AMMOXIDATION OF PROPENE OVER IRON PROMOTED BISMUTH MOLYBDATE FOR THE PRODUCTION OF ACRYLONITRILE

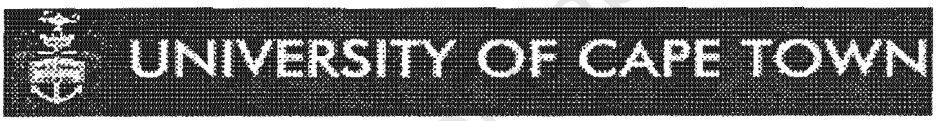

Faculty of Engineering and the Built Environment

K.D. Maripane

MSc (Applied Sciences) Dissertation (Half)

Ammoxidation of Propene over Iron Promoted Bismuth Molybdate for the Production of Acrylonitrile

Student Kgolole David Maripane

Supervisor Assoc.-Professor Eric van Steen

Internal Examiner Assoc.-Professor Eric van Steen
University of Cape Town
Department of Chemical Engineering
Rondebosch 7701, South Africa

External Examiner Professor M Scurrell
Department of Chemistry
University of the Witwatersrand
Private Bag 3
WITS
2050

Acknowledgements

I would like to thank the following individuals and organisations

Prof. Eric van Steen for his support, motivation, dedication and everything that made this work a reality.

Thanks to Dr Sadesh Sookraj for his support and organising of funds for this work.

I would like to thank my wife Virginia, my mother Shatadi and the whole family for the support they gave me throughout the entire course of study.

Special thanks to all instrumental techniques, Catalyst Characterisation and Development (CCD), SCI for analysing my catalysts

I would like to thank SASTECH RESEARCH AND DEVELOPMENT for funding this work.

Abstract

Ammoxidation of propene over iron promoted bismuth molybdate for the production of acrylonitrile.

The fundamental aim of this study is to prepare pure bismuth molybdate (α-phase) followed by iron impregnation at different ratios of iron to bismuth. The influence of iron in the ammoxidation of propene for the formation of an acrylonitrile is to be investigated.

Upon characterising the bismuth molybdate, it was found that it contains excess molybdenum oxide. After the addition of iron nitrate to the pure bismuth molybdate catalyst at different ratios, different phases started to form, which was the direct result of solid-state reaction of Fe_2O_3 and MoO_3 during calcinations at 450°C, and subsequently the reaction of Fe_2O_3 with bismuth molybdate depending on the amount of iron nitrate added. Depending on the ratio of Fe:Bi, the resulted catalysts formed were α-$Bi_2(MoO_4)_3$, α-$Bi_2(MoO_4)_3$/$Fe_2(MoO_4)_3$, $Bi_3FeO_4(MoO_4)_2$/$Fe_2(MoO_4)_3$ and $Fe_2(MoO_4)_3$.

The results from elemental analysis showed that the preparation of pure iron bismuth molybdate, $Bi_3FeO_4(MoO_4)_2$ needed pure bismuth molybdate as a starting material. This is to avoid formation of iron molybdate from reaction of iron and excess molybdenum.

The four prepared catalysts were all tested and it was found that the bismuth molybdate contributed a lot to selectivity for the formation of partial oxidation products whereas iron molybdate as a co-phase catalyst contributed to activity and the stability of the catalyst.

Iron molybdate alone showed that its ability to release oxygen from the structure is relatively lower as compared to bismuth molybdate and the mixed phased catalysts. That was showed by TPR measurements. The iron mobility plays a crucial role in regenerability and reducibility of the catalysts.

Table of Contents

		Index
Acknowledgements		i
Abstract		ii
Table of Content		iii
Chapter 1	**Literature Review**	**1**
1	Ammoxidation of propene for acrylonitrile synthesis	1
1.1	Chemistry of ammoxidation of propene	1
1.2	Uses of acrylonitrile	3
1.3	Industrial processes for the ammoxidation of propene yielding acrylonitrile	3
1.4	Mechanism of the ammoxidation of propene yielding Acrylonitrile	9
1.5	Catalyst for ammoxidation of propene	12
1.5.1	Properties of ammoxidation catalyst	12
1.5.2	Structure of ammoxidation catalyst	13
1.5.2.1	Bismuth molybdate	13
1.5.2.1.1	Preparation of bismuth molybdate	16
1.5.2.2.	Bismuth iron molybdate	18
1.5.2.3	Iron molybdate	19
1.5.2.4	Antimony based ammoxidation catalysts	19
1.5.2.5	Telluriam based ammoxidation	19
1.5.3	Role of promoters in the single or multi-component catalyst	19
1.6	Effect of reaction conditions on the ammoxidation of propene	21
1.6.1	Effect of partial pressure of the reactants	21
1.6.2	Effect of temperature	21
1.6.3	Stability and regenerability of the catalyst	21

1.7 Problem statement 22

Chapter 2 Experimental procedures 23

2.1 Catalyst preparation 23

2.1.1 Preparation of α-bismuth molybdate 23

2.1.2 Preparation of iron molybdate 23

2.1.3 Preparation of mixed iron bismuth molybdate (Bi:Fe=1) 24

2.1.4 Preparation of mixed iron bismuth molybdate (Bi:Fe=3) 24

2.2 Physio-chemical characterisation of the catalyst 24

2.2.1 Elemental analysis using AAS-ICP 25

2.2.2 Characterisation of structural features in material 25

2.2.2.1 Crystallographic characterisation using XRD 25

2.2.2.2 Infrared adsorption spectroscopy 25

2.2.2.3 Mössbauer-spectroscopy 26

2.2.3 Morphological appearance 26

2.2.3.1 Scanning Electron Microscopy (SEM) 26

2.2.3.2 Surface area and pore volume measurements 26

2.2.3.3 Particle size distribution (PSD) 26

2.2.4 Temperature programmed reduction (TPR) 27

2.3 Reaction studies 27

2.3.1. Product analysis 30

2.3.1.1 Analysis of ammonia 30

2.3.1.2 Hydrocarbon analysis 30

2.3.2 Data evaluation 32

Chapter 3 Results **33**

3.1 Catalyst preparation and characterisation 33

3.1.1 Bismuth molybdate 33

3.1.1.1 Elemental analysis 33

3.1.1.2 Structural characterisation of catalysts 34

3.1.1.2.1 X-ray diffraction 34

3.1.1.2.2 Infrared spectroscopy 36

3.1.1.3 Morphological appearance 37

3.1.1.3.1 Scanning Electron Microscopy (SEM) 37

3.1.1.3.2 Surface area and pore volume measurements 38

3.1.1.4 Particle size distribution (PSD) 38

3.1.1.5 Temperature-programmed reduction (TPR) 38

3.1.2 Iron molybdate 39

3.1.2.1 Elemental analysis using AAS-ICP 39

3.1.2.2 Characterisation of structural features in materials 40

3.1.2.2.1 Crystallographic characterisation using XRD 40

3.1.2.2.2 Infrared adsorption spectroscopy 42

3.1.2.2.3 Mössbauer-spectroscopy 42

3.1.2.3 Morphological appearance 43

3.1.2.3.1 Scanning Electron Microscopy (SEM) 43

3.1.2.3.2 Surface area and pore volume measurements 43

3.1.2.4 Particle size distribution (PSD) 44

3.1.2.5 Temperature programmed reduction (TPR) 44

3.1.3 Iron bismuth molybdate (Bi:Fe= 3:1) 45

3.1.3.1 Elemental analysis using AAS-ICP 45

3.1.3.2 Characterisation of structural features in materials 46

3.1.3.2.1 Crystallographic characterisation using XRD 46

3.1.3.2.2 Infra-red adsorption spectroscopy 48

3.1.3.2.3 Mössbauer-spectroscopy 48

3.1.3.3	Morphological appearance	49
3.1.3.3.1	Scanning Electron Microscopy (SEM)	49
3.1.3.3.2	Surface area and pore volume measurements	50
3.1.3.4	Temperature programmed reduction (TPR)	50
3.1.4	Iron bismuth molybdate (Bi:Fe= 1:1)	51
3.1.4.1	Elemental analysis using AAS-ICP	51
3.1.4.2	Characterisation of structural features in materials	52
3.1.4.2.1	Crystallographic characterisation using XRD	52
3.1.4.2.2	Infra-red adsorption spectroscopy	54
3.1.4.2.3	Mössbauer-spectroscopy	54
3.1.4.3	Morphological appearance	55
3.1.4.3.1	Scanning Electron Microscopy (SEM)	55
3.1.4.3.2	Surface area and pore volume measurements	56
3.1.4.4	Temperature programmed reduction (TPR)	56
3.2	Reaction studies over bismuth molybdate, iron molybdate and iron promoted bismuth molybdate catalysts	58
3.2.1	α-Bismuth molybdate bismuth molybdate	58
3.2.2	Iron molybdate	63
3.2.3	Iron bismuth molybdate (Bi:Mo = 3)	66
3.2.4	Iron bismuth molybdate (Bi:Mo = 1)	70
Chapter 4	**Discussion**	**75**
4.1	Catalyst preparation	75
4.2	Catalysts reducibility: Temperature programmed reduction	75
4.3	Comparison of iron bismuth molybdate as a catalyst for propene mmoxidation	77
4.4	Origin of different behaviour with tested catalyst	85
Chapter 5	**Conclusion**	**88**

Chapter 6 References **89**

Chapter 7 Appendix

Appendix 1 95
Appendix 2A 97
Appendix 2B 98
Appendix 2C 102
Appendix 3A 105
Appendix 3B 109
Appendix 3C 118

1. Ammoxidation of propene for acrylonitrile synthesis

Ammoxidation of propene represents the route for all the world's acrylonitrile production (Wittcoff and Reuben, 1980). The first ammoxidation technology was developed in 1960's by the Standard Oil Company of Ohio (now BP America). Acrylonitrile is the primary organic unit for the production of wide range of useful polymers such as nylon. It is the second largest derivative of propene. Propene is in abundance in South Africa since it is a major product of the Fischer-Tropsch synthesis. The availability of propene in SASOL creates the opportunity to expand acrylonitrile production in South Africa.

1.1 Chemistry of ammoxidation of propene

Acrylonitrile is currently produced by reacting propene and ammonia in the presence oxygen. The stoichiometric reaction equation for catalytic ammoxidation of propene is as follows:

$$C_3H_6 + \tfrac{3}{2}O_2 + NH_3 \xrightarrow{\text{catalyst, 400-500°C}} C_3H_3N + 3H_2O \qquad \Delta H^R_{25°C} = -516\ \text{kJ/mol}$$

The reaction is typically carried out at temperatures between 400 and 500°C in the presence of a catalyst. The basic components of the catalysts are bismuth molybdate, antimonite or uranium.

The ammoxidation of propene is highly exothermic. The heat of reaction per mol of acrylonitrile formed at 25°C is –516 kJ/mol. The heat of reaction does not vary much with temperature (see Figure 1.1). At typical reaction temperature of the ammoxidation of propene the heat of reaction is ca. –500 kJ/mol. In order to control the temperature during the reaction, a large amount of heat must be removed from the reactor.

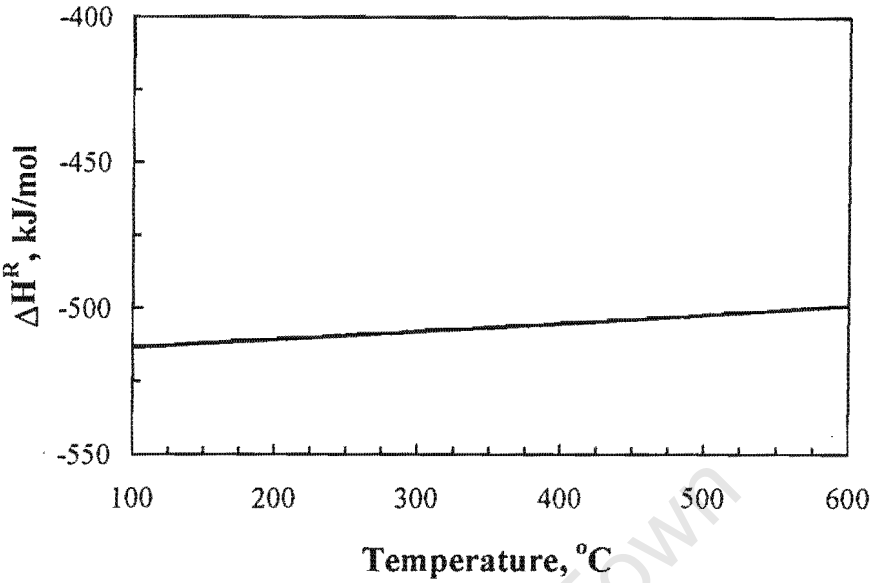

Figure 1.1: Heat of reaction in the ammoxidation of propene yielding acrylonitrile as a function of temperature (calculated using data from Perry and Green, 1984)

A typical side reaction, which may occur in gas phase oxidations, is the total oxidation of the hydrocarbon, propene, yielding CO_2/CO and the oxidation of ammonia yielding nitrogen and water. The over-oxidation of propene is even more exothermic than the selective ammoxidation of propene yielding acrylonitrile. The heat of reaction for the oxidation of propene yielding carbon dioxide equals -1925 kJ per mole of propene converted ($\Delta H^R_{25°C}$). The oxidation of ammonia yielding nitrogen and water is also exothermic ($\Delta H^R_{25°C}$=-317 kJ/mol of ammonia).

By-products, which are formed in the reaction, are hydrogen cyanide, acetonitrile and carbon oxides. The recovery or disposal of the by-products (and their corresponding impact on process economics) depends on the specific situation of each producer. Hydrogen cyanide, which has a substantial market as an intermediate for methyl methacrylate manufacture, is often recovered. Acetonitrile, on the other hand, has limited market as an industrial solvent and is usually incinerated.

1.2 Uses of acrylonitrile

The most important application of acrylonitrile is as a monomer in the production of poly-acrylonitrile. This polymer finds application in textile fibres, resins, thermoplastics and elastomers. This wide range of applications and the successful improvements in production techniques were the key reasons for dramatic expansion in acrylonitrile production in the 1980's (Weissermel and Arpe, 1993). Furthermore, acrylonitrile is used as a co-monomer in ABS and SAN plastics. In Europe and USA acrylonitrile is also used in the production of adiponitrile, which is used for Nylon®-production.

Table 1.1: Distribution of the usage of acrylonitrile (in wt-%) in 1991 (adapted from Weissermel and Arpe, 1993)

Materials	World	USA	Europe	Japan
Acrylic fibres	59	37	60	52
ABS & SAN plastics	20	20	16	26
Adiponitrile	9	22	11	6
Nitrile fibres	4	3	3	4
Other	8	18	10	12

1.3 Industrial processes for the ammoxidation of propene yielding acrylonitrile

Acrylonitrile is presently being produced by the ammoxidation of propene. The partial oxidation is either catalysed by bismuth molybdate (SOHIO-process) or iron antimonate (Nitto-process) (Albonetti et al., 1997, 1998). The introduction of the ammoxidation of propene in 1960 resulted in substantial drop in the price of acrylonitrile since this process could replace the more expensive acetylene/HCN-based route.

In the SOHIO-process for the synthesis of acrylonitrile (see Figure 1.2), propylene, ammonia and air in a volumetric ratio of 1:1:13 are fed to the fluidised bed reactor containing the catalyst. The reaction takes place at temperatures between 420 and 460 °C and a pressure of approximately 1.5-2 bar. The major by-products of the ammoxidation of propene are hydrogen cyanide and acetonitrile. The reactor effluent containing product, by-products, unconverted feed and water formed during the reaction passes through a cyclone where catalyst fines are removed and recycled.

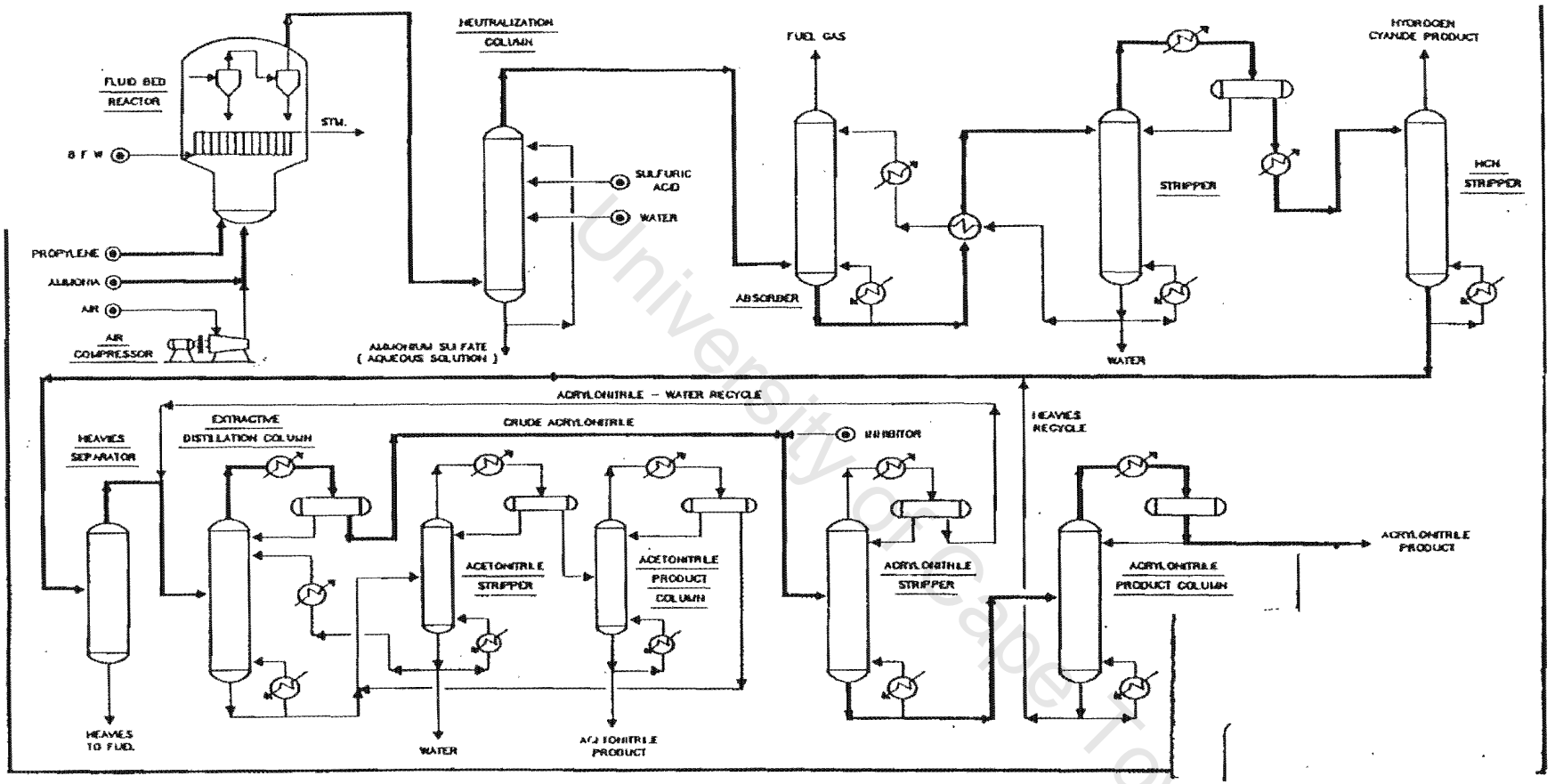

Figure 1.2: Flow sheet of the SOHIO-process for the synthesis of acrylonitrile by the ammoxidation of propene (Chem Systems, 1990)

The reactor effluent is washed in the neutralisation column with a solution of sulphuric acid and ammonium sulphate. Washing takes place at temperatures between 80 and 100°C to prevent condensation of acrylonitrile. The unconverted ammonia is neutralised, producing ammonium sulphate, which is drawn off as an aqueous solution of 30- 35 wt-% $(NH_4)_2SO_4$.

The gaseous effluent of the neutralisation column passes a water scrubber in which acrylonitrile, hydrogen cyanide, acetonitrile, and other organic side-products (such as acrolein and acrylic acid) are absorbed. Carbon oxides, unconverted propene, nitrogen are discharged from the top of the column.

The organic compounds and hydrogen cyanide in the aqueous phase leaving the water scrubber are stripped off producing a crude product. Subsequently, hydrogen cyanide is stripped off as essentially pure product.

In order to prevent the formation of condensation products, an inhibitor is added to the product stream. The inhibitor is a component of the heavies recycle stream. Condensation products, which may have formed before the addition of the inhibitor, are separated from the crude product.

Separation of acrylonitrile and acetonitrile is achieved by extractive distillation (using water as the third component), since the direct distillation is difficult. This is because of the closeness of their boiling points.

The acetonitrile/water mixture leaves the distillation column at the bottom. A two-tower system can be used to recover pure acetonitrile. The extraction column bottoms enter the acetonitrile stripper, which operate under vacuum, and acetonitrile is concentrated as an overhead while excess water is taken as bottoms for recycle to the extraction column or drained.

The overhead of the extractive distillation column (crude acrylonitrile) can be worked up to obtain essentially pure acrylonitrile. An inhibitor is added to the

acrylonitrile/water mixture in the extraction column overhead, before it enters the acrylonitrile stripper. This column operates under pressure, and the inhibitor prevents polymerisation, which would occur due to the elevated temperatures that are required. In this column, the remaining water is driven off and recycled back to the extraction column. The bottoms product, which is essentially all acrylonitrile, is sent to the acrylonitrile product column where pure acrylonitrile is taken as overhead product. The bottom product containing the inhibitor is recycled to the separator.

Processes different from the SOHIO-process have been developed for the synthesis of acrylonitrile by the ammoxidation of propene. The major differences between the other processes and the SOHIO-process lay in the choice of catalyst and catalytic reactor. In the SOHIO-process, an iron promoted bismuth molybdate is used as a catalyst. The separation of acrylonitrile from the product stream is for all these processes similar.

In the BP(Distillers)-Ugine process, the ammoxidation of propene is a two-step process. The first step is the conversion of propene to acrolein, Acrolein is subsequently converted in the presence of ammonia yielding acrylonitrile. In the Montedison route, propene is converted in a single step on fluidised bed with Te and Ce as promoters on bismuth molybdate catalyst. In the Snamprogetti/Anic route, propene is converted in a single fixed bed reaction with Mo-, V- or Mo-, Bi- as catalysts.

Most processes employ a fluidised bed reactor. Heat removal is a critical factor in the ammoxidation of propene (see section 1.1). Heat removal in a fluidised bed reactor is much more efficient than in a fixed bed reactor. In older plants two separate fluidised beds were used in the production of acrylonitrile. In the first fluidised bed reactor propene and ammonia react with the catalyst in the oxidised state. The catalyst is then re-oxidised in a second fluidised bed reactor, thus avoiding the direct contact of propene and ammonia with air. In modern plants propene and ammonia enter the fluidised bed reactor together with air (see Figure 1.3).

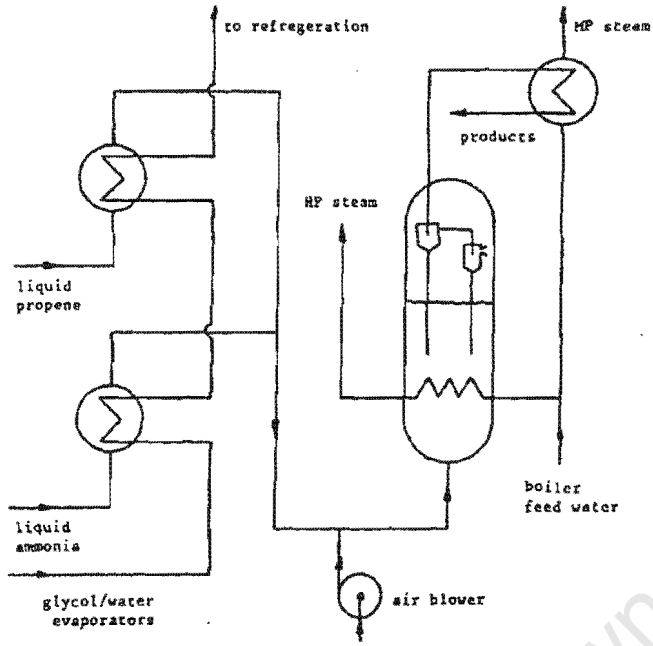

Figure 1.3: One stage reactor for the ammoxidation of propene (Pujaro et al., 1977)

The feed mixture is potentially explosive, but in practise the explosions do not occur in fluidised beds because of the high rate of heat exchange. The explosion limits of reactants and products are given in a table below.

Table 1.2: The explosive limits of reagents and products in the ammoxidation of propene in air

Gas	Explosion limits Vol.-%
Propene	2- 11
Ammonia	16- 25
Acrylonitrile	3- 17
Carbon monoxide	12- 74

1.4 Mechanism of the ammoxidation of propene yielding acrylonitrile

The ammoxidation of propene to acrylonitrile is a 6-electron oxidation (Grasselli, 1986). The whole reaction cycle is a 32-bond making and bond breaking process. The rate-determining step is the homolytic C-H bond breaking of the α-hydrogen in propene (Grasselli, 1986; Nilson et al., 1997).

Figure 1.4 shows schematically the mechanism of the ammoxidation and the oxidation of propene over bismuth molybdate catalysts (Burrington et al., 1984). Both reaction cycles proceed via a Mars-van Krevelen mechanism (Bielanski and Haber, 1991). The catalyst is reduced with the hydrocarbon (and ammonia), and re-oxidised using gaseous oxygen.

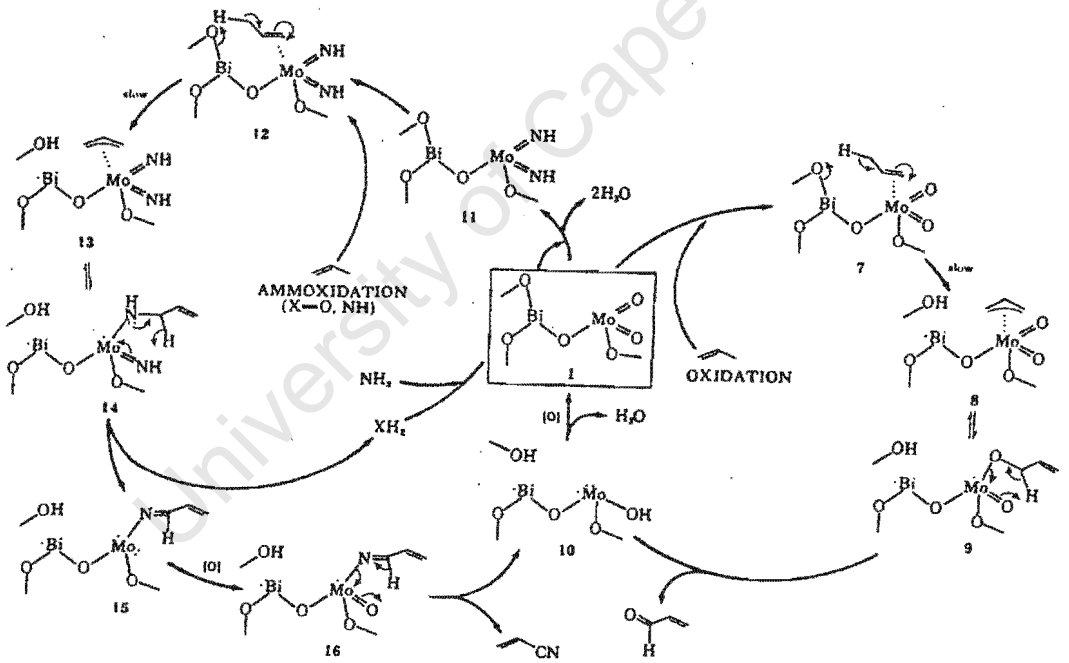

Figure 1.4: Mechanism of the selective ammoxidation and oxidation of propene over bismuth molybdate catalysts (Burrington et al., 1984)

The oxidised catalyst (**1**) adsorbs ammonia dissociatively. The Mo=O groups are thereby converted to Mo=NH groups (**11**) under simultaneous formation of water. This is a fast reaction, which can be assumed to reach equilibrium. The interaction of gaseous propene with Mo=NH sites yields a π-adsorbed complex (**12**). The π-adsorbed propene slowly undergoes α-H-abstraction by interaction with Bi-O species under formation of a hydroxyl group and a π-allylic Mo complex (**13**). The reaction of the π-allylic complex with the NH-group leads to the formation σ-N species (**14**). In this step Mo^{6+} is reduced to Mo^{5+}. The interaction of the σ-N species with the second =NH-species lead to the formation of NH_3 and 3-iminopropene Mo complex (**15**). In this step Mo^{5+} is further reduced to Mo^{3+}. In the next step Mo^{3+} is oxidised to Mo^{5+} using either lattice oxygen or gaseous oxygen resulting in an oxygen species near to the 3-iminopropene species (**16**). The oxidation state of molybdenum in complex (**16**) is Mo^{5+}. Desorption of acrylonitrile can then take place by the interaction of the 3-iminopropene species with the neighbouring oxygen, yielding a hydroxyl group (**10**). In this process Mo is reduced again to Mo^{3+}. The hydroxyl groups on the surface can recombine yielding water. The interaction with gaseous oxygen results in the restoring of the original catalytically active site (**1**).

Propene can also interact with the fully oxidised catalytically active site (**1**) yielding a π-adsorbed complex (**7**). The homolytic cleavage of the α-H species will lead to the formation of a π-allylic Mo complex (**8**) and a hydroxyl group. This is the slowest, i.e. the rate-determining step in the reaction. The interaction of the π-allylic species with Mo=O leads to the formation of a σ-O-propene complex (**9**). In this reaction Mo^{6+} is reduced to Mo^{5+}. Desorption of acrolein is accompanied by the further reduction of Mo^{5+} to Mo^{3+} and the formation of surface hydroxyl groups (**10**). The hydroxyl groups on the surface can recombine yielding water. The interaction of complex (**10**) with gaseous oxygen results in the restoring of the original catalytically active site (**1**).

The relative amounts of the various intermediates on the surface depend highly on the nature of the catalyst (see Figure 1.5), although the rate-determining step is the same

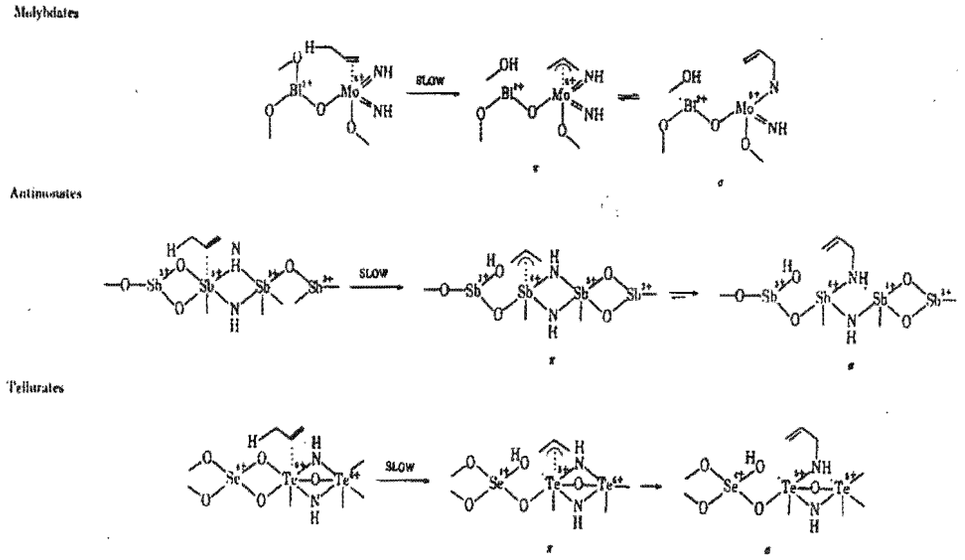

Figure 1.5: Transformation of the π-adsorbed propene complex to σ-N-species over the oxides of bismuth-molybdenum, antimony and selenium-tellurium (Grasselli, 1986)

(Grasselli, 1986). On bismuth molybdate catalyst equilibrium exists between π-allylic Mo complex and the σ-N Mo complex. With antimony based catalyst the equilibrium is shifted towards the σ-N complex. With selenium-tellurates the transformation of the π-allylic complex to σ-N complex is irreversible Mo.

Acrylonitrile and acrolein can both be formed in the ammoxidation of propene. According to the mechanism proposed by Burrington et al. (1984), acrylonitrile and acrolein are formed in parallel (see Figure 1.4). Nilsson and Andersson (1997) investigated the reaction pathway in the ammoxidation of propene (and propane) over V-Sb-oxide using transient response technique. They concluded from their results that acrylonitrile is formed as a consecutive product. According to these authors the primary product in the ammoxidation of propene is acrolein. The transformation of acrolein to acrylonitrile is thermodynamically highly favoured:

$$K_{a,500^{\circ}C} = \frac{a_{C_3H_3N} \cdot a_{H_2O}^2}{a_{C_3H_4O} \cdot a_{O_2}^{1/2}} \approx 10^{12}$$

This means that if acrolein is formed in the ammoxidation of propene, its consecutive transformation to acrylonitrile will be favoured.

1.5 Catalyst for the ammoxidation of propene

Several multi-component oxides have been reported to catalyse the ammoxidation of propene (and propane) to acrylonitrile. The challenge for the catalyst is to kinetically inhibit the over-oxidation of the reagent propene yielding CO and CO_2.

1.5.1 Properties of ammoxidation catalysts

According to Grasselli (1990), the most effective ammoxidation catalyst should have the following essential features:

- Ability to adsorb the hydrocarbon
- Ability to adsorb ammonia
- Ability to adsorb oxygen
- Ability to catalyse α-hydrogen abstraction
- Ability of insert nitrogen
- Ability to change its oxidation state

Adsorption of reagents, propene, ammonia and oxygen, needs coordinative unsaturated elements in their highest oxidation state containing empty orbital capable

of accepting electrons. The electrons originate from the double bond (in the case of propene) or from the lone pairs (in the case of ammonia). The catalyst must contain an element that has a lone electron pair imparting a partial radical character to the oxygen bound to it and thereby facilitating the abstraction of α-hydrogen as a radical from the chemisorbed olefin. The elements in the catalyst must be able to form stable =NH surface species, which can then be inserted into π-allylic surface species. The elements in the catalyst must be able to change their oxidation state readily. The ammoxidation catalysts should possess optimum metal oxygen bond strengths, isolated active sites, and a facile solid-state redox couple.

A typical ammoxidation catalyst consists of two or more elements to be effective in order to have all the essential features necessary for being an effective catalyst.

1.5.2 Structure of ammoxidation catalysts

Typical catalysts for the ammoxidation of propene contain bismuth molybdate (possibly promoted with iron), iron molybdate, antimonite or tellurate as the major component.

1.5.2.1 Bismuth molybdate

Bismuth molybdenum oxides can occur in different phases depending on the Bi:Mo ratio:

$Bi_2Mo_3O_{12}$ (α-phase)	Bi:Mo = 2:3
$Bi_2Mo_2O_9$ (β-phase)	Bi:Mo = 1:1
Bi_2MoO_6 (γ-phase)	Bi:Mo = 2:1

$Bi_2Mo_3O_{12}$ (α-phase) and $Bi_2Mo_2O_9$ (β-phase) have tetrahedrally co-ordinated Mo^{6+}-ions. The α-phase possesses a defect-scheelite structure $Bi_{2/3}\square_{1/2}MoO_4$ (Thomas and Thomas, 1997). The active site containing two Mo-dioxo groups bridged by Bi-O groups is apparent from the structure (see Figure 1.6). The boundary lines of the Scheelite structure are 5.6 along which Bi atoms and vacancies are located (ratio vacancies to Bi equals 1:2). The Mo-O polyhedra, two of which have Mo-dioxo

character, are stacked between these Bi-"layers" and provide the active sites for the ammoxidation.

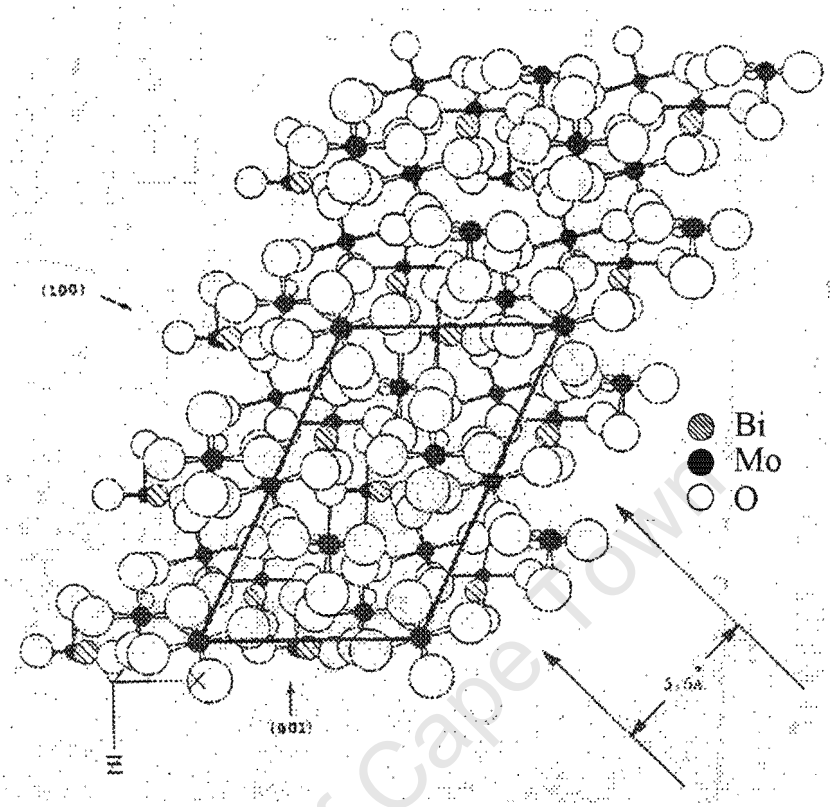

Figure1.6: Crystal structure of α-$Bi_2Mo_3O_{12}$ (010). (Burrington et al.,1984)

$Bi_2Mo_2O_9$ (β-phase) has structural features of both the α-phase and the γ-phase (Grasselli, 1997; see Figure 1.7). The molybdenum coordination is tetrahedral (as in the α-phase) and it contains vacancies. The co-ordination of bismuth is similar to that in the γ-phase.

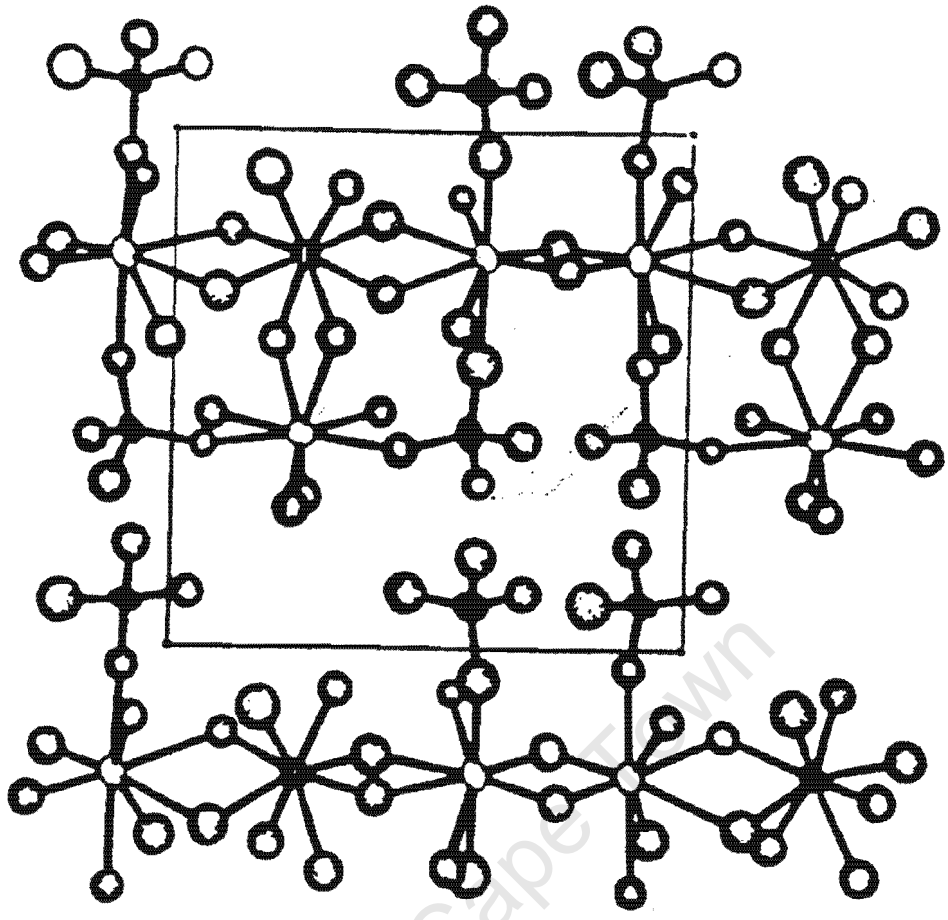

Figure 1.7: Structure of β-$Bi_2Mo_2O_9$ projected in the a-c plane. Unit cell is outlined with a as the horizontal axis. Molybdenum is tetrahedral coordinated. Bismuth is eight-coordinated. (Grasselli, 1997)

Bi_2MoO_6 (γ-phase) contains octahedral coordinated molybdenum and is similar to the naturally occurring koechlinite (see Figure 1.8; Grasselli, 1997).

Application of ESCA to the determination of electron binding energies in α-, β- and γ-phase showed those of Bi to be as in Bi_2O_3 and those of Mo to be as in MoO_3, and independent of coordination. Quantitatively, the surface composition of the α- and γ-phase was identical to that of the bulk, even after mild treatment with an alkene.

The molybdenum content becomes larger going from γ-phase to β-phase to α-phase. $Bi_2Mo_2O_9$ (β-phase) is slightly more active than the α-phase in the ammoxidation of propene, but has a lower selectivity (Grasselli, 1997). The activity of Bi_2MoO_6 (γ-

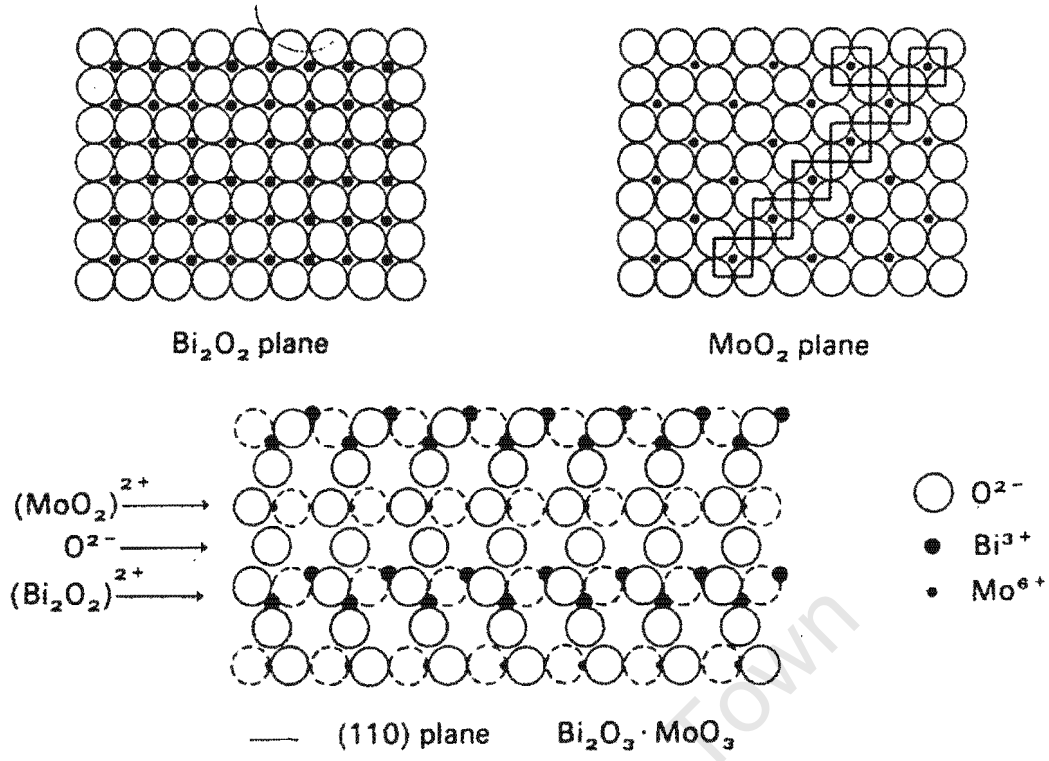

Figure 1.8: Structure of γ-Bi_2MoO_6 (koechlinite) (Grasselli, 1997)

phase) is high, but its selectivity for acrylonitrile formation is poor. This has been ascribed to loosely bound lattice oxygen which lead over-oxidation and thus to the formation of CO/CO_2 (Higgins and Hayden, 1977). Pulse experiments performed by Brazdil et al. (1980) also showed that in the absence of oxygen the activity is initially of the order of $\gamma << \alpha < \beta$, but after prolonged time (or number of pulses) the activity of α and β are comparable. The low activity of the γ-phase might be attributed to the relative low content of molybdenum in this phase. The somewhat higher initial activity of the b-phase can be attributed to the optimum ratio of Bi to Mo (1:1).

1.5.2.1.1 Preparation of bismuth molybdates

The method of preparing different phases of bismuth molybdenum oxide has been described in detail by Batist, et al. (1972). They can be prepared by reaction of $(NH_4)_6Mo_7O_{24}.4H_2O$ and $Bi(NO_3)_3.5H_2O$ in concentrated nitric acid. During preparation of each different phase, reaction conditions have to be chosen with caution to avoid transformation of the phase of interest to another phase. The required

mole ratio is essential for the preparation of the desired phase. After precipitation the precipitate must be aged. Ageing has been shown to be essential. It was observed experimentally that the un-aged catalyst has some impurities such as molybdenum trioxide. Such impurities were not observed for the catalyst of which its precipitate have been aged, as evidenced by an XRD analysis (Keulks, 1974).

Stepwise calcination is preferred to remove water and drive away any impurities, leaving a clean catalyst surface. The calcination temperature was carefully chosen to ensure that the phase of interest is not transformed to another phase. Depending on the type of phase, which need to be prepared, and the method of its preparation, it is essential to be aware of the generic connection between phases (see Figure 1.9).

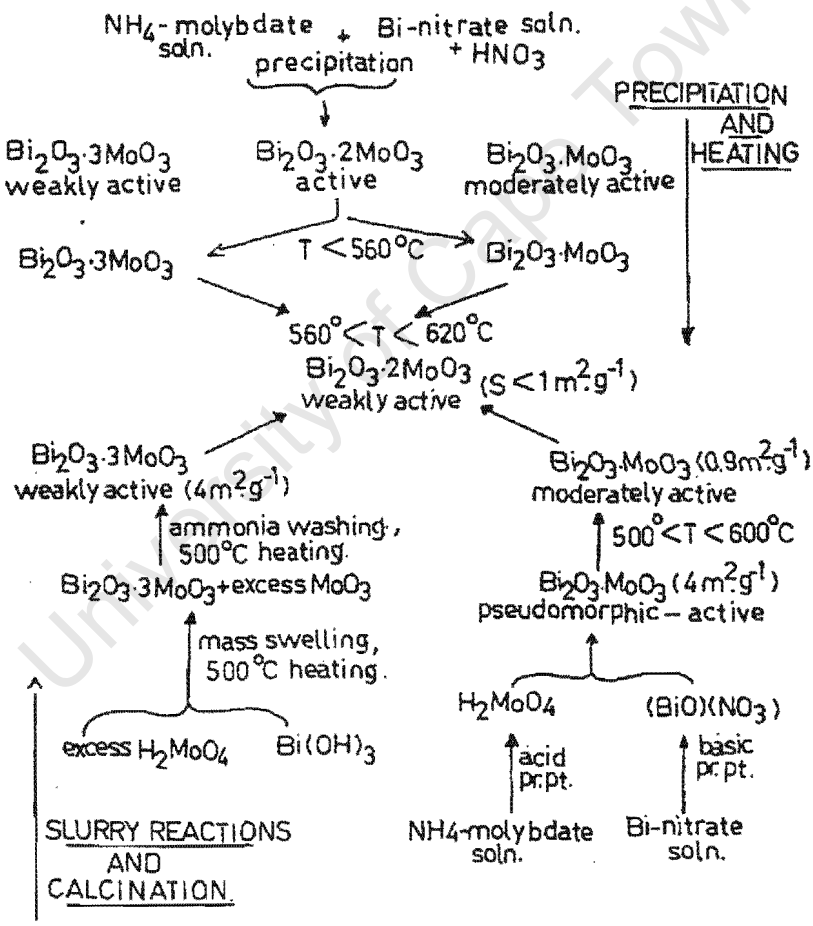

Figure 1.9: Generic connection between various phases in the BiO_3-MoO_3 systems (Batist, et al., 1972)

1.5.2.2 Bismuth iron molybdate

The efficiency of bismuth molybdate for the ammoxidation of propene can be substantially improved by incorporating additional elements in the structure, particularly redox elements (Grasselli, 1997). The solubility of these elements in the bismuth molybdate structure is however limited, and new phases can be formed. The addition of Fe^{3+} to bismuth molybdate may lead to the formation of $Bi_3(FeO_4)(MoO_4)_2$, whose structure is related to the scheelite structure with both iron and molybdenum in tetrahedral coordination (see Figure 1.10). It consists of two

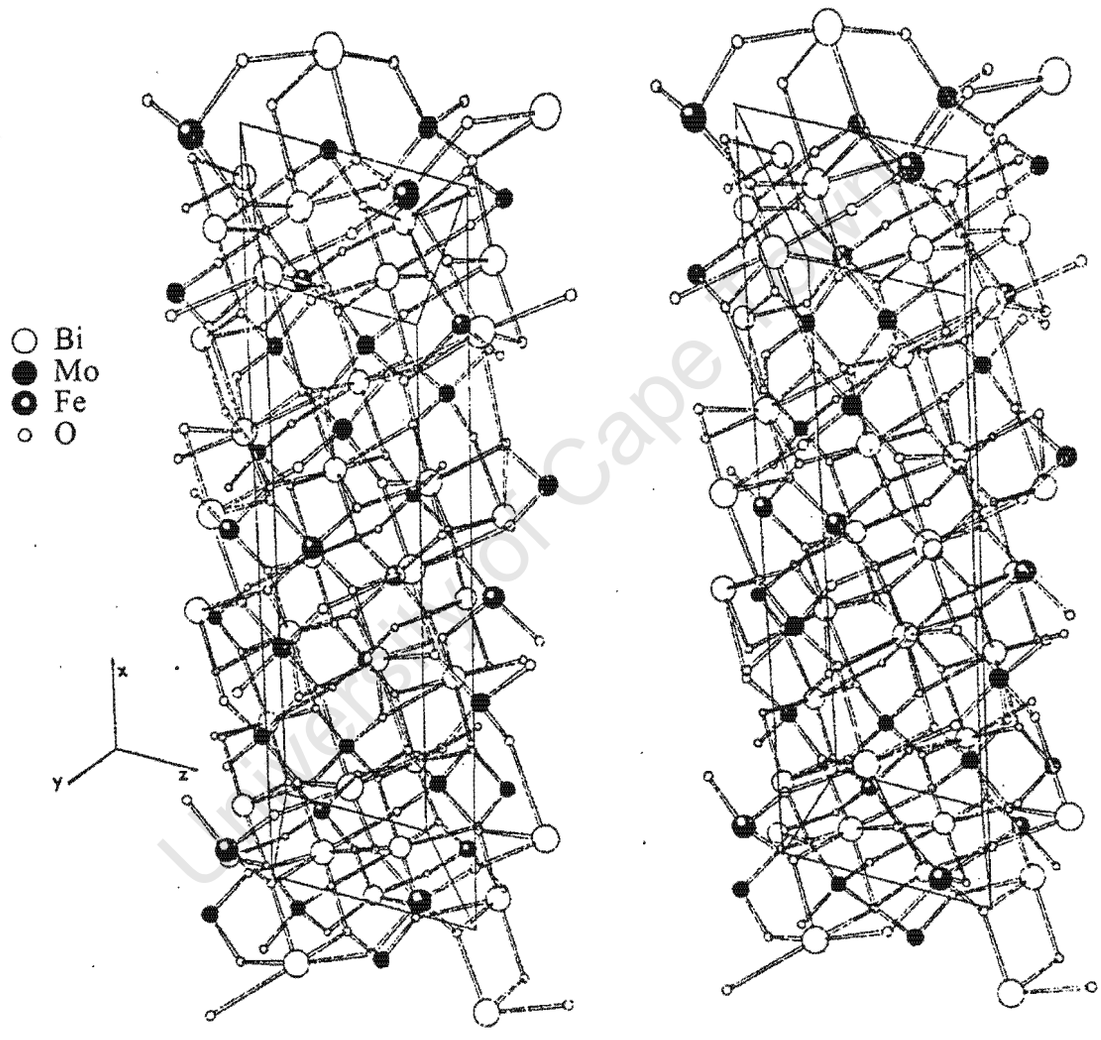

Figure 1.10: Structure of $Bi_3(FeO_4)(MoO_4)_2$ (Jeitschko et al., 1976)

crystallographically distinct Bi sites (both eight coordinated). It has a surface composition identical to that of the bulk. $Bi_3(FeO_4)(MoO_4)_2$ has two forms, the disordered and ordered one. The microcrystalline disordered form is meta-stable and

transforms to the ordered scheelite superstructure under reaction conditions or if it is heated up to 600°C to 900°C for ten hours (Jeitschko et al., 1976).

1.5.2.3 Iron molybdate

The structure of iron molybdate, $Fe_2(MoO_4)_3$, is similar to that of α-$Bi_2Mo_3O_{12}$ (Bielanski and Haber, 1991). During reaction iron molybdate can be transformed:

$$Fe_2(MoO_4)_3 \rightarrow 2FeMoO_4 + MoO_3 + \tfrac{1}{2}O_2$$

$Fe_2(MoO_4)_3$: Similar to $Bi_2Mo_3O_{12}$, the Fe in the catalyst is arranged as in Fe_2O_3 and Mo as MoO_3. The alkene ammoxidation proceed through lattice oxygen. Bulk oxygen mobility approach that of BiMo catalyst.

1.5.2.4 Antimony based ammoxidation catalysts

Iron antimonite ($FeSbO_4$) is a well-known antimony based catalysts for the ammoxidation of propene (van Steen et al., 1997). In contrast to bismuth-molybdates, which uses bulk lattice oxygen, iron antimonite only uses lattice oxygen from the upper thin layer of the catalyst, and hence tends to deactivate strongly with time on stream.

1.5.2.5 Tellurium based ammoxidation

Tellurium molybdate are moderately selective catalyst for oxidation of propene to acrolein (Bielanski and Haber, 1991). Tellurium based catalyst are problematic, because of the high volatility of TeO_2.

1.5.3 Role of promoters in the single or multi-component catalyst.

Multi-component molybdates have been developed, giving higher activity and selectivity in the ammoxidation of propene. Grasselli (1997) recommends the introduction of a redox couple. The proximity of the promoter to the active site facilitates electron transfer and thus the re-oxidation of the active surface site back to

its initial and active state once it has undergone a reduction cycle during the oxidation of the substrate (olefin) to the desired product (acrylonitrile). The typical example is the regeneration of the reduced active sites in bismuth molybdate, by the vital Fe^{3+}/Fe^{2+} redox cycle.

The role of Fe^{3+}/Fe^{2+} in bismuth molybdate and antimony based catalyst is by supplying the Fe^{3+}/Fe^{2+} redox cycle (see Table 1.3). In bismuth molybdate Fe^{2+} can structurally be stabilised by the presence of other divalent elements such as Ni, Co, Mg and Mn, which forms stable isostructural molybdate with Fe^{2+} (Grasselli, 1999). Ni and Co can also help for paraffin activation.

Table 1.3: Functions of the various elements in multi-component ammoxidation catalysts (Grasselli et al., 1990).

α-H abstraction	Olefin chemisorption/ O or NH insertion	Redox couple	Example
$Bi^{3+}5d^{10}6s^{2}6p^{0}$	$Mo^{6+}d^{0}5s^{0}$	Ce^{3+}/Ce^{4+} Fe^{2+}/Fe^{3+}	$Bi_2O_3.nMoO_4$
$Sb^{3+}4d^{10}5s^{2}5p^{0}$	$Sb^{5+}5s^{0}5p^{0}$	Fe^{2+}/Fe^{3+}	$Fe_xSb_yO_z$

It has been reported that for the direct conversion of propane to acrylonitrile using bismuth molybdate, which is efficient in olefin (amm)oxidation, combination of this catalyst with paraffin activating catalyst might be possible (Stern and Grasselli, 1997).

Alkali can be added to annihilate the most acidic cracking sites of the multi-component mixture, to serve as a spacer and contact enhancer of the two functionally distinct but epitaxially matched catalyst phases. For instance, iron molybdate can epitaxially grow onto $Bi_2Mo_2O_9$ (β-phase). This mixture of $Bi_2Mo_3O_{12}$ and $FeMoO_4$ facilitate electron and oxygen ion mobility, i.e. the redox mechanism involved in the Mars and Van Krevelen mechanism (Ponceblanc et al., 1992).

1.6 Effect of reaction conditions on the ammoxidation of propene

1.6.1 Effect of the partial pressures of the reactants

Increasing partial pressure of the reactants could result in the increase in the space velocity. The results would then be decrease in the contact time (τ) between the feed materials as well as the products and hence selectivity is enhanced. Ammonia was found to affect catalyst's degree of reduction, and also inhibiting propene chermisorption on the catalyst active sites (Van Steen et al., 1997). Increasing oxygen partial pressure could also lead to high concentration of unselective oxygenates on the surface.

1.6.2 Effect of temperature

Ammoxidation is highly exothermic reaction (see Figure 1.1). Increasing temperature will results in the decrease in selectivity.

1.6.3 Stability and regeneration of the catalyst.

The formation of selective (amm)oxidation product by an allylic mechanism with incorporation of lattice oxygen creates surface vacancies at the active site of the catalyst. These vacancies can be filled by lattice oxygen ions diffusing to the reduced centrer (Libre et al., 1983; Grasselli, 1999). After the molecular oxygen from the feed is being activated by iron for example, it thus re-oxidise the reduced bulk of the catalyst (see Figure 1.6).

The ammoxidation catalyst need to be mechanically stable and withstand inadvertent plant upsets including severe reductions. Rigidly controlled operating conditions are needed to prevent irreversible reduction of antimonate catalyst (Grasselli, 1999). The problem can partially be addressed by incorporating efficient redox component such as Fe-molybdate and Fe-tungstates to the composition.

Under hydrothermal reaction conditions, the free MoO_3 combines with steam to form volatile hydrate $MoO_2(OH)_2$.The reduction potential of a re-oxidising metal must be greater than that of the nitrogen or oxygen inserting element. In large scale industrial operation, under reaction conditions, some of the key catalytic elements partially volatilise from the respective catalytic composition, rendering the catalyst less

effective with time-on-stream. TeO_2, for example, is volatile. Its formation can be minimised by incorporating TeO_2 in antimony as well as molybdenum based catalysts. Such a redox cycle helps to keep tellurium on a microscopic time scale primarily in the less volatile 6+ oxidation state.

If Fe-Sb-O catalyst is used for (amm)oxidation, the degree of reduction of this catalyst is influenced by antimony content in the surface of the catalyst (van Steen et al., 1997). Catalyst with an enriched antimony surface exhibits a higher selectivity.

Chemisorption of molecular oxygen for the formation of O^{2-} needs an efficient redox couple, such as $Fe^{3+/2+}$. Fe^{2+} is capable of efficient di-oxygen chemisorption, reducing and transforming it to lattice O^{2-} and its incorporation into the lattice (Grasselli, 1999; Bielansky and Haber 1991; Schnobel and van Steen, 1997). Dissociation of the solid continues even in the absence of the gaseous oxygen without the change in the yield of the product up to 7% catalyst reduction (Bielansky and Haber, 1991). That suggests that it is the lattice oxygen, which is responsible for hydrocarbon activation.

1.7 Problem statement

From the literature review, it has become clear that bismuth molybdates, and especially iron promoted bismuth molybdates, are effective catalysts for the ammoxidation of propene. Up to now, a kinetic comparison of the different phases has not been attempted. In this study, the effect of the ammonia partial pressure on the performance of iron promoted bismuth molybdates will be investigated. The phase composition and the structural features on the activity and selectivity for the propene ammoxidation will be evaluated.

2. Experimental

2.1 Catalyst preparation

Initially, it was attempted to synthesise the pure phases of α-$Bi_2Mo_3O_{12}$, $Fe_2(MoO_4)_3$ and mixed iron bismuth molybdate with varying ratios of bismuth to iron.

2.1.1 Preparation of α-$Bi_2Mo_3O_{12}$

The method described by Batist et al. (1972) was followed for the preparation of α-$Bi_2Mo_3O_{12}$. An aqueous solution of bismuth nitrate was prepared by dissolving 96.80g $Bi(NO_3)_3.5H_2O$ in 225ml distilled water and adding 25 ml concentrated nitric acid. 52.80g ammonium heptamolybdate ($(NH_4)_6Mo_7O_{24}.4H_2O$) was dissolved in 200ml distilled water. The solution of $(NH_4)_6Mo_7O_{24}.4H_2O$ was added drop-wise to the solution containing $Bi(NO_3)_3.5H_2O$ at room temperature. A white precipitate was formed, filtered and washed with distilled water. The precipitate was dried at 110°C overnight. After calcination in an oven in air at 450°C for 16 hours, the material changed to slightly yellow coloured powder.

2.1.2 Preparation of $Fe_2(MoO_4)_3$

Iron molybdate ($Fe_2(MoO_4)_3$) was prepared by co-precipitation from solutions containing iron nitrate and ammonium heptamolybdate in adoption of the recipe escribed by Cadus et al. (1994). An aqueous solution of iron nitrate was prepared by dissolving 21.8g $Fe(NO_3)_3.5H_2O$ in 100ml distilled water. An aqueous solution of ammonium heptamolybdate was prepared by dissolving 17.35g $(NH_4)_6Mo_7O_{24}.4H_2O$ in 100ml distilled water. The ammonium heptamolybdate solution was added to the iron nitrate solution under vigorous stirring at room temperature. The resulting green precipitate was washed with distilled water and dried at 110°C in an oven. A brownish-yellow catalyst precursor was obtained, which turned green after calcination in air at 450°C for 16 hours.

2.1.3 Preparation of mixed iron bismuth molybdate with Bi:Fe = 1

The iron bismuth molybdate with a ratio of iron to bismuth of 1 was prepared by slurry impregnation technique. It was expected that the highly dispersed iron ions would be incorporated into the matrix of the catalyst by a solid-state reaction at elevated temperatures. 17.65g $Fe(NO_3)_3.5H_2O$ was dissolved in 150ml distilled water. 24.00g α-$Bi_2Mo_3O_{12}$ was suspended in this solution. The water was slowly removed in a rotavapor at 60°C under reduced pressure. The catalyst was finally dried at 110°C overnight. The brownish-yellow mass was obtained which changed to light brown after calcination in an oven in air at 450°C for 16 hours.

2.1.4 Preparation of mixed iron bismuth molybdate with Bi:Fe = 3

The iron bismuth molybdate with a ratio of iron to bismuth of 3 was prepared by slurry impregnation technique. It was expected that the highly dispersed iron ions would be incorporated into the matrix of the catalyst by a solid-state reaction at elevated temperatures. 5.51g $Fe(NO_3)_3.5H_2O$ was dissolved in 150ml distilled water. 23.75g α-$Bi_2Mo_3O_{12}$ was suspended in this solution. The water was slowly removed in a rotavapor at 60°C under reduced pressure. The catalyst was finally dried at 110°C overnight. The light brown-orange mass was obtained which changed to yellow after calcination in an oven in air at 450°C for 16 hours.

2.2 Physio-chemical characterisation of the catalysts

The synthesised materials were characterised for the elemental and structural composition and morphological appearance. The elemental analysis was performed using AAS-ICP. The structural characterisation included the crystallographic characterisation, and the characterisation of the chemical surrounding of the various elements within the catalyst. The ability of the materials to release oxygen from the bulk of the structure was determined using temperature programmed reduction (TPR).

2.2.1 Elemental analysis using AAS-ICP

Atomic adsorption spectroscopy coupled with inductive coupled plasma (AAS-ICP) was used to determine the bismuth, iron and molybdenum content of the materials. For this purpose the calcined material was digested using.

Method 1.

0.5g of catalyst was dissolved in 10ml of HCl, 10ml of HF and 10ml of HNO_3. The solution was left in a Teflon beaker for about five hours. The residue was dissolved in 20ml concentrated HCl and make up to 100ml.

Method 2.

0.4g Lithiumborate fuse and 0.5g sample was mixed in Pt dish. The mixture was left for 1 hour at 800°C. The mixture was dissolved in concentrated HCl and made up to 100ml.

Calibration

A standard solutions of bismuth nitrate (100 ppm), iron nitrate (100ppm) and molybdenum (100ppm) in nitric acid all from Sollulab were used to prepare different concentrations for calibration.

2.2.2 Characterisation of structural features in materials

2.2.2.1 Crystallographic characterisation using XRD

The crystallographic composition of the materials was determined using X-ray diffraction (XRD). X-ray diffraction (XRD) was performed using a Siemens diffractometer with Cu K_α radiation operating at 40 kV.

2.2.2.2 Infrared adsorption spectroscopy

The structural features of the materials were characterised using vibration spectroscopy. IR spectra were obtained using the Perkin Elmer FT-IR spectrometer using KBr cells at KBr to catalyst ratio of 10. The wafer was prepared by applying 10

Tons of pressure to the KBr/catalyst mixture. The spectra obtained were compared with those reported in literature.

2.2.2.3 Mössbauer-spectroscopy

Mössbauer spectroscopy experiments were performed with a 50 mCi (initial activity) Co-57 source in a Rhodium matrix. The spectrometer was operated in a symmetric constant acceleration mode with 100 μs of dwell time per channel. The spectrum was collected over 1024 channels in mirror image format.

2.2.3 Morphological appearance

2.2.3.1 Scanning Electron Microscopy (SEM)

SEM photographs were obtained a Cambridge S360 Stereoscan operating at 17.2 kV. The sample as adhered to carbon tab on aluminium stab followed by Ar-Au-Pb sputtering for 30 seconds, four times.

2.2.3.2 Surface area and pore volume measurements

Nitrogen physiosorption at –195.8°C was used to determine the BET-surface area of the calcined materials and their pore volume. The catalyst was degassed by exposing it to a temperature of 250 °C at constant nitrogen flow for a period of eight hours. The surface area was obtained from the adsorbed amount of nitrogen using the BET-equation.

2.2.3.3 Particle size distribution (PSD)

The particle size distribution of the calcined materials was obtained using LS 30 Particle Size Analyser at a pump speed of 35 rpm.

2.2.4 Temperature programmed reduction (TPR)

Temperature programmed reduction was performed using a Micromeritics TPD/TPR 2900. 0.03g of catalyst was exposed to H_2 as a reducing gas at a flow rate of 40 cm^3/min.

2.3 Reaction studies

The ammoxidation of propene was performed in continuous flow conditions at a fixed bed reactor. The flow sheet of the experimental set-up is given in Figure 2.1. The flow of a gas mixture containing 1.7% C_3H_6, 2.03% O_2 with the balance being balance N_2 (Afrox) was using a Brooks mass flow controller (calibration see Appendix 2A). The ammonia flow was regulated by the usage of a needle valve. The two feed streams were mixed and passed over the reactor. The reactor is connected to a pressure relieve valve at the top of the reactor to ensure that any unexpected pressure built-up can be relieved to the vent line. This valve opens at 7000 kPA bar. The reactor has a by-pass line for analysing the feed composition.

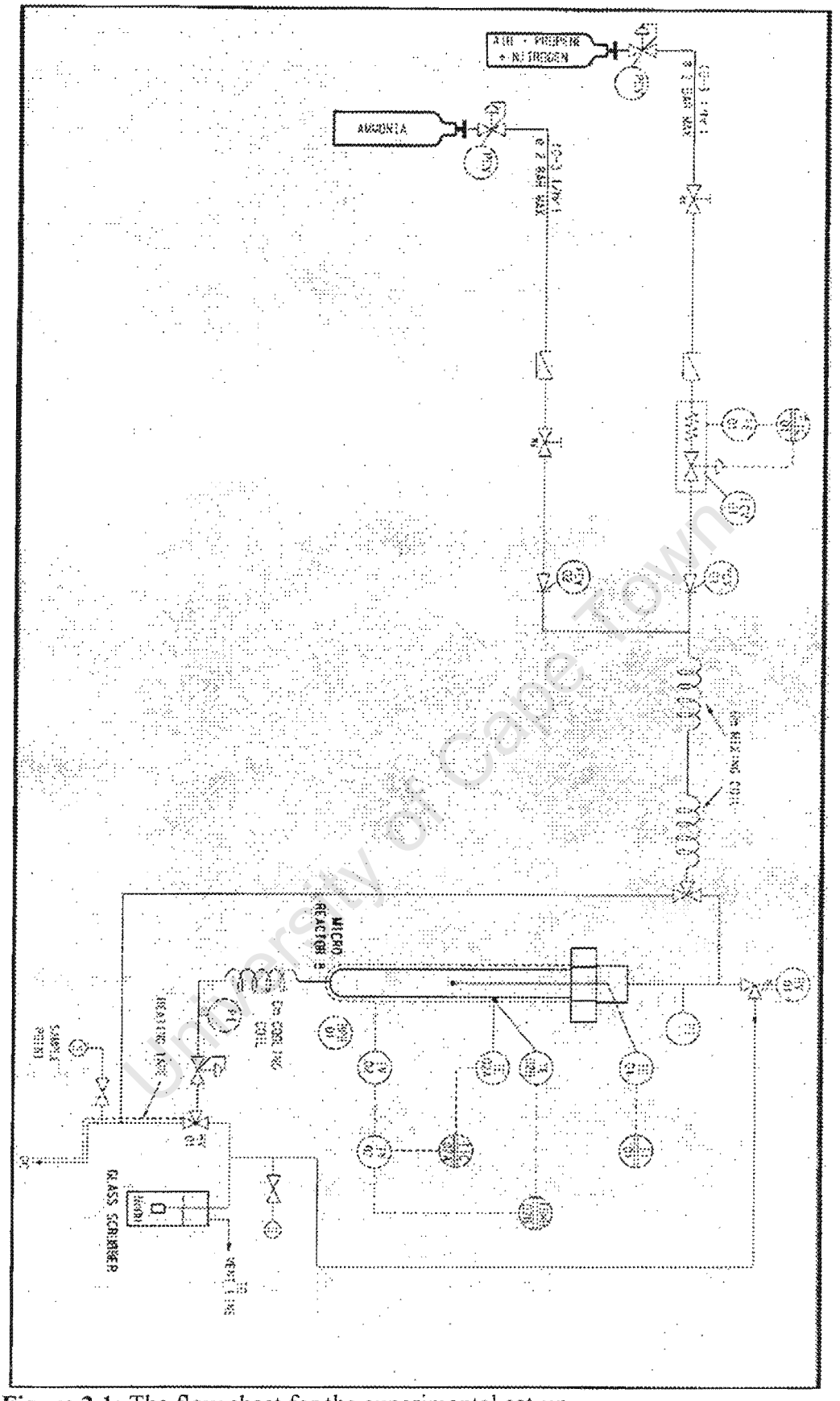

Figure 2.1: The flow sheet for the experimental set-up

Figure 2.2 shows schematically the reactor. The reactor is made out of stainless steel and has a length of 200 mm and a diameter of 13.5 mm. The catalyst bed is loaded in the isothermal zone of the reactor (see Figure 2.2); 1g of catalyst is diluted with 4g of 24-grit carborundum loaded to ensure isothermal operation.

The effluent passes a back-pressure regulator for maintaining a constant pressure of 1.9 bar. Ammonia was trapped in a 1M sulphuric acid scrubber. The product stream then passes a 2M NaOH base scrubber to neutralise poisonous HCN gas side product before it goes out to the vent. The reactor effluent can also be directed through a sample valve for GC analysis.

All the experiments were conducted using 1g of catalyst at 450°C and a total pressure of 1.9 bar. The flow rate of the gas mixture containing propene was kept constant at 22.5 ml/min (containing 1.7% propene, 2.03% oxygen, with balance nitrogen). The ammonia molar flow rate was varied between 0.1 and 23 ml/min.

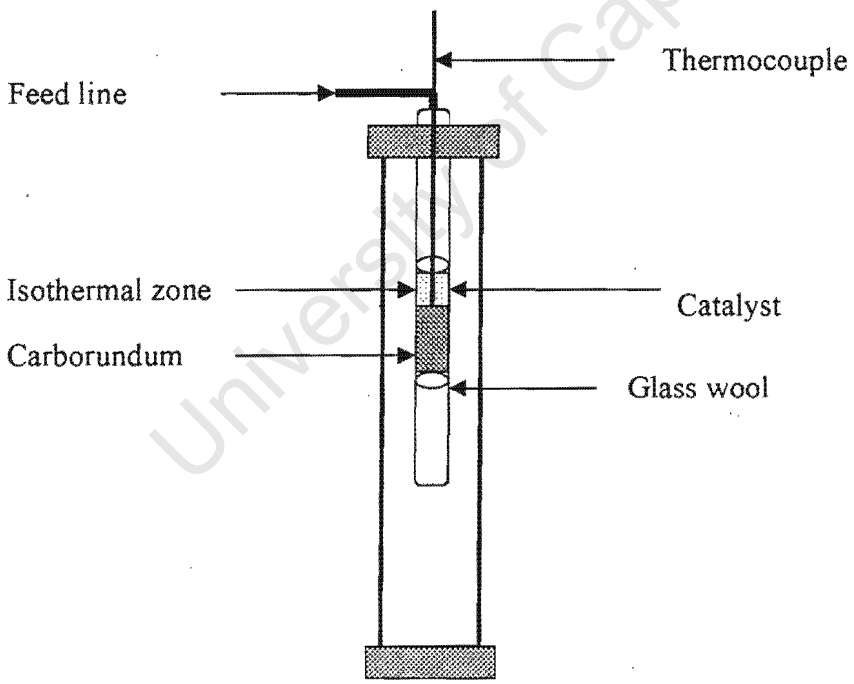

Figure 2.2: The schematic representation of the reactor

2.3.1 Product analysis

The products and unreacted feed materials all need to be analysed in order to determine a mass balance for the system.

2.3.1.1 Analysis of ammonia

To measure the amounts of ammonia going through the reactor, the feed stream was by-passed through 1M sulphuric acid to convert ammonia into ammonium sulphate in one minute. Unreacted ammonia was analysed by passing the product stream through 1M sulphuric acid. Unconverted sulphuric acid is back titrated with a standard solution of potassium hydroxide. The difference gives the reacted sulphuric acid, of which on stoichiometric relations the amount of ammonia reacted and unreacted could be determined.

$H_2SO_4 + (2NH_3)_i \rightarrow (NH_4)_2SO_4$

$H_2SO_4 + (2NH_3)_f \rightarrow (NH_4)_2SO_4$

The conversion of ammonia was determined as follows:

$$X_{NH3} = \frac{(NH_3)_i - (NH_3)_f}{(NH_3)_i},$$

where $(NH_3)_i$ and $(NH_3)_f$ is the amount of ammonia going in and out of reactor respectively.

2.3.1.2 Hydrocarbon analysis

The expected hydrocarbon products and feed materials to be analysed were propene, acrolein, acrylonitrile, acetonitrile, hydrogen cyanide and carbon-oxide gasses (CO/CO_2). The product stream is directed the GC which is monitored by a computer. The GC is equipped with two columns, the capillary column (30m CP Sil 24) and the packed column (0.6m Chromosorb WHP-SP). All product compounds pass the capillary column. Carbon monoxide and carbon dioxide are directed to the packed column. All other compounds are detected immediately after the capillary using a Flame ionisation detector (FID 2). Carbon monoxide and carbon dioxide, passed over

a methaniser, which convert CO and CO_2 to methane in order to be detected by the FID 1. The operating conditions of the GC are given in Table 2.1 and appendix 2B.

Table 2.1: Operating conditions of the GC

Operatioal parameters	Conditions
Carrier Gas (CG)	Nitrogen
Flow rate of CG	35 ml/min
Pressure of CG	50 kPa
Injection Temp,	200 °C
Heating rate	8 °C/min
Heating range	50 – 190 °C
Detector Temp, FID1	370 °C
Detector Temp, FID2	250 °C

The FID was calibrated for the various compounds (see Appendix 2B). Table 2.2 gives the obtained calibration factors. The method for determining the number of moles in a sample is then given by multiplying the obtained peak area with the calibration factor. This method required that the split ratio remains constant for all the analyses.

Table 2.2: Calibration factors for GC analysis

Compound	Calibration factor μmol/count
Propene	$3\ 10^7$
Acrylonitrile	$3\ 10^7$
Acrolein	$2\ 10^7$
Carbon monoxide	$2\ 10^8$
Carbon dioxide	$1\ 10^8$

2.3.2 Data evaluation

The peak areas for the various compounds will be converted to the corresponding mole amounts.

$$n_{compound} = Area_{compound} . f_{compound} ,$$

with $Area_{compound}$: peak area obtained for a compound

$f_{compound}$: calibration factor (see table 2.2)

$n_{compound}$: number of moles of compound in the sample

The conversion for propene was calculated as follows:

$$X_{C3H6} = 100(1-n_{out}/n_{in})$$

The yield of the various product compounds were determined as follows:

$$Y_i = 100(1-n_{i,out}/n_{C3H6,\,in})$$

Selectivity expressed as the ratio of the yield to the conversion.

The acrylonitrile content is the fraction of selectivity to acrylonitrile in the partial oxidation products, acrylonitrile plus acrolein:

$$\text{Acrylonitrile content} = Y_{ACN}/(Y_{ACN}+Y_{ACO})*100$$

3 Results

The following catalysts were prepared and characterised: bismuth molybdate, iron molybdate, iron bismuth molybdate (Bi:Fe=3:1) and iron bismuth molybdate (Bi:Fe=1:1). The intention was to study the behaviour of iron promoted bismuth molybdate catalysts in the ammoxidation of propene.

3.1 Catalyst preparation and characterisation

The catalyst samples were prepared as described in chapter 2 and after calcination characterised.

3.1.1 Bismuth molybdate

3.1.1.1 Elemental analysis

The elements, bismuth and molybdenum, in the calcined catalyst sample were analysed using AAS-ICP. For this method the sample has to be digested. Two different methods for digestion were used (see Section 2.2.1), viz. the dissolution using a mixture of $HCl/HF/HNO_3$ (method 1) and the dissolution of the ashed sample (using $LiBO_2$) in HCl (method 2). Table 3.1 summarizes the results of the AAS-ICP using both methods. Included in the table is the amount of oxygen in the sample as obtained by the difference of the total mass and the mass attributable to the amount of bismuth and molybdenum.

Table 3.1: Weight and molar fraction of the elements present in bismuth molybdate as determined by two different digestion methods (see Section 2.2.1) using AAS-ICP (oxygen calculated by difference).

	Method 1		Method 2	
Element	**wt.-%**	**mol-%**	**wt.-%**	**mol-%**
Bismuth	42.7	10.3	37.2	10.3
Molybdenum	34.8	18.4	33.5	20.2
Oxygen	22.5	71.3	19.2	69.5

Both analyses seem to give approximately the same results. However, the bismuth content using method 1 seems to be slightly higher. Both analyses indicate that the molybdenum to bismuth ratio is higher than the expected ratio of 1.5 (method 1 yielded a result of 1.8 and method 2 yielded 2.0). If it can be assumed that α-$Bi_2Mo_3O_{12}$ is a component in the sample (see chapter 3.1.2), the elemental analysis indicate an excess of molybdenum oxide in the sample. According to the analysis by method 1 the excess molybdenum is in the form of $Mo_{0.3}O$ and according to method 2 it is in the form of $Mo_{0.5}O$. Based on the difference analyses, method 1 seems to be more accurate, since the oxidation state of Mo is expected to be 6+. The elemental analysis seems to indicate, that if the sample contains α-$Bi_2Mo_3O_{12}$, it also contains MoO_3. The ratio of MoO_3 to α-$Bi_2Mo_3O_{12}$ is then equal to 1:3 on a molar basis.

3.1.1.2 Structural characterisation of catalysts

The structural features of the bismuth molybdate were characterised using X-ray diffraction and infra-red spectroscopy.

3.1.1.2.1 X-ray diffraction

Figure 3.1 shows the X-ray diffraction pattern obtained with bismuth molybdate. The XRD-spectrum shows a crystalline material, the bismuth molybdate (α-phase) and an amorphous material, possibly molybdenum oxide. In Table 3.2 the observed d-spacing is compared with those of α-$Bi_2Mo_3O_{12}$ (as reported by Batist et al., 1972), and those of MoO_3 (as reported by Kahmer et al., 1997).

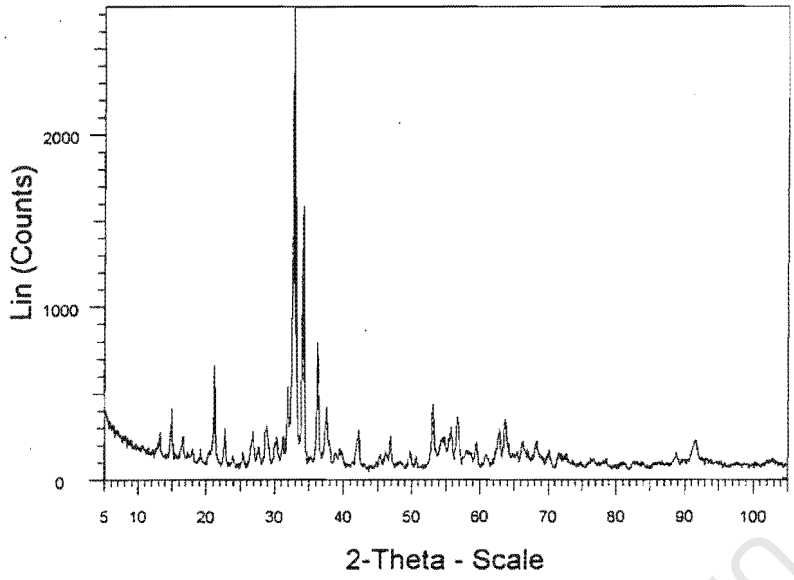

Figure 3.1: XRD diffraction spectrum of bismuth molybdate

Table 3.2: Characteristic lines of α-$Bi_2Mo_3O_{12}$, and MoO_3 (Batist et al., 1972; Kahmer et al., 1997) compared with XRD-bands obtained with the prepared bismuth molybdate catalyst

Literature d, (A°)	Exp d, (A°)	Exp(I/I_o)
6.90	6.965	14.8
4.89	4.891	20.4
3.57*	3.597	9.4
3.26*	3.261	18.6
3.18	3.184	100.00
3.05*	3.053	63.3
3.81•	3.801	5.4
2.88	2.877	30.5
2.79	2.789	13.4
2.004	2.003	13.4
1.915	1.915	10
1.690*	1.694	10.31

*d-spacing: For both α-$Bi_2Mo_3O_{12}$ and MoO_3; •d-spacing for MoO_3

Based on the characteristics lines, it is indicated that both α-$Bi_2Mo_3O_{12}$ and MoO_3 are present in the prepared bismuth molybdate. The appearance of MoO_3 is also indicated from the AAS-ICP results.

3.1.1.2.2 Infrared spectroscopy

The observed infrared spectrum for bismuth molybdate catalyst is shown in figure 3.2. The characteristic Mo-O stretching vibrations can be seen in the region 950-700 cm^{-1} of the infrared spectrum of the bismuth molybdate (α-phase) and Bi-O stretching vibration and deformation in the 600- 400 cm^{-1} region (Carson et al., 1983). The characteristic infrared bands of bismuth molybdate (α-phase) appear at 950 cm^{-1}, 935 cm^{-1} and 900 cm^{-1} (Trifiró et al., 1972). At higher molybdenum concentration, the 725 $cm^{-1}$and 850 cm^{-1} band are broader and there is more absorption and/ or bands above 900 cm^{-1} (Mitchell, et al., 1970; Grzybows, 1992)

The bismuth molybdate (β-phase) is characterised by the broad featureless peak in the region of 800 cm^{-1} (Carson et al., 1983) with some others at 890 cm^{-1} (sharp), 800cm^{-1} (broad), 470 cm^{-1}, 440 cm^{-1} and 350 cm^{-1}.

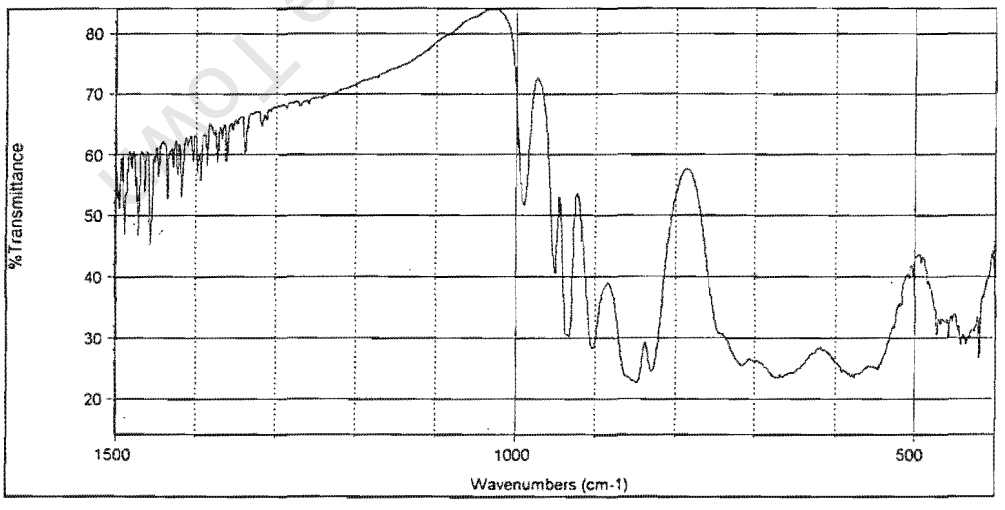

Figure 3.2: Infrared spectra of prepared bismuth molybdate catalyst.

Figure 3.2 spectrum shows Mo-O stretching vibration bands at 861 cm^{-1} (broad) and some characteristic bands at 902 cm^{-1}, 935 cm^{-1} and 950 cm^{-1}. These bands give an indication that the bismuth molybdate (α-phase) is formed. It is difficult to assign the band appeared at 471 cm^{-1} and 457 cm^{-1} since that particular region can characterise all bismuth molybdate phases.

3.1.1.3 Morphological appearance

The morphology of the catalyst is determined by using the scanning electron microscopy as well as surface area measurements.

3.1.1.3.1 Scanning Electron Microscopy (SEM)

Figure 3.3 shows the Scanning electron microgram picture of prepared bismuth molybdate catalyst. The bismuth molybdate crystals seem to be needle shaped. There are some islets of amorphous material on the matrix of the bigger particles. These small materials could possibly be molybdenum oxide as indicated by ICP-AAS and XRD (see Section 3.1.1.1 and 3.1.1.2).

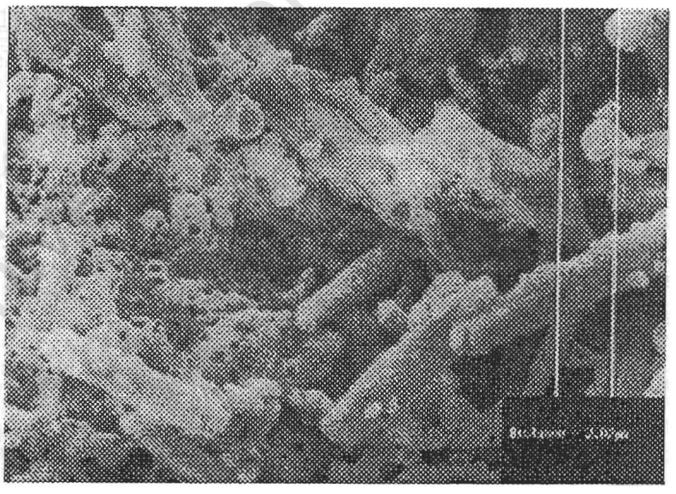

Figure 3.3: Scanning Electron Micrograms of prepared bismuth molybdate catalyst

3.1.1.3.2 Surface area and pore volume measurements

The surface area of the catalyst was found to be 1.9 m^2/g, which correspond to literature value of 1.9 m^2/g for α-$Bi_2Mo_3O_{12}$ (Carson et al., 1983). The pore volume of the catalyst is found to be 0.0095 cm^3/g.

3.1.1.4 Particle size distribution (PSD)

Figure 3.4 shows the distribution of particle sizes in the total catalyst matrix. There are two distinct particle distribution regions, 5- 12 μm and the other fraction is between 20- 100 μm. A fraction of the particles are between 2 μm and 20 μm diameter.

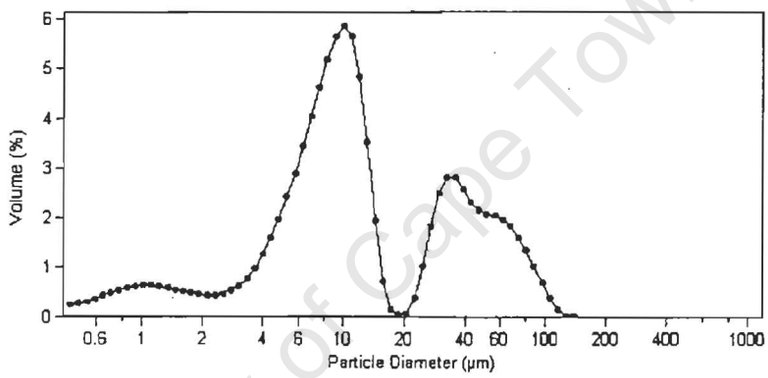

Figure 3.4: Particle size distribution of prepared bismuth molybdate catalyst.

3.1.1.5 Temperature-programmed reduction (TPR)

Figure 3.5 shows the temperature-programmed reduction of prepared bismuth molybdate catalyst and pure oxides of MoO_3 and Bi_2O_3, which are all calcined at 450 °C. The TPR showed three regions that are reduced at different temperatures, 577 °C, 660 °C and a shoulder at 713 °C. The first peak at 577 °C indicates the reduction of Bi^{3+} to Bi. The reduction is comparable to the reduction of pure oxide of Bi_2O_3 at 447 °C. The difference in reduction temperatures of Bi^{3+} in Bi_2O_3 and $Bi_2Mo_3O_{12}$ is due to the interaction of bismuth and molybdenum. The second and the third reductions peaks matches Mo^{5+} to Mo^{4+} to Mo according to comparison with the reduction of pure MoO_3 as shown in figure 3.5.

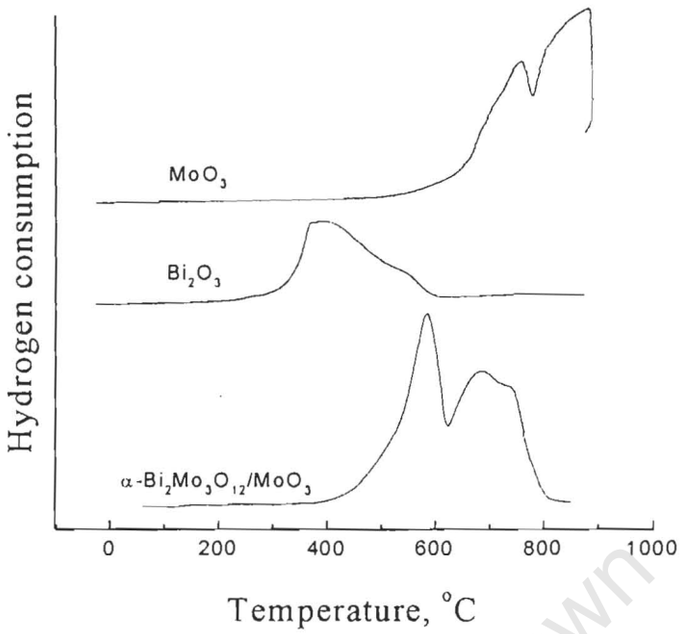

Figure 3.5: Temperature Programmed-reduction profile of prepared bismuth molybdate catalyst, bismuth oxide and molybdenum(VI) oxide.

3.1.2 Iron molybdate

3.1.2.1 Elemental analysis using AAS-ICP

The elements, iron and molybdenum, in the calcined catalyst sample were analysed using AAS-ICP. The digestion method prior for analysis is method 1, i.e. the dissolution using a mixture of HCl/HF/HNO_3 (see Section 2.2.1). Table 3.3 indicates the results of the AAS-ICP using this digestion method. Included in the table is the amount of oxygen in the sample as obtained by the difference of the total mass and the mass attributable to the amount of bismuth and molybdenum.

Table 3.3: Weight and molar fraction of the elements present in iron molybdate using AAS-ICP (oxygen calculated by difference).

Element	wt.-%	mol-%
Iron	15.6	8.4
Molybdenum	42.9	13.5
Oxygen	41.5	78.1

The expected molybdenum to bismuth ration is 1.5. The ratio is slightly higher as the analysis yielded 1.6 is found for these results. These indicate that the catalyst have slight excess of molybdenum oxide. The iron molybdate is therefore not expected to be the only phase. According to this analysis the excess molybdenum is in the form of $Mo_{0.1}O$. The elemental analysis seems to indicate that if the sample contains iron molybdate, it also contains molybdenum oxide.

3.1.2.2 Characterisation of structural features in materials

The structural features of the bismuth molybdate were characterised using X-ray diffraction, infrared spectroscopy and Mössbauer spectroscopy.

3.1.2.2.1 Crystallographic characterisation using XRD

Figure 3.6 shows XRD spectra of iron molybdate. A crystalline material as well as an amorphous material is observable from the spectra. The crystalline one is iron molybdate (Fe:Mo=2:3) and the amorphous material is MoO_3, as also indicated by AAS-ICP analysis.

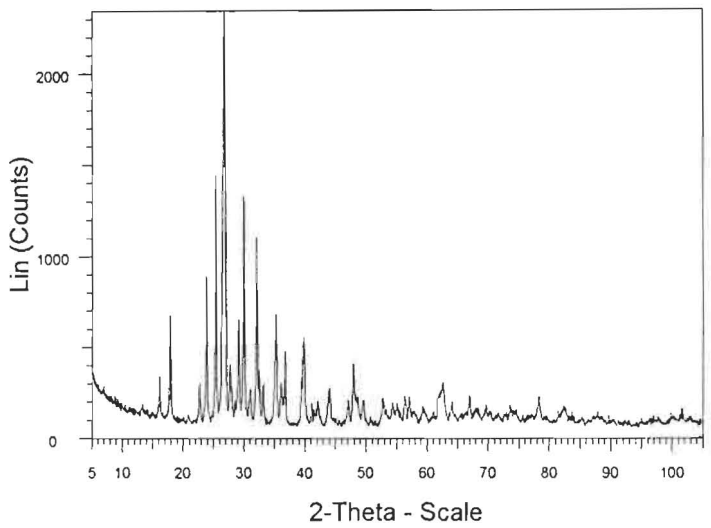

Figure 3.6: XRD diffraction spectrum of prepared iron molybdate catalyst.

Table 3.4: Characteristic lines of $Fe_2Mo_3O_{12}$ (Kahmer et al., 1997) compared with XRD-bands obtained with the prepared iron molybdate catalyst

Literature d, (A^o)	Exp d, (A^o)	Exp(I/I_o)
5.65	5.794	28.7
4.08	4.09	61.6
3.92	3.924	61.3
3.88	3.876	100
3.79	3.744	17.1
3.56	3.568	27.7
3.5	3.465	56.7
3.37	3.35	11.3
3.24	3.242	47
2.57	2.632	23.7
2.39	2.392	11.6

3.1.2.2.2 Infrared adsorption spectroscopy

Figure 3.7 shows an infrared spectrum of the prepared iron molybdate catalyst. The sharp-broad peak at 842 cm^{-1} indicates the Mo-O stretching vibration of the catalyst (Trifiró et al., 1972).

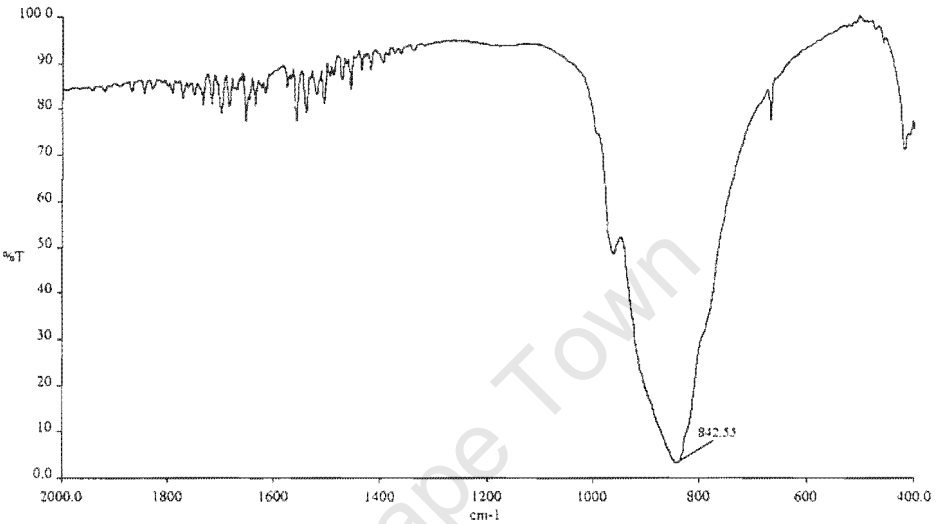

Figur 3.7: Infrared spectra of prepared iron molybdate catalyst.

3.1.2.2.3 Mössbauer-spectroscopy

Table 3.5 shows the hyperfine interaction parameters for the prepared iron molybdate catalyst. The Mössbauer spectra are given in appendix 3C. The Mössbauer data of iron molybdate indicate that iron in this catalyst is present as high spin Fe^{3+}. The Mössbauer spectra for this sample indicate that the iron in this catalyst is in same environment, as indicated by the appearance of two quadruple doublets with similar isomeric shift values (IS). If iron molybdate (Fe:Mo=2:3) is a component in this catalyst, it could hence be deduced that it is the only iron containing phase. The difference in quadruple splitting values (QS) for the doublets is an indication that this catalyst have both ordered and disordered phase (Jeitschko et al., 1976).

Table 3.5: Hyperfine interaction parameters for prepared iron molybdate catalyst

IS $(mms^{-1})_{Fe}$	QS (mms^{-1})	RA Intensity	Phase % Fe
0.40	0.67	24.7	Fe^{3+}
0.40	0.19	75.3	Fe^{3+}

3.1.2.3 Morphological appearance

The morphology of the catalyst is determined by using the scanning electron microscopy as well as surface area measurements.

3.1.2.3.1 Scanning Electron Microscopy (SEM)

Figure 3.8 shows a SEM picture of calcined, prepared iron molybdate catalyst. An amorphous material is observable from the picture. The crystals seem to be of irregular shape.

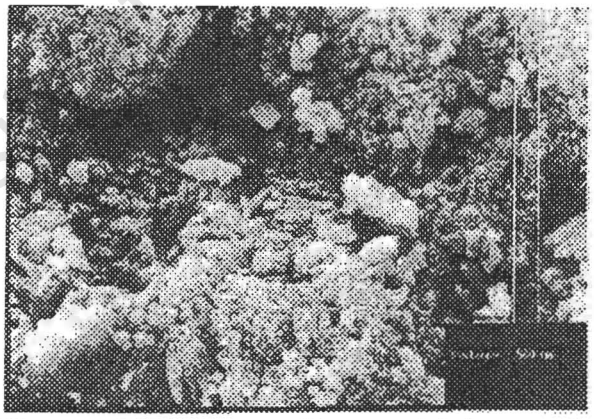

Figure 3.8: Scanning Electron Micrograms of iron molybdate catalyst.

3.1.2.3.2 Surface area and pore volume measurements

The surface area of prepared iron molybdate catalyst from BET measurements is found to be 8.6 m^2/g. The pore volume of the catalyst is found to be 0.042 cm^3/g.

3.1.2.4 Particle size distribution (PSD)

Figure 3.9 shows the particle size distribution of calcined, prepared iron molybdate catalyst. The particles show a skewed distribution around 100 μm in diameter.

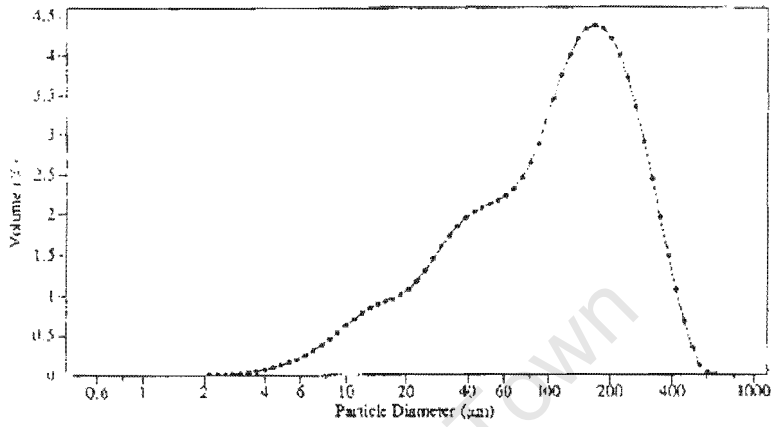

Figure 3.9: Particle size distribution of prepared iron molybdate catalyst

3.1.2.5 Temperature programmed reduction (TPR)

Figure 3.10 shows the temperature-programmed reduction of prepared iron molybdate catalyst, Fe_2O_3 and MoO_3. There are three distinct reduction regions for iron molybdate at 485 °C (shoulder) and 635 °C (sharp) and 800 °C (broad). The first reduction peaks at 485 °C corresponds with the partial reduction of Fe^{3+} to $Fe^{3/2+}$ ($Fe_2O_3 \rightarrow Fe_3O_4$). The second one at 635 °C should correspond with the reduction of $Fe^{3/2+}$ to Fe^{2+} ($Fe_3O_4 \rightarrow FeO$). Complete reduction of iron is at 800 °C, which overlaps with the reduction of Mo^{6+} to Mo^{5+} to Mo according to the comparison with pure oxide of Fe_2O_3 and MoO_3 as shown in the figure.

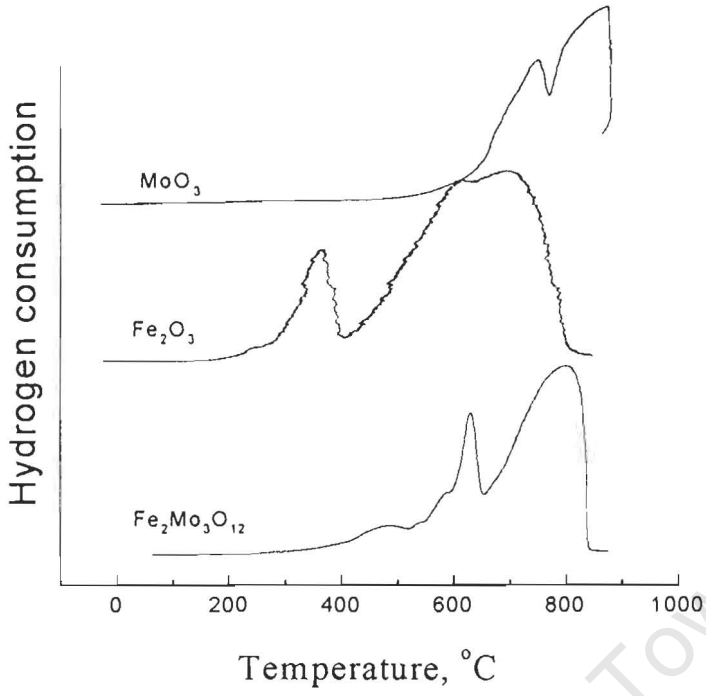

Figure 3.10: Temperature Programmed-reduction profile of prepared iron molybdate catalyst, iron(III) oxide, and molybdenum(VI) oxide.

3.1.3 Iron bismuth molybdate (Bi:Fe= 3:1)

3.1.3.1 Elemental analysis using AAS-ICP

The elements, bismuth, iron and molybdenum, in the calcined catalyst sample were analysed using AAS-ICP. The digestion method for this catalyst prior for analysis is method 2, as described in section 2.2.1. Table 3.6 summarizes the results of the AAS-ICP. Included in the table is the amount of oxygen in the sample as obtained by the difference of the total mass and the mass attributable to the amount of bismuth, iron and molybdenum.

Table 3.6: Weight and molar fraction of the elements present in iron bismuth molybdate (Bi:Fe=3:1) using AAS-ICP (oxygen calculated by difference).

Element	wt.-%	mol-%
Bismuth	40.2	10.9
Iron	3.6	3.7
Molybdenum	38.5	22.7
Oxygen	17.7	62.7

The results indicate that the ratio of bismuth to iron is 3:1 as expected. No excess molybdenum was observed. This results correlate with the fact that since the starting material for the preparation of this catalyst is bismuth molybdate (α-phase), and it was found that it contains $1/3MoO_3$. It is therefore not surprising to find that this catalyst contains bismuth molybdate (α-phase) and iron molybdate, which is yielded by the reaction of iron oxide and molybdenum oxide.

3.1.3.1 Characterisation of structural features in materials

The structural features of the iron molybdate were characterised using X-ray diffraction, infrared spectroscopy and Mössbauer spectroscopy.

3.1.3.1.1 Crystallographic characterisation using XRD

Figure 3.11 shows the XRD spectrum of iron bismuth molybdate (Bi:Fe=3). Two crystallites are observable, the α-bismuth molybdate and iron molybdate. The appearances of two phases in one catalyst matrix are evidenced by characteristic line as tabulated in table 3.7. The more intense line at d-spacing = 3.183 is a characteristic line for bismuth molybdate (α-phase), while the one at d-spacind = 3.88 is the most characteristic line for iron molybdate. The difference in intensity for the lines does not necessarily quantify the amount of the phases present.

Table 3.7: Characteristic lines of iron bismuth molybdate (Bi:Fe=3) (Batist et al., 1972; Kahmer et al., 1997) compared with XRD-bands obtained with the prepared bismuth molybdate catalyst

Literature d, (A^o)	Exp d, (A^o)	Exp(I/I_o)
6.9	6.95	14.9
4.89	4.895	23.8
4.08	4.084	5.8
3.92	3.917	7
3.88	3.867	9.9
3.79	3.747	6.7
3.57	3.601	11.3
3.5	3.455	7.7
3.26	3.26	19.4
3.18	3.185	100
3.05	3.056	57.9
2.88	2.88	28.7

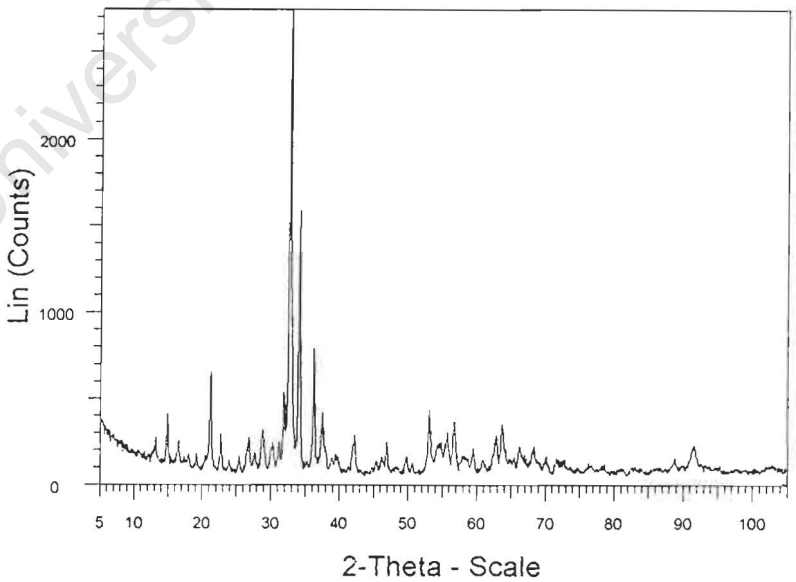

Figure 3.11: XRD diffraction spectrum of prepared iron bismuth molybdate (Bi:Fe=3)

3.1.3.1.2 Infra-red adsorption spectroscopy

Figure 3.12 shows the IR spectra of iron bismuth molybdate (Bi:Fe=3). The features of iron molybdate and bismuth molybdate (α-phase) are highly observable from this spectrum. The characteristic infrared band of bismuth molybdate (α-phase) appears at 830 cm^{-1}, which by the nature of its broadness also characterise iron molybdate (Mitchell et al., 1970; Grzybows, 1992). This spectrum seems to be mixing features of bismuth molybdate (α-phase) and iron molybdate.

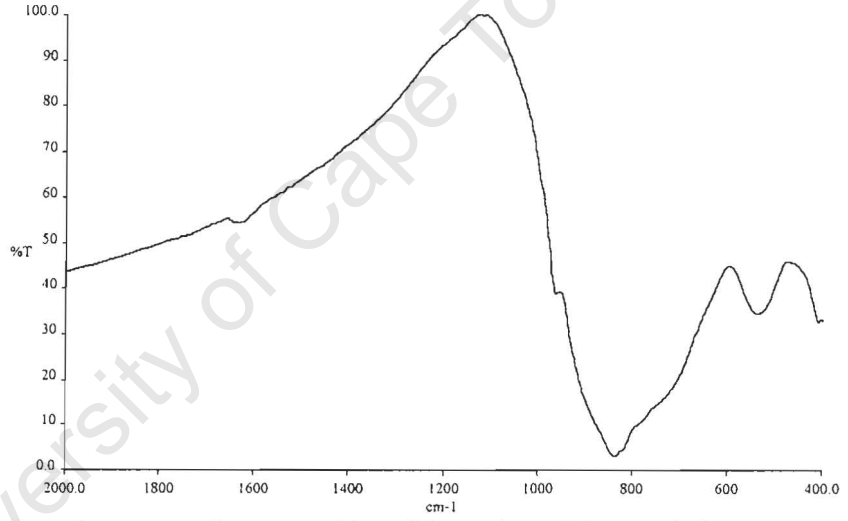

Figure 3.12: Infrared spectra of prepared iron bismuth molybdate (Bi:Fe=3)

3.1.3.1.3 Mössbauer-spectroscopy

Table 3.8 shows the hyperfine interaction parameters for the prepared iron bismuth molybdate catalyst. The Mössbauer spectra are given in appendix 3C. The Mössbauer data of iron bismuth molybdate (Bi:Fe=3) catalyst indicate that iron in these catalyst is present as high spin Fe^{3+}. The Mössbauer spectra for this sample indicate that the iron in this catalyst is in same environment. Similarly to iron molybdate (Fe:Mo=2:3) described in section 3.1.2.2.3. This is shown by the appearance of two quadruple doublets with similar isomeric shift values (IS) (see Table 3.8). If iron molybdate

(Fe:Mo=2:3) is a component in this catalyst, it could hence be deduced that it is the only iron containing phase. The difference in quadruple splitting values (QS) for the doublets is an indication that this catalyst have both ordered and disordered phase (Jeitschko et al., 1976).

Table 3.8: Hyperfine interaction parameters for the prepared iron bismuth molybdate (Bi:Fe=3)

IS $(mms^{-1})_{Fe}$	QS (mms^{-1})	RA Intensity	Phase % Fe
0.40	0.70	32.3	Fe^{3+}
0.40	0.18	67.7	Fe^{3+}

3.1.3.2 Morphological appearance

The morphology of the catalyst is determined by using the scanning electron microscopy as well as surface area measurements.

3.1.3.2.1 Scanning Electron Microscopy (SEM)

The Scanning Electron Microscopy (SEM) of the prepared iron bismuth molybdate (Bi:Fe=3) is shown by figure 3.13. Small roud-like crystalites are observed, revealing also some islets of irregular particles over the surface of the catalyst. This observation may indicate that there are two phases making up the iron bismuth molybdate catalyst as also indicated by XRD analysis.

Figure 3.13: Scanning Electron Micrograms of iron bismuth molybdate (Bi:Fe=3) catalyst.

3.1.3.2.2 Surface area and pore volume measurements

The surface area measurement by BET resulted in total surface area of 2.4 m^2/g. This surface area is a contribution from two-phased, bismuth molybdate plus iron molybdate catalyst as observed by XRD. The pore volume of the catalyst was found to be 0.012 cm^3/g.

3.1.3.3 Temperature-Programmed Reduction (TPR)

Figure 3.14 shows the Temperature-Programmed reduction of iron bismuth molybdate (Bi:Fe=3), Fe_2O_3, Bi_2O_3 and molybdenum oxide. The reducibility of this catalyst shifted slightly higher as compared to pure bismuth molybdate (α-phase). The presence of iron molybdate makes this catalyst to be in highly oxidising atmosphere. The reduction peak at 595 °C for iron bismuth molybdate (Bi:Fe=3) indicates the reduction of Bi^{3+} overlapping with the reduction of Fe^{3+}. The second broad peak at 750 °C is the complete reduction of iron overlapping with the reduction of molybdenum(VI).

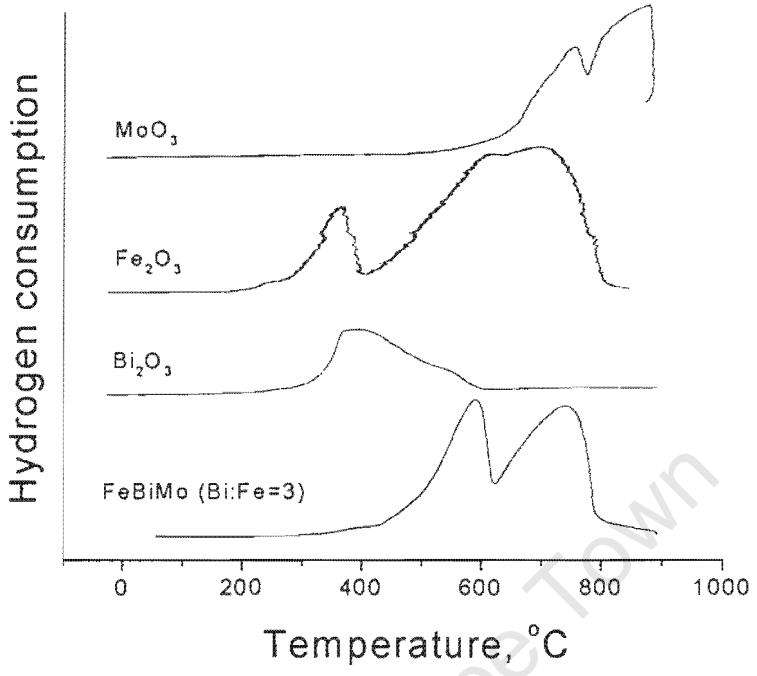

Figure 3.14: Temperature Programmed-reduction profile of prepared iron bismuth molybdate (Bi:Fe=3) catalyst, iron(III) oxide, bismuth oxide and molybdenum(VI) oxide.

3.1.4 Iron bismuth molybdate (Bi:Fe= 1:1)

3.1.4.1 Elemental analysis using AAS-ICP

The elements, bismuth, iron and molybdenum, in the calcined catalyst sample were analysed using AAS-ICP. For this method the sample has to be digested. The digestion method is as described in section 2.2.1 (method 1), viz. the dissolution using a mixture of HCl/HF/HNO_3 (method 1). Table 3.9 summarizes the results of the AAS-ICP using method x. Included in the table is the amount of oxygen in the sample as obtained by the difference of the total mass and the mass attributable to the amount of bismuth and molybdenum.

Table 3.9: Weight and molar fraction of the elements present in iron bismuth molybdate (Bi:Fe=1:1) using AAS-ICP (oxygen calculated by difference).

Element	wt.-%	mol-%
Bismuth	43.1	12
Iron	10.3	10.7
Molybdenum	30.4	18.4
Oxygen	16.2	58.9

The expected bismuth to iron ration is 1. The results for this analysis yielded bismuth to iron ration equal to 1.1. This analysis showed a slight excess of bismuth.

3.1.4.2 Characterisation of structural features in materials

The structural features of the bismuth molybdate were characterised using X-ray diffraction, infrared spectroscopy and Mössbauer spectroscopy.

3.1.4.3.1 Crystallographic characterisation using XRD

Figure 3.15 shows the X-ray diffraction pattern obtained for iron bismuth molybdate (Bi:Fe=1). In Table 3.10 the observed d-spacing is compared with those of $Bi_3FeMo_2O_{12}$ (as reported by Sleight et al., 1974), and those of $Fe_2Mo_3O_{12}$ (Kahmer et al., 1997).

Table 3.10: Observed d-spacing of prepared iron bismuth molybdate (Bi:Fe=1) is compared with those of $Bi_3FeMo_2O_{12}$ (Sleight et al., 1974), and those of $Fe_2Mo_3O_{12}$ (Kahmer et al., 1997).

Literature d, (A^o)	Exp d, (A^o)	Exp(I/I_o)
9.47	9.54	8.6
4.79	4.83	12.7
4.09	4.088	12.7
3.87	3.88	21.8
3.5	3.46	13.8
3.15	3.157	100
2.91	2.907	15.5
2.33	2.328	6.7

The experimental d-spacing corresponds with the one from literature. The XRD spectrum shows that there are two crystallites making up this catalyst. Both $Bi_3FeMo_2O_{12}$ and $Fe_2Mo_3O_{12}$ were detected.

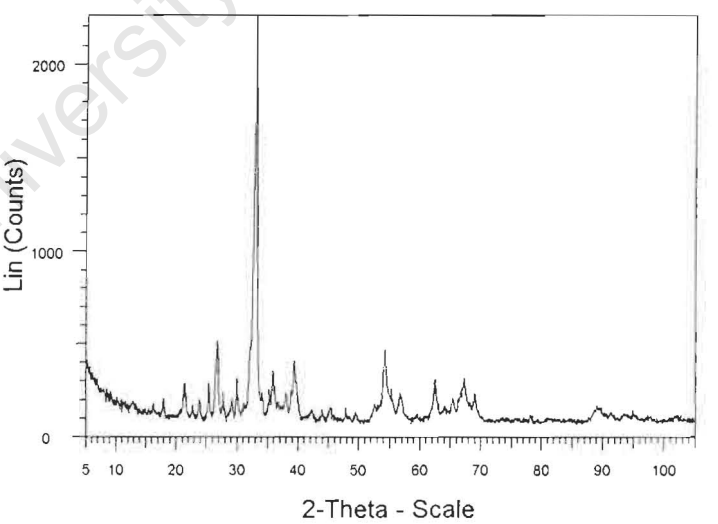

Figure 3.15: XRD diffraction spectrum of prepared iron bismuth molybdate (Bi:Fe=1)

3.1.4.3.2 Infrared adsorption spectroscopy

Figure 3.16 shows an infrared spectrum of prepared iron bismuth molybdate (Bi:Fe=1)

This spectrum is similar to the spectrum of an ordered phase $Bi_3(FeO_4)(MoO_4)_2$ (Jeitschko et al., 1976). According to this author, all MoO_4 groups should be equivalent in an ordered structure of $Bi_3(FeO_4)(MoO_4)_2$. At short range figure 3.16 shows some broadening behaviour. This could imply either the presence of the trace amount of disordered $Bi_3(FeO_4)(MoO_4)_2$ or characterising Mo-O vibration in iron molybdate as a co-phase.

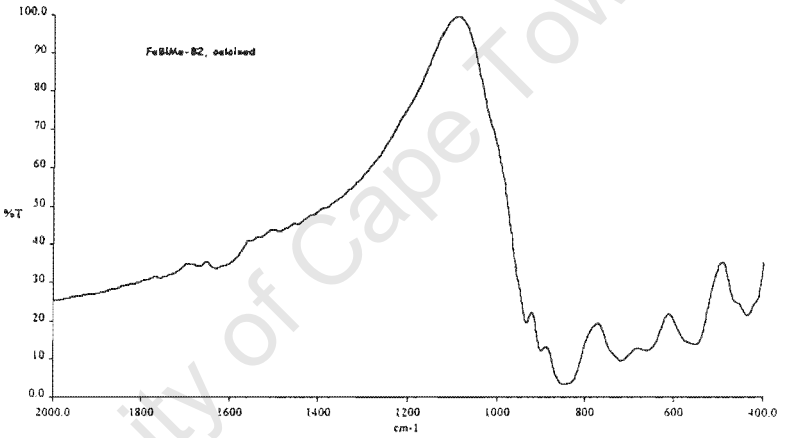

Figure 3.16: Infrared spectra of iron bismuth molybdate (Bi:Fe=1)

3.1.4.3.3 Mössbauer-spectroscopy

Table 3.11 shows the hyperfine interaction parameters for the prepared iron bismuth molybdate catalyst. The Mössbauer spectra are given in appendix 3C. The Mössbauer data for iron bismuth molybdate (Bi:Fe=1) indicates that the catalyst contains iron as high spin Fe^{3+}. The Mössbauer results for this catalyst indicates that there are two kinds of iron. This is shown by the appearance of two quadruple doublets with different isomeric shift values. It could hence be deduced that this catalyst as characterised by XRD is composed of iron containing phased ($Fe_2(MoO_4)_3$) and $Bi_3(FeO_4)(MoO_4)_2$ with iron in different environment. The hyperfine parameters obtained from the Mössbauer analyses of the samples are summarised in Table 3.11.

Table 3.11: Hyperfine interaction parameters for iron bismuth molybdate (Bi:Fe=1)

IS $(mms^{-1})_{Fe}$	QS (mms^{-1})	RA Intensity (% Fe)	Phase
0.35	0.89	41	Fe^{3+}
0.46	0.22	59	Fe^{3+}

The difference in quadruple splitting values for the doublets is an indication of the presence of markedly different local environments of the Fe^{3+} atoms, i.e., large quadruple reflects a departure from cubic symmetry (Jeitschko et al., 1976). For $Bi_3FeMo_2O_{12}$ and $Fe_2(MoO_4)_3$ this indicates that the iron phase has both an ordered and disordered structure, whereas the different isomer shift values observed with this catalyst are indicative of different Fe-O distances as would be expected for different phases.

3.1.4.3 Morphological appearance

The morphology of the catalyst is determined by using the scanning electron microscopy as well as surface area measurements.

3.1.4.3.1 Scanning Electron Microscopy (SEM)

Figure 3.17 shows a Scanning Electron Microscopy picture of prepared iron bismuth molybdate (Bi:Fe=1). Some round shaped crystalline material is observable together with the amorphous material.

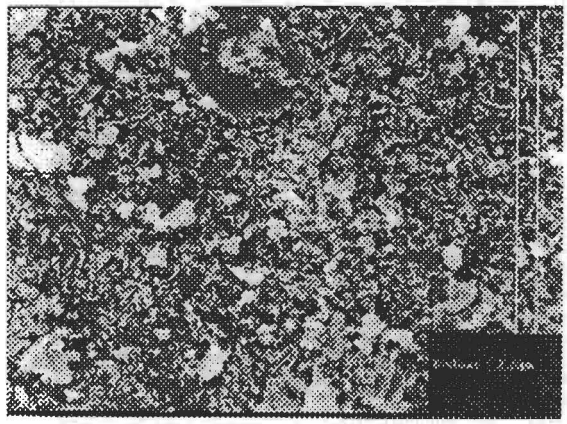

Figure 3.17: Scanning Electron Micrograms of iron bismuth molybdate (Bi:Fe=1) catalyst.

3.1.4.3.2 Surface area and pore volume measurements

The surface area of iron bismuth molybdenum (Bi:Fe=1) was found to be 4.7 m^2/g. This surface area is a contribution of two faces, $Bi_3FeMo_2O_{12}$ and $Fe_2(MoO_4)_3$. The smaller particles, probably $Fe_2(MoO_4)_3$ contributed highly to the total surface area. The pore volume of the catalyst is 0.037 cm^3/g.

3.1.4.4 Temperature programmed reduction (TPR)

Figure 3.18 shows the temperature-programmed reduction of iron bismuth molybdate (Bi:Fe=1), Fe_2O_3, Bi_2O_3 and MoO_3. There are four reduction peaks observable for iron bismuth molybdate (Bi:Fe=1). The first one appears as a shoulder at 400 °C, which matches exactly the reduction of Bi^{3+} according to comparison with pure oxides. The second reduction peak at 540 °C corresponds with partial reduction of Fe^{3+} ($Fe_2O_3 \rightarrow Fe_3O_4$). At 570 °C is the reduction of Fe_3O_4 to Fe_2O_3. The complete reduction of iron overlaps with the reduction of Mo^{6+} at 715 °C.

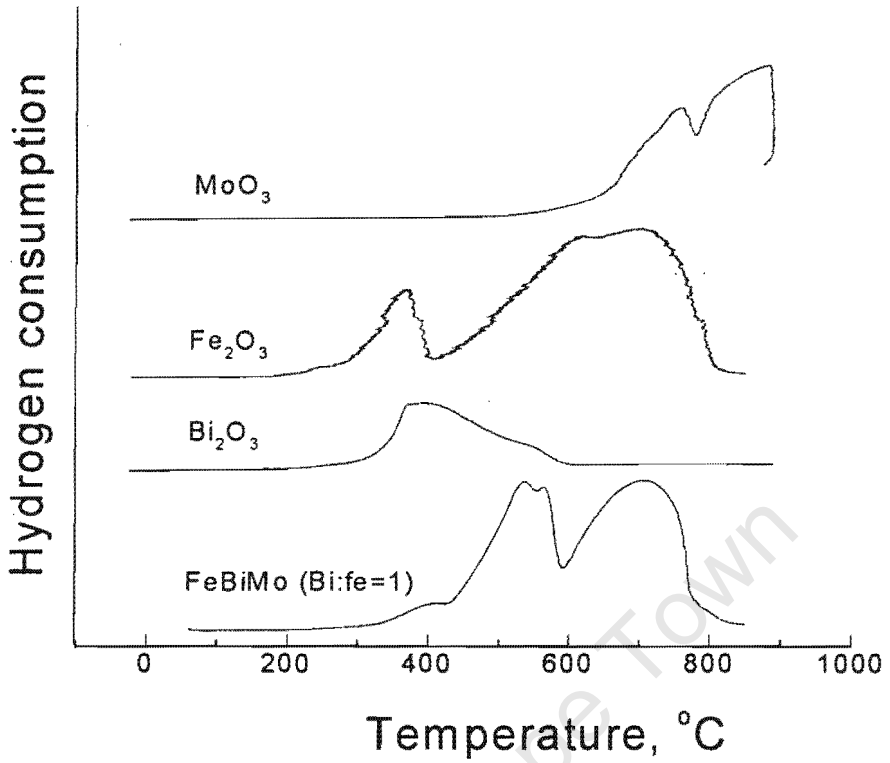

Figure 3.18: Temperature Programmed-reduction profile of iron bismuth molybdate (Bi:Fe=1) catalyst, iron(III) oxide, bismuth oxide and molybdenum(VI) oxide.

3.2 Reaction studies over bismuth molybdate, iron molybdate and iron promoted bismuth molybdate catalysts

Four of the catalysts of which their characterisation results were reported in the previous section were tested. The results for their catalytic performance were obtained and recorded in appendix 2C. The key variable during the testing was ammonia molar flow rate with molar flow rate for both propene and oxygen being kept constant. Upon changing the molar flow rate of ammonia, the resistance time decreases, the partial pressure of ammonia increases and propene and oxygen decreases. The conversions for propene and ammonia were kept low in order to suppress the formation of by-products. The main products formed for all tested catalysts were acrylonitrile, acrolein, carbon dioxide and carbon monoxide.

3.2.1 α-Bismuth molybdate

Figure 3.19 shows the conversion of propene as a function of molar flow rate of ammonia. The conversion decreases with an increase in the molar flow rate of ammonia. The decreasing trend in conversion could be due to an increase in the space velocity as the partial pressure of ammonia is increased and hence decreasing contact time of propene and the catalyst. Figure 3.20 shows the conversion of ammonia as a function of molar flow rate of ammonia. The conversion of ammonia passes through the maximum with increasing molar flow rate of ammonia. The decrease in conversion of ammonia from maximum point could be due the oxidation of ammonia at the catalyst surface. The selectivity for the formation of partial oxidation products and hence for combustion products was affected by the increase in the molar flow rate of ammonia.

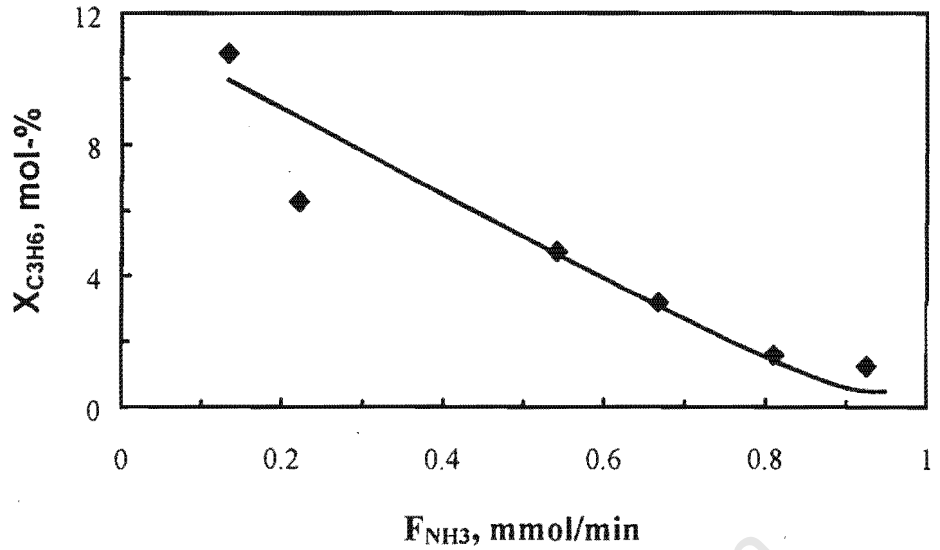

Figure 3.19 Propene conversion over α-bismuth molybdate as a function of ammonia molar flow rate (F_{C3H6} = 0.012 mmol/min; F_{O2} = 0.014 mmol/min; F_{N2} = 0.68 mmol/min; T = 450°C; p = 190 kPa; $m_{catalyst}$ = 1 g)

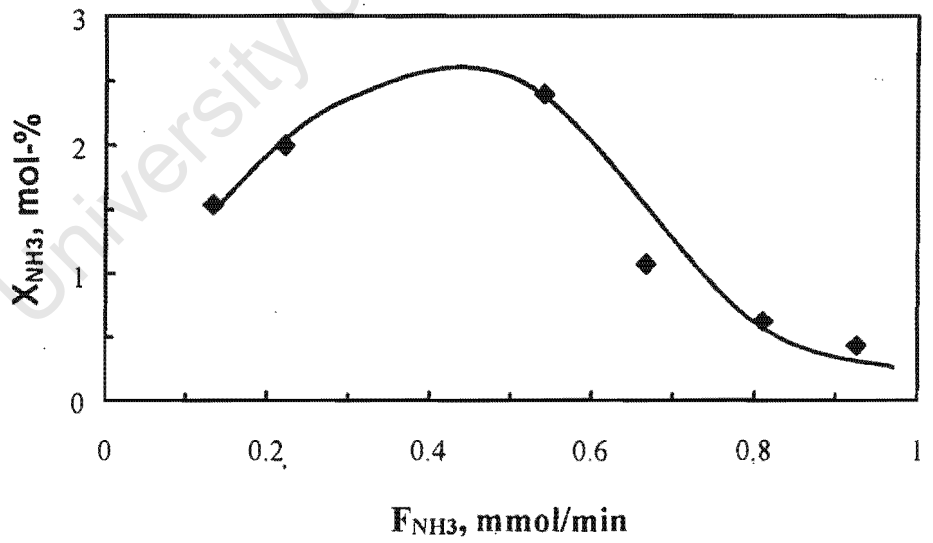

Figure 3.20: Ammonia conversion over α-bismuth molybdate as a function of ammonia molar flow rate of ammonia (F_{C3H6} = 0.012 mmol/min; F_{O2} = 0.014 mmol/min; F_{N2} = 0.68 mmol/min; T = 450°C; p = 190 kPa; $m_{catalyst}$ = 1 g).

Figure 3.21 shows the selectivity for the partial oxidation products, acrylonitrile and acrolein, as a function of the molar flow rate of ammonia (the selectivity for the total oxidation products, CO and CO_2, follows the opposite trend). The selectivity for the partial ammoxidation products passes a maximum. The occurrence of a maximum is unexpected. It has been reported in literature (Van Steen et al., 1997), that ammonia will inhibit the formation of total oxidation products. Furthermore, by increasing the molar flow rate of ammonia, the contact time decreases, which should lead to a decreased extent of consecutive oxidation of the primary formed products. It might thus be speculated that ammonia alters the catalyst behaviour, which favours the formation of CO and CO_2.

Figure 3.22 shows the content of acrylonitrile in the fraction of partial oxidation products, acrylonitrile plus acrolein. The acrylonitrile content seems to pass a maximum with increasing molar flow rate of ammonia. Burrington et al. (1984) described the ratio of the rate of formation of acrylonitrile to that of acrolein. According to these authors, the acrylonitrile content should increase with increasing partial pressure of ammonia. Increasing space velocity decreases the extent of secondary reactions. The observed decrease in the acrylonitrile content can be explained by assuming that both acrolein and acrylonitrile are primary products of the ammoxidation of propene. The conversion of acrolein into acrylonitrile is thermodynamically highly favoured. Thus, if acrolein is not allowed to react further by having a high flow rate, the acrylonitrile content can become lower with increasing molar flow rate of propene.

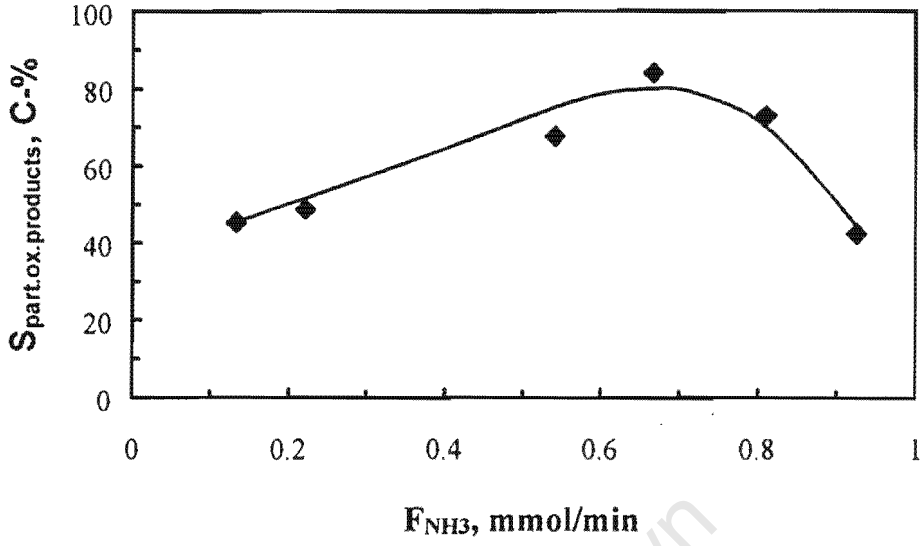

Figure 3.21: Selectivity for partial oxidation products over α-bismuth molybdate as a function of molar flow rate of ammonia (F_{C3H6} = 0.012 mmol/min; F_{O2} = 0.014 mmol/min; F_{N2} = 0.68 mmol/min; T = 450°C; p = 190 kPa; $m_{catalyst}$ = 1 g)

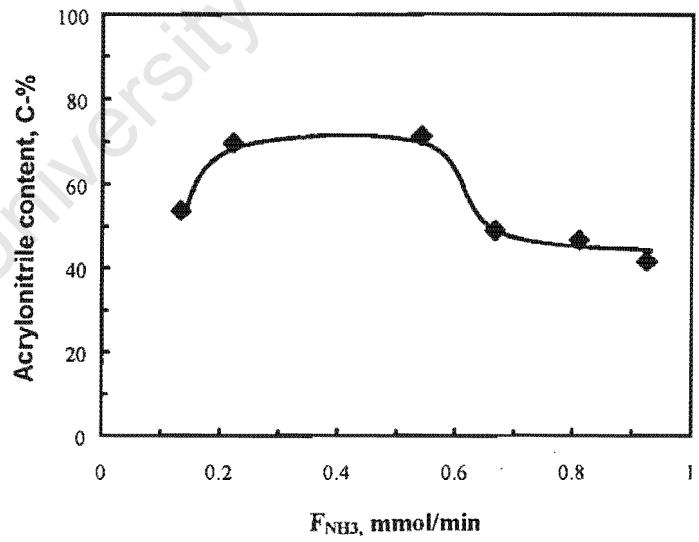

Figure 3.22: Acrylonitrile content in the fraction of partial oxidation products (acrylonitrile plus acrolein) as a function of molar flow rate of ammonia (F_{C3H6} = 0.012 mmol/min; F_{O2} = 0.014 mmol/min; F_{N2} = 0.68 mmol/min; T=450°C; p = 190 kPa; $m_{catalyst}$ = 1 g)

Figure 3.23 shows the content of CO in the fraction of the total oxidation products, CO and CO_2. The carbon monoxide content passes as a function of the molar flow rate of ammonia passes through the maximum. This is due to increase in the partial pressure of ammonia and hence decreasing the residence time, which then inhibit the consecutive oxidation of carbon monoxide to carbon dioxide. The decrease in the carbon monoxide content co-incised with the increase in the selectivity for partial oxidation products.

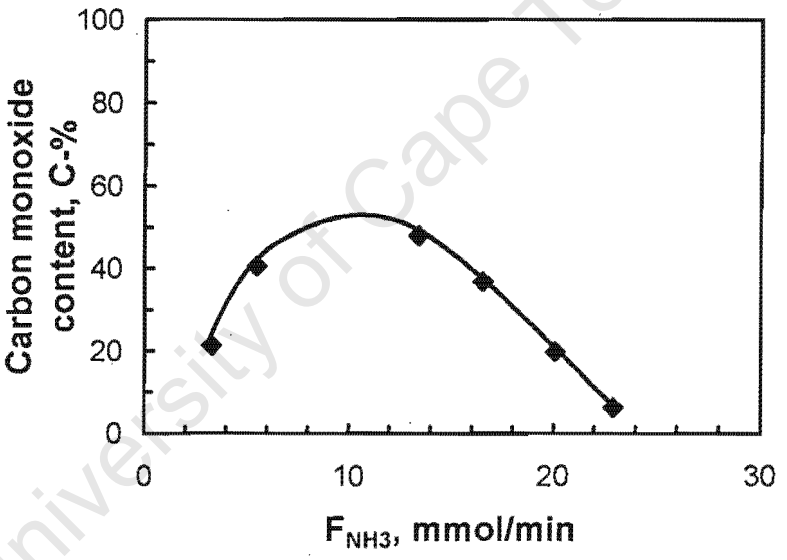

Figure 3.23: CO content in the fraction of total oxidation products (carbon monoxide plus carbon dioxide) as a function of molar flow rate of ammonia (F_{C3H6} = 0.012 mmol/min; F_{O2} = 0.014 mmol/min; F_{N2} = 0.68 mmol/min; T=450°C; p = 190 kPa; $m_{catalyst}$ = 1 g)

3.2.2. Iron molybdate

Figure 3.24 shows the conversion of propene over iron molybdate as a function of molar flow rate of ammonia. Conversion of propene as a function of ammonia flow rate is difficult to explain, due to the lack of sufficient data points. The conversion for ammonia over iron molybdate as a function of molar flow rate is shown in figure 3.25. The rapid decline in ammonia conversion with increasing flow rate of ammonia can be speculated to be a result of oxidation of ammonia at the surface to form water and nitrogen. The increase in ammonia flow rate resulted in an increase in the selectivity of partial ammoxidation products at high flow rate. This indicates that this catalyst is highly unselective for ammoxidation of propene (see Figure 3.26). The sudden increase in partial oxidation selectivity at higher flow rate of ammonia suggests that the total combustion is mainly from consecutive reaction of partial oxidation products. The selectivity for partial ammoxidation products is low at lower ammonia flow (30%) and higher (70%) at higher flow rate of ammonia.

In figure 3.27 the acrylonitrile content as a function of a molar flow rate of ammonia is shown. Although the low selectivity for partial oxidation products is observed for this catalyst (see Figure 3.26), the acrylonitrile content in the fraction of the partial oxidation products, acrylonitrile and acrolein, is high (70 – 90 C-%). The decline of the acrylonitrile content with increasing molar flow rate of ammonia might be attributed to the decreasing consecutive conversion of acrolein to acrylonitrile.

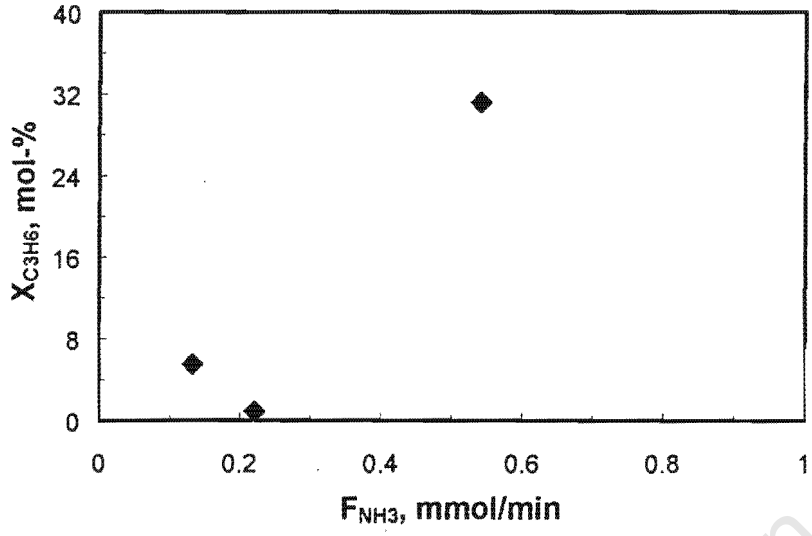

Figure 3.24: Propene conversion over iron molybdate as a function of ammonia molar flow rate (F_{C3H6} = 0.012 mmol/min; F_{O2} = 0.014 mmol/min; F_{N2} = 0.68 mmol/min; T = 450°C; p = 190 kPa; $m_{catalyst}$ = 1 g)

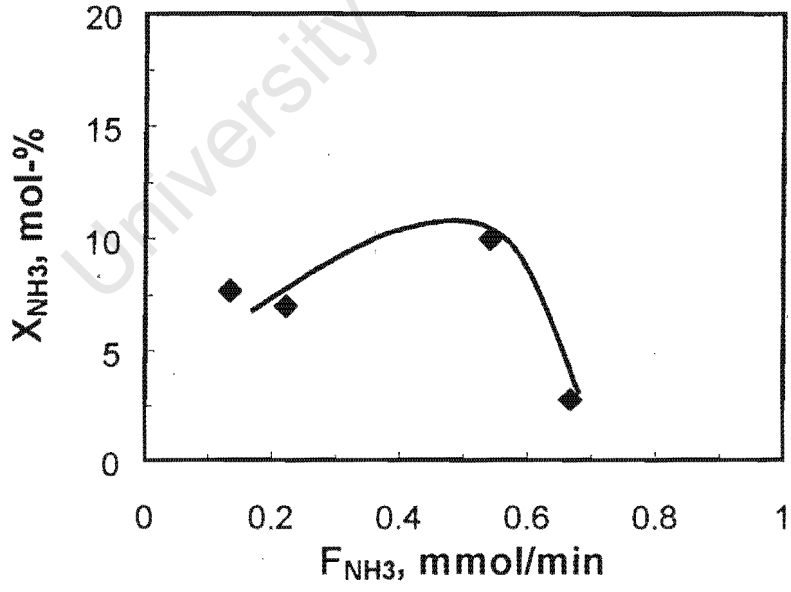

Figure 3.25: Ammonia conversion over iron molybdate as a function of ammonia molar flow rate (F_{C3H6} = 0.012 mmol/min; F_{O2} = 0.014 mmol/min; F_{N2} = 0.68 mmol/min; T = 450°C; p = 190 kPa; $m_{catalyst}$ = 1 g)

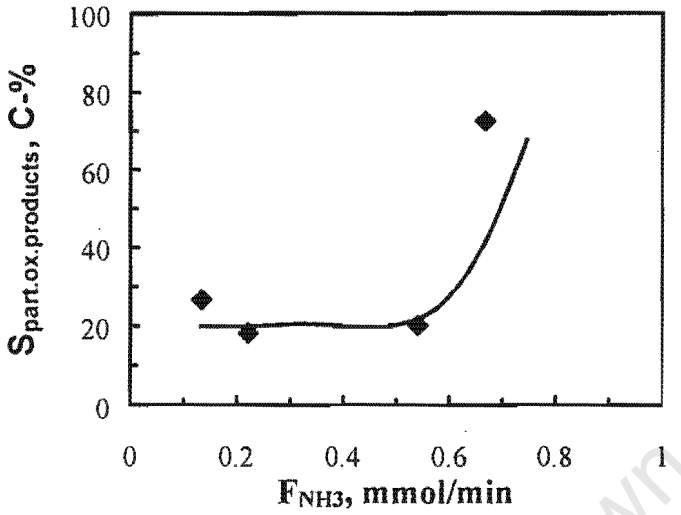

Figure 3.26: Selectivity for partial oxidation products over iron molybdate as a function of molar flow rate of ammonia (F_{C3H6} = 0.012 mmol/min; F_{O2} = 0.014 mmol/min; F_{N2} = 0.68 mmol/min; T = 450°C; p = 190 kPa; $m_{catalyst}$ = 1 g).

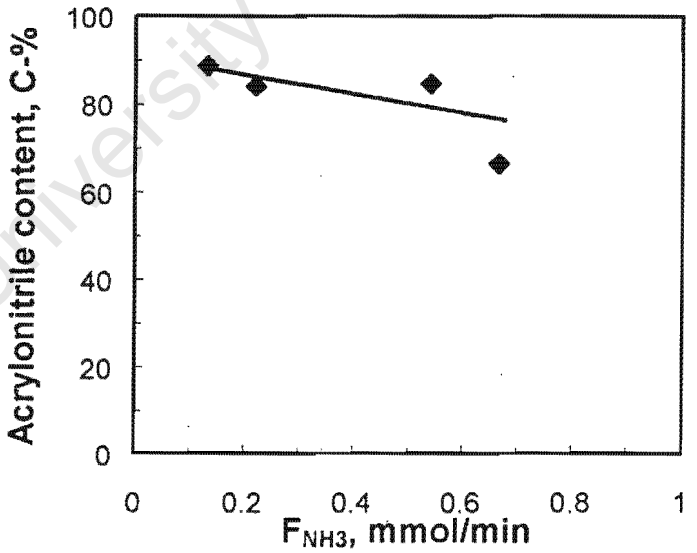

Figure 3.27: Acrylonitrile content in the fraction of partial oxidation products (acrylonitrile plus acrolein) as a function of molar flow rate of ammonia (F_{C3H6} = 0.012 mmol/min; F_{O2} = 0.014 mmol/min; F_{N2} = 0.68 mmol/min; T = 450°C; p = 190 kPa; $m_{catalyst}$ = 1 g).

Figure 3.28 describes the dependency of the carbon monoxide content in the fraction of total oxidation products, carbon monoxide and carbon dioxide. The carbon monoxide content in the total oxidation products is very low. The slight increase in the content of carbon monoxide corresponds with the increase in the selectivity of the partial oxidation products.

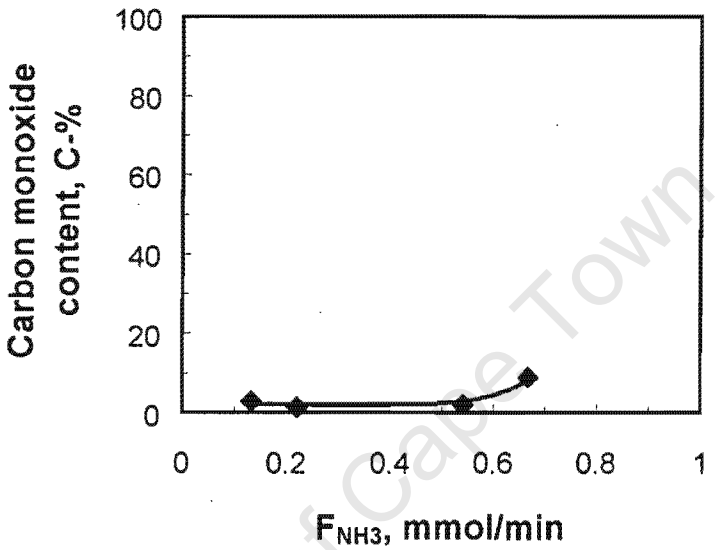

Figure 3.28: CO content in the fraction of total oxidation products (carbon monoxide plus carbon dioxide) as a function of molar flow rate of ammonia (F_{C3H6} = 0.012 mmol/min; F_{O2} = 0.014 mmol/min; F_{N2} = 0.68 mmol/min; T=450°C; p = 190 kPa; $m_{catalyst}$ = 1 g)

3.2.3. Iron bismuth molybdate (Bi:Fe = 3:1)

The influence of increasing molar flow rate of ammonia on propene ammoxidation was further investigated on iron promoted bismuth molybdate (Bi:Fe = 3:1). Figure 3.29 shows the conversion of propene as a function of molar flow rate of ammonia. The trend in conversion indicates that the catalyst does not show a strong declining rate in conversion with increasing molar flow rate of ammonia. Iron is known to regenerate the catalyst by facilitating oxygen mobility.

Figure 3.30 shows conversion of ammonia as a function of molar flow rate of ammonia. The conversion of ammonia decreases with the increasing molar flow rate of ammonia. The reason for a decrease could be resulting from the high space velocity induced by increasing molar flow rate of ammonia, which could result in a decrease in a space-time (τ).

Figure 3.31 shows the influence of partial oxidation selectivity with increasing molar flow rate of ammonia. Selectivity increases from 50 C-% to 70 C-% with increasing molar flow rate of ammonia. That implies on increasing the flow rate of ammonia the total space velocity is getting increased and hence minimising the total oxidation of products in favour of partial oxidation products.

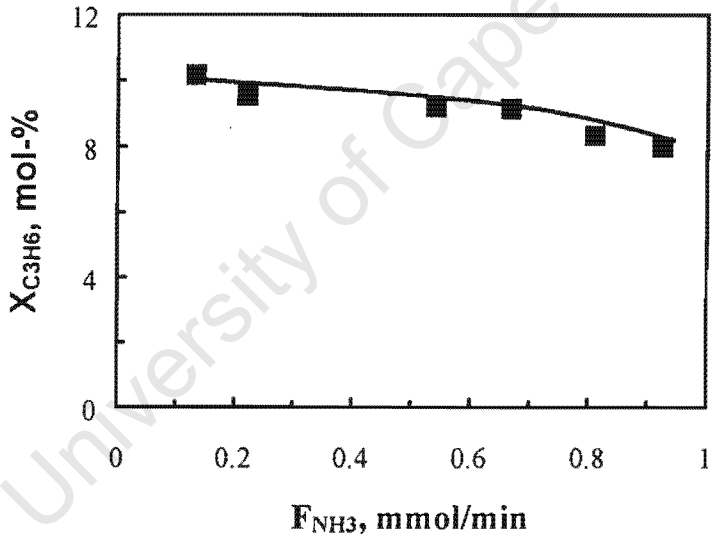

Figure 3.29: Propene conversion over iron bismuth molybdate (Bi:Fe=3) as a function of ammonia molar flow rate (F_{C3H6} = 0.012 mmol/min; F_{O2} = 0.014 mmol/min; F_{N2} = 0.68 mmol/min; T = 450°C; p = 190 kPa; $m_{catalyst}$ = 1 g)

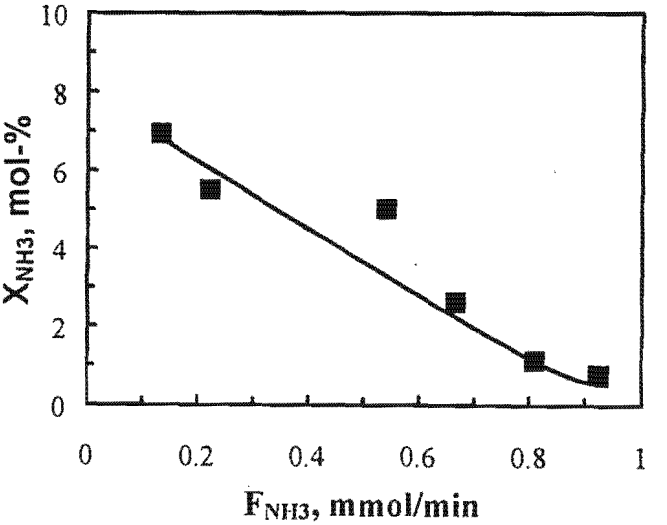

Figure 3.30: Ammonia conversion over iron bismuth molybdate (Bi:Fe=3) as a function of ammonia molar flow rate (F_{C3H6} = 0.012 mmol/min; F_{O2} = 0.014 mmol/min; F_{N2} = 0.68 mmol/min; T = 450°C; p = 190 kPa; $m_{catalyst}$ = 1 g)

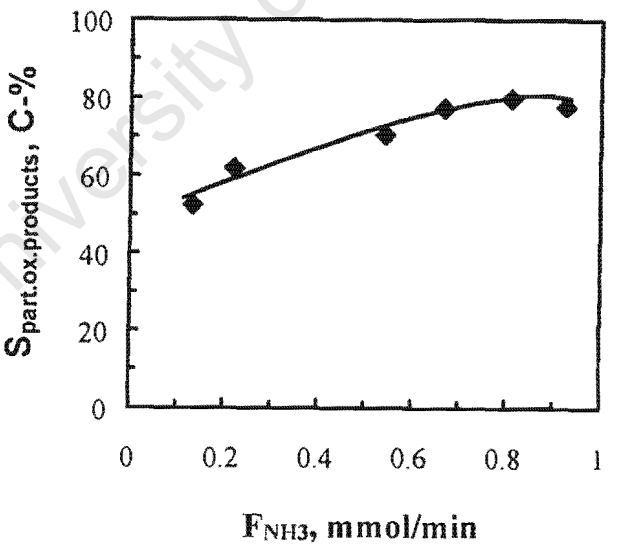

Figure 3.31: Selectivity to partial oxidation products over iron bismuth molybdate (Bi:Fe=3) as a function of molecular flow rate of ammonia (F_{C3H6} = 0.012 mmol/min; F_{O2} = 0.014 mmol/min; F_{N2} = 0.68 mmol/min; T=450°C; p = 190 kPa; $m_{catalyst}$ = 1 g)

Figure 3.32 shows acrylonitrile content in the fraction of partial oxidation products, acrylonitrile and acrolein, as a function of molar flow rate of ammonia. Acrylonitrile content is rather high (ca 79 C-%) and does not change with molar flow rate of ammonia. Figure 3.33 shows carbon monoxide content in the fraction of total oxidation products, carbon monoxide and carbon dioxide, as a function of molar flow rate of ammonia. The carbon monoxide content was initially low (30 C-%) and very high (95 C-%). The trend is similar to partial oxidation selectivity (see Figure 3.29) at higher molar flow rate of ammonia.

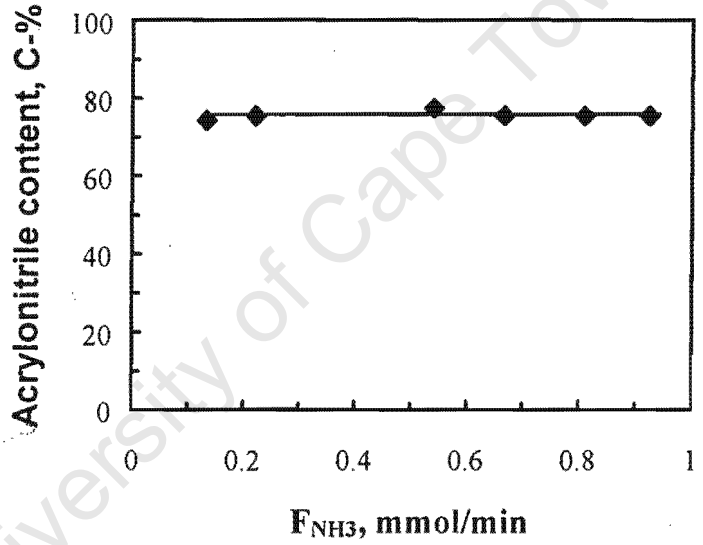

Figure 3.32: Acrylonitrile content in the fraction of partial oxidation products as a function of a molar flow rate of ammonia (F_{C3H6} = 0.012 mmol/mi-*n; F_{O2} = 0.014 mmol/min; F_{N2} = 0.68 mmol/min; T=450°C; p = 190 kPa; $m_{catalyst}$ = 1 g).

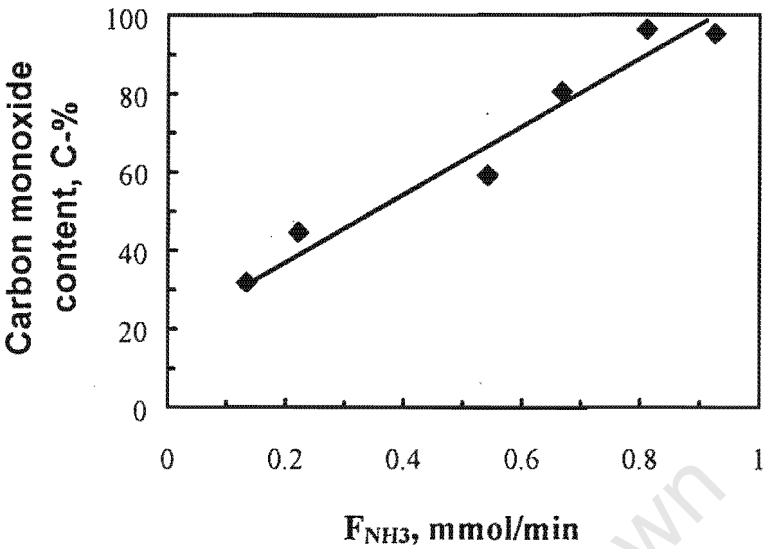

Figure 3.33: Carbon monoxide content in the fraction of total oxidation products (carbon-monoxide plus carbon-dioxide) as a function of molar flow rate of ammonia (F_{C3H6} = 0.012 mmol/min; F_{O2} = 0.014 mmol/min; F_{N2} = 0.68 mmol/min; T=450°C; p = 190 kPa; $m_{catalyst}$ = 1 g)

3.2.4. Iron bismuth molybdate (Bi:Fe = 1:1)

Figure 3.34 shows the conversion of propene as a function of molar flow rate of ammonia. The conversion decreases linearly with increasing molar flow rate of ammonia. The decrease could be due to an increasing space velocity in the catalyst bed, which reduces contact time between catalyst and the propene as well as products.

Figure 3.35 shows ammonia conversion as a function of molar flow rate of ammonia. The conversion of ammonia passes through maximum with increasing molar flow rates of ammonia. The increase at lower flow rates could be attributed to the initial increase in the formation of acrylonitrile from both ammoxidation of propene and acrolein as well. That is evidenced by the linear increase in the acrylonitrile content in the fraction of partial oxidation products, acrylonitrile plus acrolein partial (see Figure 3.37).

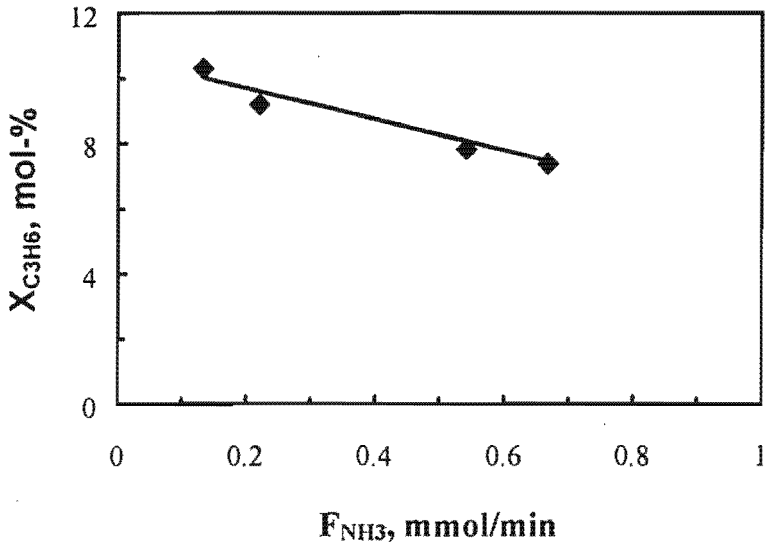

Figure 3.34: Propene conversion over iron bismuth molybdate (Bi:Fe=1) as a function of ammonia molar flow rate (F_{C3H6} = 0.012 mmol/min; F_{O2} = 0.014 mmol/min; F_{N2} = 0.68 mmol/min; T = 450°C; p = 190 kPa; $m_{catalyst}$ = 1 g)

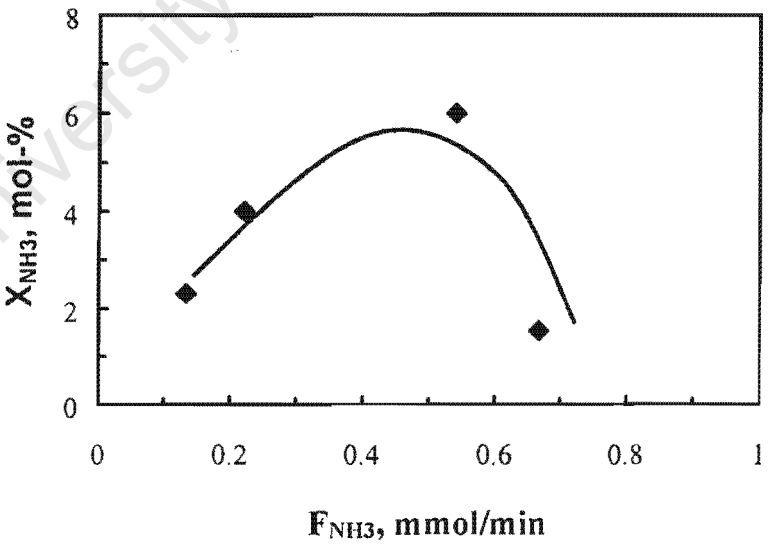

Figure 3.35: Ammonia conversion over iron bismuth molybdate (Bi:Fe=1) as a function of ammonia flow rate rate (F_{C3H6} = 0.012 mmol/min; F_{O2} = 0.014 mmol/min; F_{N2} = 0.68 mmol/min; T = 450°C; p = 190 kPa; $m_{catalyst}$ = 1 g)

Figure 3.36 shows partial oxidation selectivity as a function of molar flow rate of ammonia. The selectivity to partial oxidation products passes through the maximum with increasing molar flow rate of ammonia. The increase of partial oxidation products with an increasing molar flow rates is due to the increasing space velocity which ensures the removal of products from the active sites of the catalysts as they get formed. The selectivity to oxidation products is high, ranging from 50 C-% to 95 C-%.

Figure 3.37 shows the acrylonitrile content in the partial oxidation products, acrylonitrile and acrolein as a function of molar flow rate of ammonia. Despite the decline in partial oxidation selectivity at higher flow rate of ammonia, acrylonitrile content is increasing with the increase with the molar flow rate of ammonia. That may indicate that the formation of acrylonitrile is also from the consecutive ammoxidation of acrolein.

Figure 3.38 shows the carbon monoxide content in the fraction of total oxidation products, carbon monoxide and carbon dioxide. The carbon monoxide content passes through the maximum.

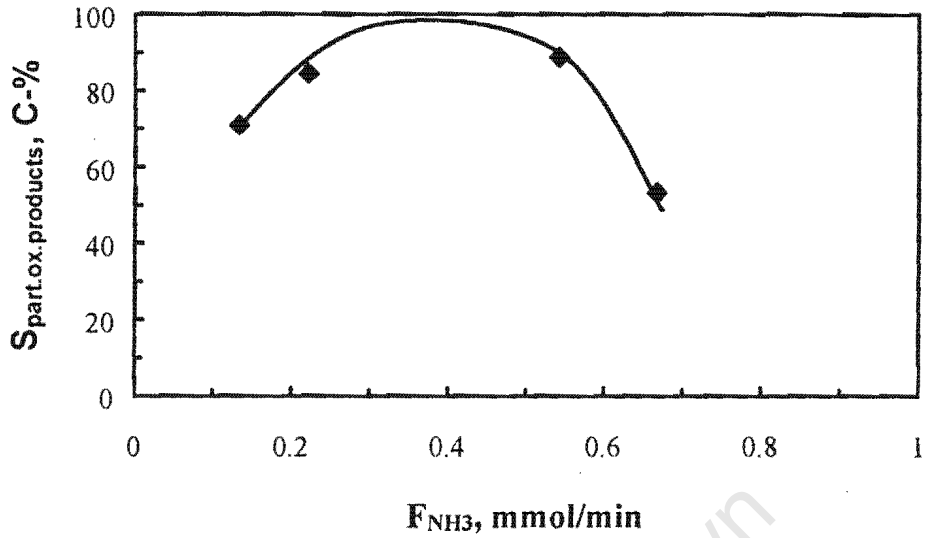

Figure 3.36: Selectivity to partial oxidation products over iron bismuth molybdate (Bi:Fe=1) as a function of molecular flow rate of ammonia (F_{C3H6} = 0.012 mmol/min; F_{O2} = 0.014 mmol/min; F_{N2} = 0.68 mmol/min; T=450°C; p = 190 kPa; $m_{catalyst}$ = 1 g)

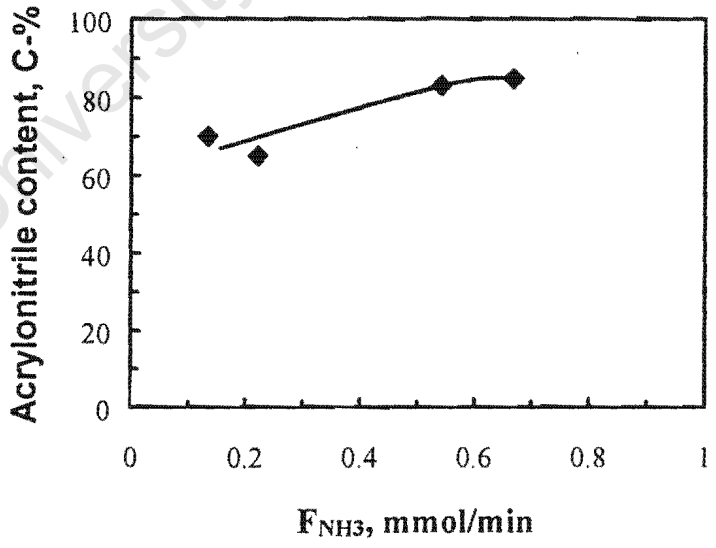

Figure 3.37: Acrylonitrile content in the fraction of partial oxidation products as a function of a molar flow rate of ammonia (F_{C3H6} = 0.012 mmol/min; F_{O2} = 0.014 mmol/min; F_{N2} = 0.68 mmol/min; T=450°C; p = 190 kPa; $m_{catalyst}$ = 1 g).

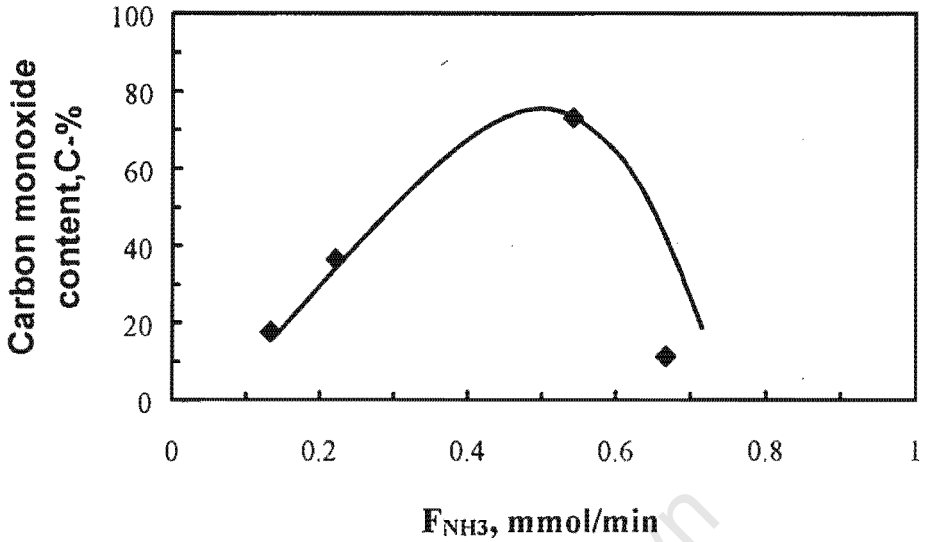

Figure 3.38: Carbon monoxide content in the fraction of total oxidation products (carbon-monoxide plus carbon dioxide) as a function of molar flow rate of ammonia (F_{C3H6} = 0.012 mmol/min; F_{O2} = 0.014 mmol/min; F_{N2} = 0.68 mmol/min; T=450°C; p = 190 kPa; $m_{catalyst}$ = 1 g)

4 Discussion

4.1 Catalyst preparation

Bismuth molybdate (α-phase):

The stoichiometric preparation of pure bismuth molybdate (α-phase) resulted with some excess MoO_3 (see Section 3.1.1.1). For pure bismuth molybdate (α-phase) preparation, excess bismuth is therefore needed.

Iron molybdate (Fe:Mo=1.5):

The preparation of iron molybdate ($Fe_2Mo_3O_{12}$) is almost stoichiometric. The AAS-ICP analysis showed the results with slight excess MoO_3. Therefore for pure preparation of iron molybdate (Fe:Mo=1.5), a slight excess of iron might result in the pure phase.

Iron bismuth molybdate (Bi:Fe=3):

Because the starting material is the prepared bismuth molybdate (α-phase) with some excess MoO_3 in it, the results for this reaction, as described in section 2.1.4 resulted in the reaction of Fe_2O_3 and MoO_3 leading to $Fe_2Mo_3O_{12}$. Bismuth molybdate remained unchanged in this reaction.

Iron bismuth molybdate (Bi:Fe=1):

The increase in the amount of iron to the amount of bismuth molybdate (α-phase) resulted in the formation of $Bi_3FeO_4(MoO_4)_2$ and $Fe_2Mo_3O_{12}$. The formation of $Fe_2Mo_3O_{12}$ is formed from reaction of excess MoO_3 present in prepared bismuth molybdate. In order to prepare pure $Bi_3FeO_4(MoO_4)_2$, pure bismuth molybdate (α-phase) is needed.

4.2 Catalyst reducibility: Temperature programmed reduction

The reducibility of the catalysts at lower temperatures could imply that the catalysts do have high mobility of oxygen at the surface, and possibly to the bulk. For the catalysts that need high temperatures to be reduced, that could be a sign of low

oxygen mobility. The temperature programmed reduction for various catalysts that have been tested for their catalytic performance have been described individually in chapter 3. Figure 4.1 shows the comparisons in reducibility among different ammoxidation catalysts. The indication is that the reduction of bismuth containing catalysts starts at lower temperatures. The ease of reduction for the first peak decreases as follows: $Bi3FeO4(MoO_4)_2/Fe_2Mo_3O_{12}$ > $Bi_2Mo_3O_{12}/Fe_2Mo_3O_{12}$ ≈ α-$Bi_2Mo_3O_{12}$ > $Fe_2Mo_3O_{12}$. The difference in reducibility implies that the catalysts have the different reduction potentials. Assuming that the oxygen mobility determines the ease of reduction {Brazdil et al., 1980 and Krenzke et al., 1980}, then the oxygen mobility in the multi-component catalyst, $Bi_3FeO_4(MoO_4)_2/Fe_2Mo_3O_{12}$ is the highest. The amount of oxygen participating in the reaction contributes to the hydrogen consumption. The high hydrogen consumption for the first reduction step showed by $Bi_3FeO_4(MoO_4)_2/Fe_2Mo_3O_{12}$ catalyst indicated that this catalyst has multiple layers participating in the reaction.

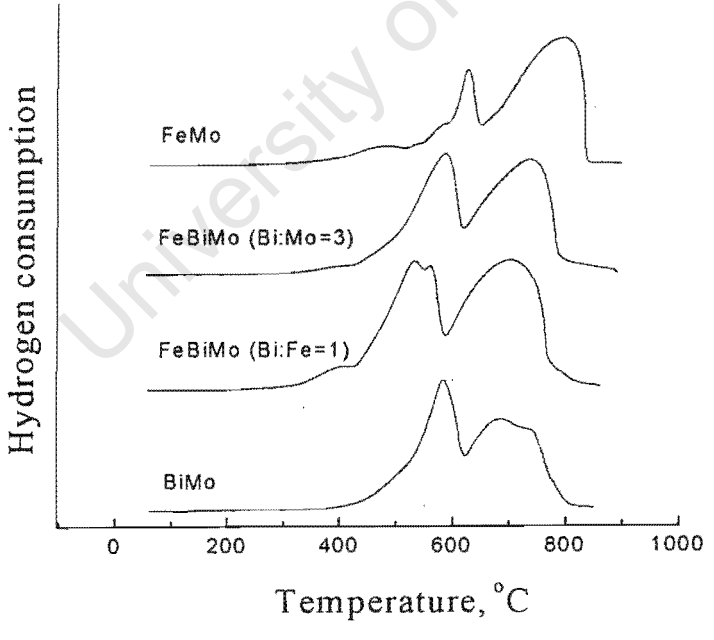

Figure 4.1: Temperature programmed reduction of the four-tested ammoxidation catalysts

The total number of lattice oxygen utilisation in the ammoxidation of propene (Brazdil et al., 1980) was found to decrease as follows: Multi-component > α-$Bi_2Mo_3O_{12}$ > $Bi_3FeO_4(MoO_4)_2$. The second reduction peak takes place at the same temperature for $Bi_3FeO_4(MoO_4)_2/Fe_2Mo_3O_{12}$, $Bi_2Mo_3O_{12}/Fe_2Mo_3O_{12}$ and α-$Bi_2Mo_3O_{12}$, with α-$Bi_2Mo_3O_{12}$ getting reduced totally with lower hydrogen consumption. Iron molybdate needed relatively higher temperature to be reduced.

4.3 Comparison of iron bismuth molybdate as a catalyst for propene ammoxidation

The activity for the four catalysts, which were tested for the ammoxidation of propene, was evaluated by looking at the rate of consumption of both propene and ammonia. The activity describes the catalytic nature of the catalyst under testing and the optimum rate of formation of partial oxidation products.

Figure 4.2 shows the rate of propene consumption as a function of partial pressure of ammonia. All catalyst shows same trend as their catalytic rate decreases with increasing partial pressure of ammonia, showing an inhibition of the propene consumption by the reactant ammonia. The increase in the partial pressure of ammonia was found to inhibit the conversion of both propane and propene over iron antimonate catalyst (Van Steen et al., 1997). Similar studies were done for the ammoxidation of propane over vanadium antimony catalyst (Catani et al., 1992), whereby the increase in ammonia partial pressure inhibited the conversion of propane to propene, as an intermediate product to an acrylonitrile formation.

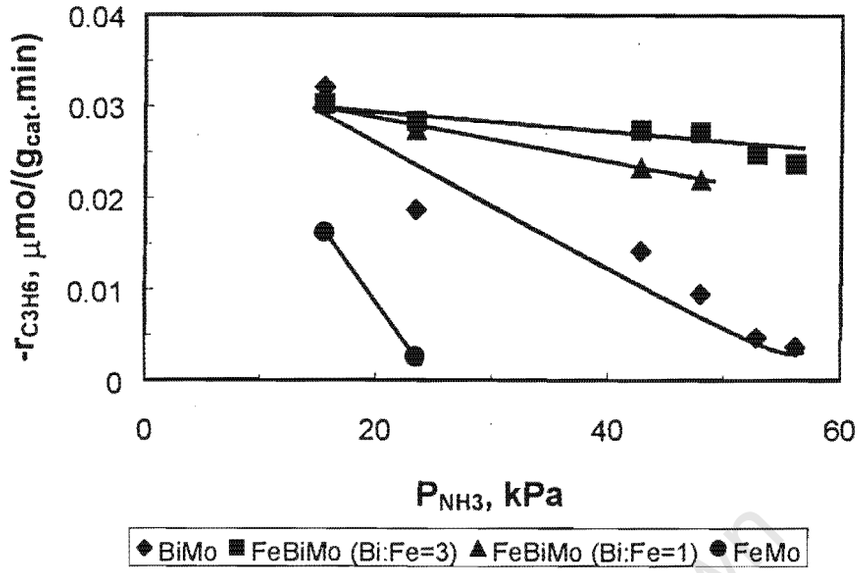

Figure 4.2: Rate of consumption of propene over iron bismuth molybdenum catalysts as a function of partial pressure of ammonia (F_{C3H6} = 0.012 mmol/min; F_{O2} = 0.014 mmol/min; F_{N2} = 0.68 mmol/min; T = 450°C; p = 190 kPa; $m_{catalyst}$ = 1 g).

The most active catalysts are the iron bismuth molybdate (Bi:Fe=3) and iron bismuth molybdate (Bi:Fe=1). The XRD analysis indicated that the said catalysts are composed of α-$Bi_2Mo_3O_{12}$/$Fe_2Mo_3O_{12}$ and $Bi_3FeO_4(MoO_4)_2$/$Fe_2Mo_3O_{12}$ respectively. The order of activity with reference to propene rate of consumption decreases as follows: α-$Bi_2Mo_3O_{12}$/$Fe_2Mo_3O_{12}$ > $Bi_3FeO_4(MoO_4)_2$/$Fe_2Mo_3O_{12}$ > α-$Bi_2Mo_3O_{12}$ > $Fe_2Mo_3O_{12}$.

The rate constants and reaction orders for the prepared bismuth molybdate, iron molybdate and iron promoted bismuth molybdate were determined. The following equation expresses the relationship between rate of consumption of propene as a function of partial pressure of ammonia.

$$-r_{C3^=} = kP^n$$

Table 4.1 and Figure 4.3 summarises the results for the determined reaction orders and rate constants. The reaction order and rate constant for iron molybdate catalyst could not be done because of lack of sufficient data points. The negative order of reaction observed means the ammonia partial pressure inhibited the consumption of propene. At high partial pressure deviations are observed. α-Bismuth molybdate deviates strongly at high partial pressure of ammonia, which imply that the consumption of propene is strongly inhibited by increasing ammonia partial pressure. The presence of iron in $Bi_2Mo_3O_{12}/Fe_2Mo_3O_{12}$ resulted in only slight change in reaction order as compared to iron free Bi_2MoO_3/MoO_3.

Table 4.1: Rate constant (k) and the order of reaction (n) for propene rate of consumption over prepared iron promoted bismuth molybdate catalysts

Catalyst	n	k
Bi_2MoO_3/MoO_3	-0.8	$0.3\mu mol/(g_{cat}.min(kPa^{-0.8}))$
FeBiMo (Fe:Bi=3)	-0.1	$0.04\mu mol/(g_{cat}.min(kPa^{-0.1}))$
FeBiMo (Fe:Bi=1)	-0.3	$0.07\mu mol/(g_{cat}.min(kPa^{-0.3}))$

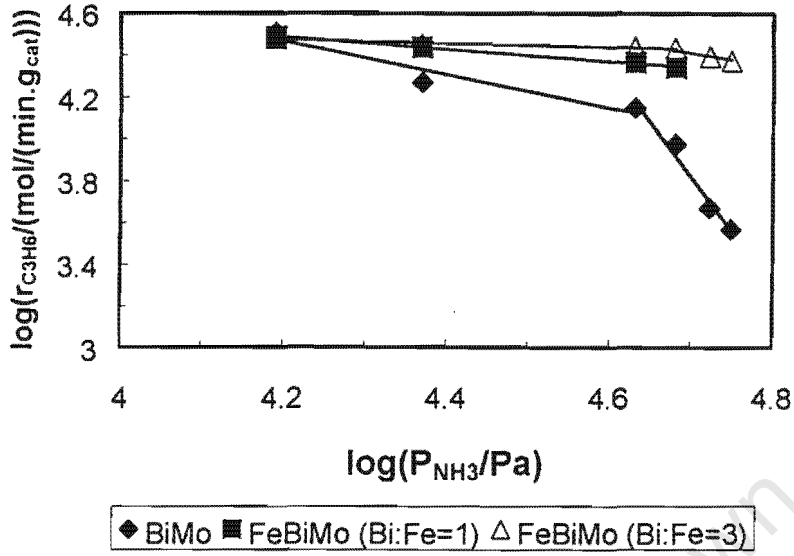

Figure 4.3: Log scale for the rate of consumption of propene versus partial pressure of ammonia

At high partial pressure of ammonia, the activity of α-$Bi_2Mo_3O_{12}/Fe_2Mo_3O_{12}$ (Bi:Fe=3) > $Bi_3FeO_4(MoO_4)_2/Fe_2Mo_3O_{12}$ (Bi:Fe=1) > α-$Bi_2Mo_3O_{12}/MoO_3$.

Figure 4.4 shows the rate of consumption of ammonia as a function of the partial pressure of ammonia. The rate of consumption of ammonia as a function of the ammonia partial pressure seems to pass a maximum, indicating a more complex relationship. The passing through a maximum is typical for a function, such as

$$-r_{NH_3} = \frac{k' \cdot p_{NH_3}}{\left(1 + K \cdot p_{NH_3}\right)^2}$$

describing the reaction involving two active sites. A fitting of the data to this function was not attempted due to the small number of data points available.

Ammonia is not only used for the production of acrylonitrile. In the systems under investigation the non-selective consumption of ammonia (i.e. the oxidation of ammonia to nitrogen and water) is much more than the selective conversion of ammonia, as can be seen by comparing the rate of propene consumption and the rate

of ammonia consumption. This can be ascribed to the large excess of ammonia used in these experiments.

The rate of ammonia consumption does not follow the same pattern of activity for propene consumption over the same catalysts. The relatively less active catalyst for propene activation, iron molybdate, is one of the most active for ammonia activation or oxidation. This is due to the fact that if $Fe_2Mo_3O_{12}$ is present as a single phase during oxidation reactions, its reduction to unselective $FeMoO_4$ is common (Cadus et al., 1994).

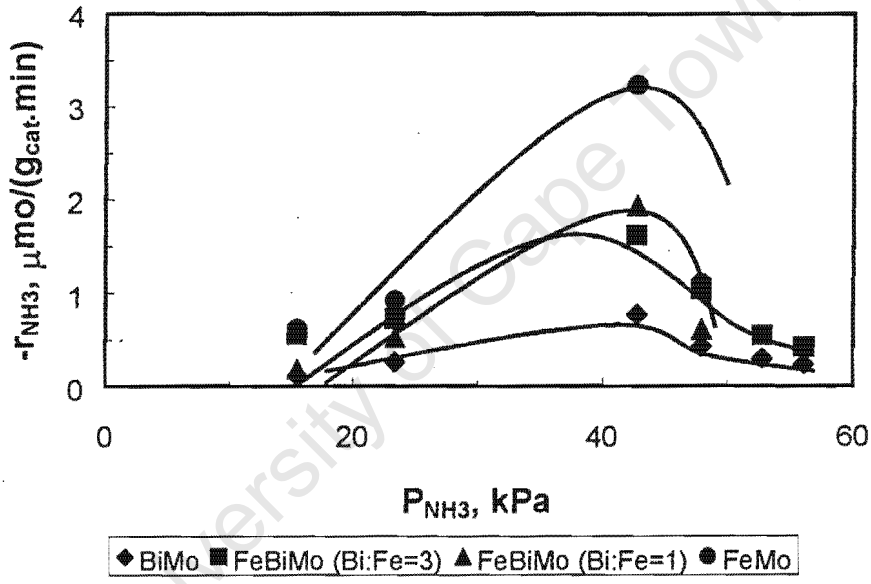

Figure 4.4: Rate of consumption of ammonia over iron bismuth molybdenum catalysts as a function of partial pressure of ammonia (F_{C3H6} = 0.012 mmol/min; F_{O2} = 0.014 mmol/min; F_{N2} = 0.68 mmol/min; T = 450°C; p = 190 kPa; $m_{catalyst}$ = 1 g).

The rate of formation of partial oxidation products, acrylonitrile and acrolein as a function of partial pressure of ammonia is as shown in figure 4.4. The largest rate of formation for partial oxidation products at lower partial pressure of ammonia is given by iron molybdate, which decreases with increasing partial pressure of ammonia. With all other catalysts the rate of formation of partial oxidation products as a

function of the partial pressure of ammonia passes through a maximum, indicating a rate expression such as:

$$-r_{NH_3} = \frac{k' \cdot p_{NH_3}}{(1 + K \cdot p_{NH_3})^2}$$

describing the reaction involving two active sites. A fitting of the data to this function was not attempted due to the small number of data points available.

The relative activity among the catalysts for the rate of formation of partial oxidation products at partial pressures of ammonia decreases as follows: $Fe_2Mo_3O_{12}$ > α-$Bi_2Mo_3O_{12}/Fe_2Mo_3O_{12}$ > $Bi_3FeO_4(MoO_4)_2$/ $Fe_2Mo_3O_{12}$ >>> α-$Bi_2Mo_3O_{12}$. The relative activity among the catalysts for the rate of formation of partial oxidation products at higher partial pressures of ammonia decreases as follows: α-$Bi_2Mo_3O_{12}/Fe_2Mo_3O_{12}$ ≈ $Bi_3FeO_4(MoO_4)_2/Fe_2Mo_3O_{12}$ >>> α-$Bi_2Mo_3O_{12}$, with $Fe_2Mo_3O_{12}$ catalyst possibly being before or after α-$Bi_2Mo_3O_{12}$.

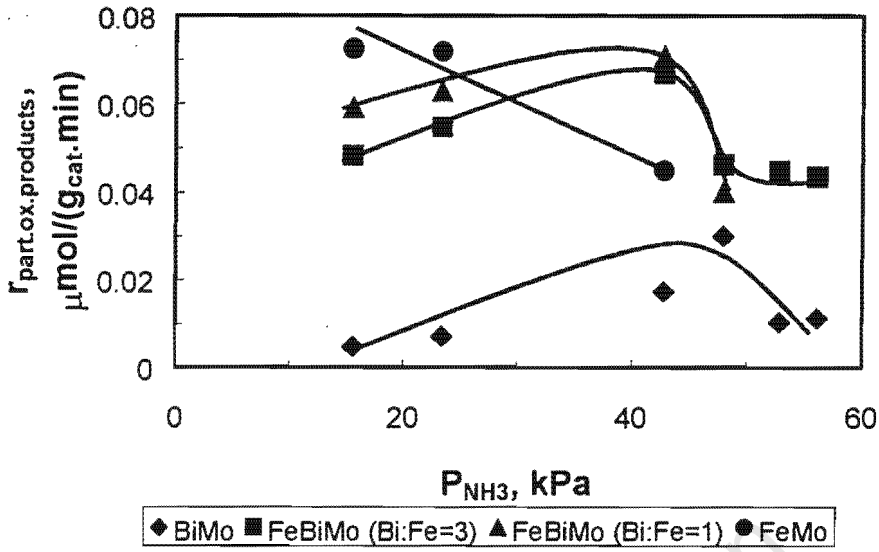

Figure 4.5: Rate of formation of partial oxidation products, acrylonitrile plus acrolein over iron bismuth molybdenum catalysts as a function of partial pressure of ammonia (F_{C3H6} = 0.012 mmol/min; F_{O2} = 0.014 mmol/min; F_{N2} = 0.68 mmol/min; T = 450°C; p = 190 kPa; $m_{catalyst}$ = 1 g).

The rate of total oxidation products, carbon monoxide and carbon dioxide as a function of partial pressure of ammonia for the tested catalysts is as shown in figures 4.6 and 4.7. Iron molybdate shows extremely large rate of formation of combustion products (see Figure 4.6). The decline in the rate of combustion products with increasing partial pressure of ammonia is not surprising. The activity for the rate of formation of combustion products decreases as follows: $Fe_2Mo_3O_{12}$ >>> α-$Bi_2Mo_3O_{12}/Fe_2Mo_3O_{12}$ > $Bi_3FeO_4(MoO_4)_2/Fe_2Mo_3O_{12}$ > α-$Bi_2Mo_3O_{12}$, except at higher flow rates whereby $Bi_3FeO_4(MoO_4)_2/Fe_2Mo_3O_{12}$ shows some deviation as it shows an exponential increase in rate of formation of combustion products.

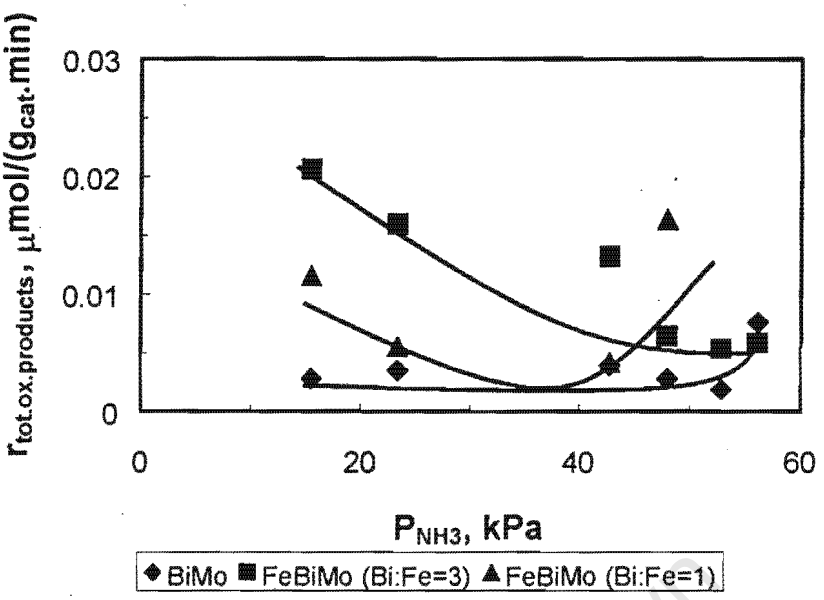

Figure 4.6: Rate of formation of total oxidation products, carbon dioxide plus carbon monoxide plus carbon dioxide over iron bismuth molybdenum catalysts as a function of partial pressure of ammonia (F_{C3H6} = 0.012 mmol/min; F_{O2} = 0.014 mmol/min; F_{N2} = 0.68 mmol/min; T = 450°C; p = 190 kPa; $m_{catalyst}$ = 1 g).

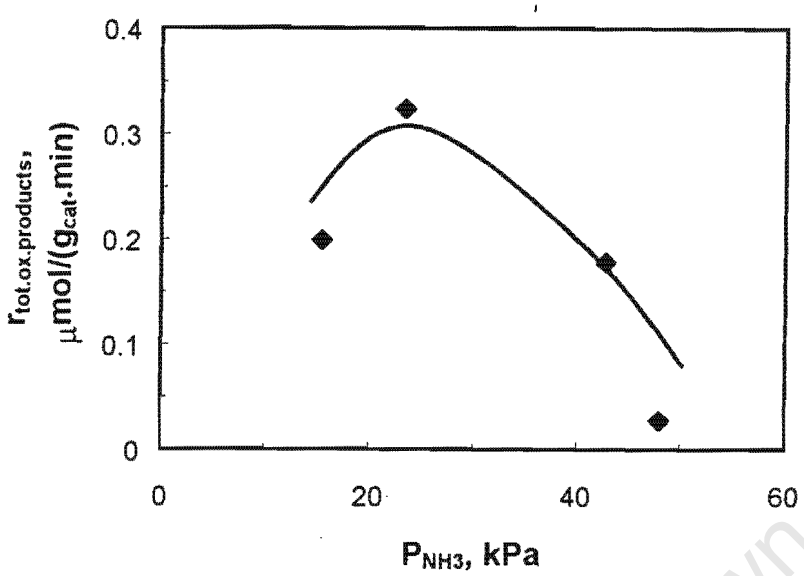

Figure 4.7: Rate of formation of total oxidation products, carbon dioxide plus carbon monoxide plus carbon dioxide over iron molybdate catalyst as a function of partial pressure of ammonia (F_{C3H6} = 0.012 mmol/min; F_{O2} = 0.014 mmol/min; F_{N2} = 0.68 mmol/min; T = 450°C; p = 190 kPa; $m_{catalyst}$ = 1 g).

4.4 Origin of different behaviour with tested catalysts

The activities of the different tested catalysts have been discussed at the previous section. It was found that iron molybdate is the most active catalyst even though highly unselective. The low selectivity could be ascribed to the reduction of $Fe_2Mo_3O_{12}$ to $FeMoO_4$ and MoO_2 as described in section 1.5.2.3. The reduction is irreversible, and the new phases are highly unselective. If pure $Fe_2Mo_3O_{12}$ works alone, more rapid reduction occurs during partial oxidation reactions than in mixed phased catalysts (Weng et al., 1992 and Castillo et al., 1994).

Figure 4.8 shows the yield of partial oxidation products as a function of partial pressure of ammonia. Iron molybdate contribute to activity. The high activity of iron molybdate may be due to an increasing over oxidation induced by unselective $FeMoO_4$ and MoO_2 formed during reduction of $Fe_2Mo_3O_{12}$ under catalytic condition.

Figure 4.9 shows the selectivity for partial oxidation products as a function of molar flow rate of ammonia. The selectivity is high for bismuth containing catalysts, while the activity appears to be high for iron molybdate as a co-catalyst. The preparation of bismuth molybdate (α-phase) resulted in the presence of some excess MoO_3 in the catalyst matrix. The activity of this catalyst may have been by the influence of the labile material, MoO_3. During ammoxidation conditions, molybdenum depletion is experienced due to volatility of unbound MoO_3 when in contact with steam. It is unavoidable since steam is generated during the reaction. MoO_3 is highly labile and moves as the molecular specie MoO(OH) (Grasselli, 1990; 1999). This observation is further evidenced by the high selectivity for partial oxidation products over a wide range of partial pressure of ammonia (see Figure 4.9). $Bi_3FeO_4(MoO_4)_2/Fe_2Mo_3O_{12}$ is the catalyst which carries both activity and selectivity. It is a multi-component catalyst, which was found by other authors to have an ability to utilise a multiple layers during catalytic reaction more than the other tested catalysts (Brazdil et al., 1980). $Bi_2Mo_3O_{12}/Fe_2Mo_3O_{12}$ come closer to the former in terms of both activity and selectivity. The durability of these two catalysts is driven by the rapid regenerability as described in section 1.5.3. The presence of $Fe_2Mo_3O_{12}$ in the catalyst mixture facilitates electron transfer and re-oxidation of the active sites. The reduction of $Fe_2Mo_3O_{12}$ to $FeMoO_4$ is the most important step in these mixtures because the redox cycle needs both Fe^{3+}/Fe^{2+}. The regenerability and the stability of the catalysts depend also on the epitaxial match between the phases. Although the stability of the catalysts was found to be influence the iron promotion, the selectivity seems to depend primarily on the nature of the elements and bonds stability. The fact that $Bi_3FeO_4(MoO_4)_2$ has three metals in single structure does not necessarily means the pure phase will be more active than $Bi_2Mo_3O_{12}$. In fact it was found in literature that bismuth molybdate (α-phase) is more active and selective than $Bi_3FeO_4(MoO_4)_2$. The mobility of irons in a single component catalyst is highly restricted than in multi-component system.

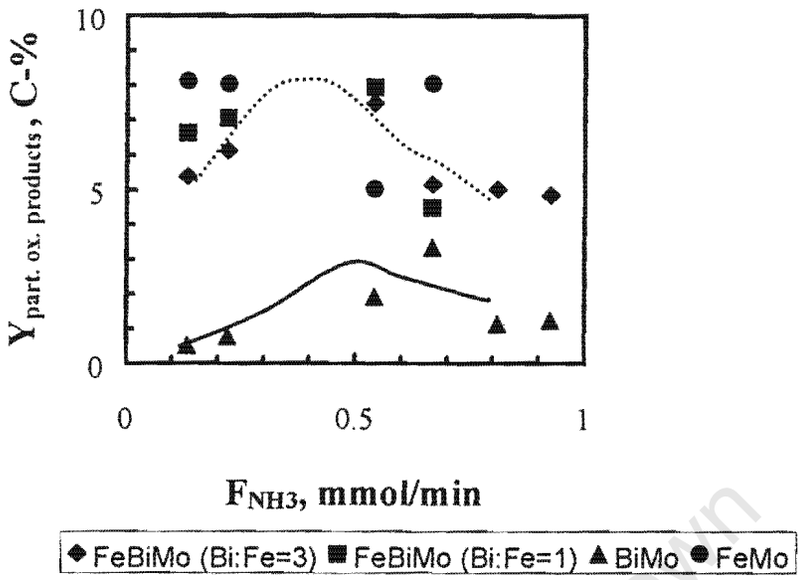

Figure 4.8: Yield for partial oxidation products as a function of the molar flow rates of ammonia ammonia (F_{C3H6} = 0.012 mmol/min; F_{O2} = 0.014 mmol/min; F_{N2} = 0.68 mmol/min; T = 450°C; p = 190 kPa; $m_{catalyst}$ = 1 g)

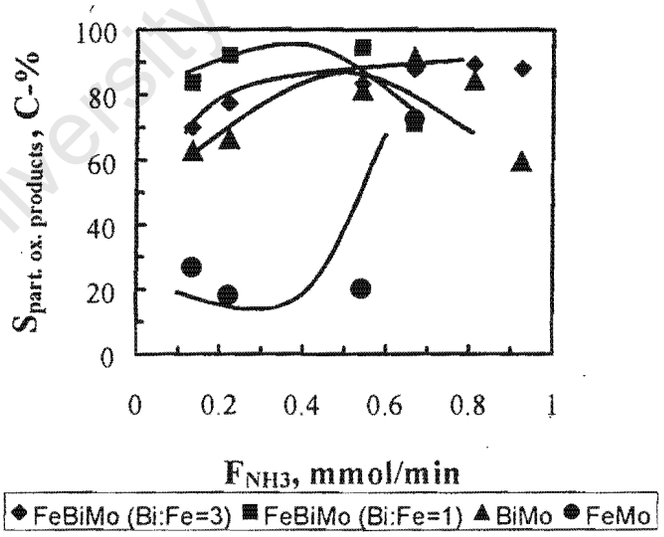

Figure 4.9: Selectivity for partial oxidation products as a function of the molar flow rates of ammonia ammonia (F_{C3H6} = 0.012 mmol/min; F_{O2} = 0.014 mmol/min; F_{N2} = 0.68 mmol/min; T = 450°C; p = 190 kPa; $m_{catalyst}$ = 1 g)

The preparation of iron promoted bismuth molybdate needs some special precautions. It was found that the only catalyst which could possibly contain the elements Fe, Bi and Mo in single phase is $Bi_3FeO_4(MoO_4)_2$. An attempt to increase the ratio of iron resulted in a mixed phased catalyst of $Bi_3FeO_4(MoO_4)_2/Fe_2(MoO_4)_3$. The mixed phase catalyst was the results of impure prepared bismuth molybdate (α-phase), which contains excess molybdenum oxide. Therefore to prepare pure $Bi_3FeO_4(MoO_4)_2$, it is essential to start with pure bismuth molybdate (α-phase).

Although an excess molybdenum resulted in the formation of iron molybdenum during catalyst impregnation, an excess molybdenum is important to facilitate an epitaxial match between promoter phase (e.g. $Fe_2(MoO_4)_3$) and phase of interest (i.e . $Bi_2(MoO_4)_3$. It is therefore vital to bring some amount of excess molybdenum oxide in the catalyst matrix during catalytic reaction. It could also serve as a spectator phase to supplement any decline in molybdenum.

Bismuth molybdate (α-phase) appeared to be selective for the formation of partial oxidation products. Its activity was enhanced by the introduction of iron molybdate. The iron molybdate alone is not selective, but promoted the activity of bismuth molybdate (α-phase) and $Bi_3FeO_4(MoO_4)_2$ by generating stability through the formation of redox couple and thereby enhancing electron mobility. The most active and selective catalyst was found to be $Bi_3FeO_4(MoO_4)_2/Fe_2(MoO_4)_3$, but very close to $Bi_2(MoO_4)_3/Fe_2(MoO_4)_3$. This two mixed phased catalysts consist of promoter phase $Fe_2(MoO_4)_3$ and most selective $Bi_3FeO_4(MoO_4)_2$ and $Bi_2(MoO_4)_3$ respectively.

The selectivity to partial oxidation products, increase with the increase in the partial pressure of ammonia. This was due to an increasing space velocity, which reduces the contact time (τ). The selectivity for partial oxidation over $Bi_2(MoO_4)_3$, $Bi_3FeO_4(MoO_4)_2/Fe_2(MoO_4)_3$ and $Bi_2(MoO_4)_3/Fe_2(MoO_4)_3$ products passes through the maximum. The decline in selectivity at higher partial pressure of ammonia may be due to the inhibiting behaviour of ammonia by reducing the surface, and possibly inducing non-selective oxygen species, which over oxidise the products and also oxidise ammonia to nitrogen and water.

TPR measurements indicated that the mixed phase catalysts get reduced relatively at lower temperature as compared to iron molybdate alone. That could be the fact that iron molybdate as a single phase has relatively lower iron mobility as compared to mixed phases of $Bi_2(MoO_4)_3/MoO_3$, $Bi_2(MoO_4)_3/Fe_2(MoO_4)_3$ and $Bi_3FeO_4(MoO_4)_2/Fe_2(MoO_4)_3$.

6 References

Albonetti, S., Blanchard, G., Burattin, P., Masetti, S. and Trifiro, F. *A new catalyst for propane ammoxidation:* the Sb/V/Sb mixed oxide, In 3rd World Congress on Oxidation Catalysis. Grasselli, R.K., Oyama, S.T. and Gaffney, A.M. (Editors). **1997** Elsevier Science B.V.

Albonetti, S., Blanchard, G., Burattin, P., Cassidy, T.J., Masetti, S. and Trifiro, F. *Mechanism of ammoxidation of propane on a Sb/V/O system.* Cat. Lett., **45** (1997) 119-123.

Albonetti, S., Blanchard, G., Burattin, P., Masetti, S., Tagliani, A. and Trifiro, F. *A new ternary mixed oxide catalyst for ammoxidation of propane: Sn/V/Sb.* Cat. Lett., **50** (1998) 17-23.

Batist, PH.A., Bouwens, J.F.H. and Schuit G.C.A. *Bismuth Molybdate Catalysts. Preparation, Characterization and Activity of Different Compounds in the Bi-Mo-O Systems.* Journal of Catalysis, **25** (1972) 1-11.

Bielañski, A. and Haber, J. *Oxygen in Catalysis.* Marcel Dekker, Inc. 1991.

Brazdil, J.F., Suresh, D.D. and Grasselli, R.K. *Redox Kinetics of Bismuth Molybdate Ammoxidation Catalyst.* J. of Catal., **66** (1980) 347-367.

Burrington, C.T., Kartisek, C.T. and Grasselli, R.K. *Surface Intermemediates in Selective Propylene Oxidation over Heterogeneous Molybdate and Antimonate catalyst.* J. of Catal., **87** (1984) 363-380.

Cadus, L.E., Xiong, Y.L., Gotor, F.J., Acosta, D., Naud, J., Ruiz, D. and Delmon, B. *Synergy In The Fe-Mo-Sb-O Multiphase System.* In New Developments in Selective Oxidation II. Corberán, V.C. and Bellón, S.V. (Editors). **1994** Elsevier Science B.V.

Carrazan, S.R.G., Cadus. L., Dieu, Ph., Ruiz. P. and Delmon, B. *Synergetic effects in multiphase catalysts: the role of* $FeSbO_4$ as *donor-acceptor of* the *spill over oxygen.* Catalysis Today **32** (1996) 311-319.

Carson, D., Coudurier, G., Forissier, M. and Vedrine, J.C. *Synergy Effect in the Catalytic properties of Bisbuth Molybdate.* J. Chem. Soc., Faraday Trans.1, **79** (1983) 1921-1929.

Castillo, R., Awasarkar, P.A., Papadopoulou, Ch., Acosta, D. and Ruiz, P. *Creation of new Selective Sites By Spill-Over Oxygen Via a-Sb2O4 in the Oxidation of Ethanol.* In New Developments in Selective Oxidation II. Corberán, V.C. and Bellón, S.V. (Editors). **1994** Elsevier Science B.V.

Catani, R., Centi, G. and Trifiro, F. *Kinetics and Reaction Network in the Ammoxidation to acrylonitrile on V-Sb-Al Based Mixed Oxides.* Ind. Eng. Chem. Res. **31** (1992) 107-119.

Centi, G., Grasselli, R.K. and Trifiro, F. *Propane Ammoxidation to Acrylonitrile-An Overview.* Catalysis Today, **13** (1992) 661-666.

Centi, G., Marchi, F. and Perathoner S. *Surface chemistry of V-Sb-oxide in relation to the mechanism of acrilonitrile synthesis from propane. Part 2. Reactivity towards ammonia and relationship with catalytic behaviour.* Journal of Chemical Society, Faraday Trans **92(24)** (1996) 5151-5159.

Centi, G., Marchi, F. and Perathoner Siglinda. *Effect of ammonia chemisorption on the surface reactivity of V-Sb-Oxide catalysts for propane ammoxidation.* Applied Catalysis A: Genaral **149** (1997) 225-244

Centi, G., Foresti, E. and Guarnieri, F. *Structure and Stability during the catalytic Reaction of Unsupported V-Antimonate Catalysts for the direct Selective Ammoxidation of Propane Acrylonitrile.* In New Developments in Selective oxidation II. **1994** Elsevier Science B.V.

Centi, G., Marchi, F. and Perathoner Siglinda. *Surface chemistry of V-Sb-oxide in relation to the mechanism of acrilonitrile synthesis from propane. Part 1. Chemisorption and transformationof possible intermediates.* Journal of Chemical Society, Faraday Trans **92(24)** (1996) 5141-5149.

Chem Systems. Acrylonitrile ex Propane www.chemsystems.com. 1990

Fattore, V., Fuhrman, Z.A ., Manara G. and Notari, B. *Oxidation of Propene in the Absence of Gaseous Oxygen.* II. *Bismuth Molybdates and Iron Antimonates.* J. of Catal., **37** (1975) 223-231.

Grasselli, R.K. *Adavances and future trends in selective oxidation and ammoxidation catalysis.* Catalysis Today, **49** (1999) 141-153.

Grasselli, R.K. *Ammoxidation.* In Handbook of Heterogeneous Catalysis. **5** (1997) 2302-2324. VCH.

Grasselli, R.K. *Selective Oxidation and Ammoxidation of Olefins by Heterogeneous Catalysis.* Journal of Chemical Education **63**(3) (1986) 216-221.

Grasselli, R.K., Brazdi, J.F. and Burrington, J.D. *Fe-Se-Tellurates as ammoxidation catalysts..* Applied Catalysis. **25** (1986) 335-344.

Grasselli, R.K., Centi, G. and Trifiro, F. *Selective Oxidation of Hydrocarbons Employing Tellurium Containing Heterogeneous Catalysts.* App.Catal. **57** (1990) 149 -166.

Grzybowska, B., Harber, J. and Komorek, J. *The Chemistry of Bi-Mo Oxide Catalysts: 1. Phase Composition of Catalysts and its Relation to the structure of Precursors.* J. of Catal., **25** (1992) 25-32.

Han, Y., Ueda, W. and Moro-Oka, Y. *Lattice oxide ion-transfer effect demonstrated in the selective oxidation of propene over silica-supported bismuth molybdate catalysts.* Appl. Catal. A: General, **176** (1999) 11-16.

Higgins, R. and Hayden, P. *Selective Oxidation of Hydrocarbons Over Mixed Oxide Catalysts.* In Specialist Periodical Reports. Kemball, C. (Editor). Catal., **1** (1977) 168-203.

Jeitschko, W., Sleight, A.W., McClellan, W.R. and Weiher, J.F. *A Comprehensive Study of Disordered and Ordered Scheelite-Related $Bi_3(FeO_4)(MoO_4)_2$.* Acta Cryst., **B32** (1976) 1163.

Kahmer, T., McClune, W.F., Clark, H.E., Dickson, B. and Lannol, L. *Powder Diffraction File for Inorganic Phases.* International Centre for Diffraction Data., 1997.

Keulks, G.W. and Matsuzaki, T. *The Nature of Active Oxygen In Selective Oxidation Reactions*: In Adsorption and Catalysis on Oxide surfaces. Che, M. and Bond, G.C. (Editors). Elsevier Science Publishers B.V., Amsterdam, **1985**.

Keulks, G.W., Hall, J.L., Daniel, C. and Suzuki, K. *Catalytic Oxidation of Propylene. IV. Preparation and Characterisation of α-Bisbuth Molybdate.* J. of Catal., **34** (1974) 77-79.

Krenzke, L.D. and Keulks, G.W. *The Catalytic Oxidation of Propylene. VI. Mechanistic Studies Utilizing isotopic Tracers.* J. of Catal., **61** (1980) 316-325.

Kim, Y.-C., Ueda, W. and Moro-oka, Y. *Catalytic (amm)oxidation of propane with molecular oxygen over complex metal oxides: Involvement of homogeneous reaction in gas phase.* Catalysis Today, **13** (1992) 673 - 678.

Libre, J.M., Barbaux, Y., Grzybowska, B., Conflant, P and Bonnelle, J.P. *Catalytic oxidation of propene: Surface potential measurements and structural properties of α-$Bi_2Mo_3O_{12}$, α-Bi_2O_3 and MoO_3.* Applied Catalysis **6** (1983) 315-328.

Levenspiel, O., Chemical Reaction Engineering. 2nd Edition. 1972, John Wiley & Sons.

Matsuura, I. And Schuit, G.C.A. *Adsorption and Reaction of Adsorbed Species on Bi_2MoO_6 Catalyst: Influence on Sintering and of Temperature of Reduction.* J. of Catal., **25** (1972) 314-325.

Mitchell, P.C.H. and Trifiro, F. *Spectroscopic Investigation of Bismuth-Molybdenum-Oxide Catalysts.* J. Chem. Soc. (A), 1970,

Miura, H., Morikawa, Y. and Shirasaki, T. *Studies on the Reduction –Reoxidation of Bismuth Molybdate Catalysts by Temperature Programmed Reoxidation method.* J. Catal., **39** (1975) 22-28.

Nilsson, J., Landa-Canovas, A.R., Hansen, S. and Andesson, A. *Formation of active phases in the Sb-V-, Al-Sb-V-, and Al-Sb-V-W-Oxide systems for propane ammoxidation,* In 3rd World Congress on Oxidation Catalysis. Grasselli, R.K.., Oyama, S.T. and Gaffney, A.M.(Editors). **1997** Elsevier B.V.

Nilsson, R. and Andersson, A. *Transient Response Study of the Ammoxidation of Propene and Propane on an Sb-V-Oxide Catalyst.* Ind. Eng. Chem. Res. **36** (1997) 5207-5219.

Nilsson, R., Lindblad,T. and Anderson, A. *Ammoxidation of Propane over Antimony-Vanadium-Oxide Catalysts.* J. of Catal., **148** (1994) 501-513.

Perry, R.H., Gree, D. Perry's Chemical Engineering Handbook. six edition, 1984.

Patterson, W.R. *Selective Hydrocarbon Oxidation, in:* Catalysis and Chemical Processes. Pearce, R. and Patterson, W.R. (editors). Blackie & Son Ltd. 1981.

Ponceblanc, H., Millet, J.M.M., Coudurier, G. and Vedrine, J.C. *Synergy Effect of Multicomponent Co, Fe, and Bi Molybdates in Propene Partial oxidation, in* : Catalytic Selective Oxidation. Oyama, S.T. and Hightower, J.W., (editors). ACS Symposium Series, **523** (1992) 262-272.

Schnobel, M. and Van Steen, E. *Kinetics of Selective Partial Oxidation of C_3-C_6 α-Olefins over an Iron Antimony Oxide Catalyst.* Ind. Eng. Che. Res. **36(9)** (1997) 3568 - 3575.

Sleight, A.W. and Jeitschko, W. *$Bi_3(FeO_4)(MoO_4)_2$ and $Bi_3(GaO_4)(MoO_4)_2$ – New Compounds with Scheelite related structures*. Mat. Res, Bull., **9** (1974) 951-954.

Stern, D.L. and Grasselli, R.K. *Mechanistic Aspects of Propane Oxidation over Ni-Co-Molybdate Catalysts*, In 3rd World Congress on Oxidation Catalysis. Grasselli, R.K.., Oyama, S.T. and Gaffney, A.M.(Editors). **1997** Elsevier B.V.

Trifiró, F., Hoser, H. and Scarle, R.D. *Relationship between Structure and Activity of the Mixed Oxides as Oxidation Catalysts: 1. Preparation and Solid State Reactions of Bi-molybdate.* J. of Cat., **25** (1972) 12-24.

Ueda, W., Moro-oka, Y. and Tsuneo Ikawa. *Study of Ternary-Components Bismuth Molybdate Catalysts by $^{18}O_2$ Tracer in the Oxidation of Propylene to Acrolein.* Journal of Catalysis **70** (1981) 409-417

Van der Baan, H.S. *The Acrylonitrile Process,* in Chemistry and Chemical Engeneering of Catalytic Processes. Prins, R. and Schuit, G.C.A.(Editors). Sijthoff and Noordhoff **1980**.

Van Steen, E., Kuwert, G., Naidoo, A. and Williams, M. *Influence of Antimony content in the Iron Antimony Oxide Catalyst and Reaction Conditions on the*

(Amm)Oxidation of Propene and Propane, in 3rd World Congress on Oxidation Catalysis. Grasselli, R.K.., Oyama, S.T. Gaffney, A.M. and Lyons J.E.(Editors). **1997** Elsevier Science B.V.

Van Steen, E., Schnoebel, M., Walsh, R. and Riedel, T. *Time on streem behaviour in the partial oxidation of propene over iron antimony oxide.* Appl. Catal. A: general. **165** (1997) 349-356.

Weissermel, K. and Arpe, H. Industrial Organic Chemistry. VCH publishers. 1993.

Weng, L.T., Cadus, L., Ruiz, P. and Delmon, P. *Protection Against Deactivation of Selective Oxidation Catalysts Due To Spill Over Oxygen.* Catalysis Today, **11** (1992) 455-464. Elsivier Science Publishers B.V., Amsterdam.

Wittcoff, H.A. and Reuben B.G., *Industrial Organic Chemicals, John Wiley & Sons, Inc,* 1980.

Zanthoff, H.W., Buchholz, S.A., Ovsitser O.Y., *Ammoxidation of propane to acrylonitrile on V-Sb-O catalysts. Role of ammonia in the reaction pathways.* Catalysis Today **32** (1996) 291-296

Chapter 7- Appendix 1

Thermodynamics

Temp, °C	ΔHr, kJ/mol	Temp, °C	ΔHr, kJ/mol	Temp, °C	ΔHr, kJ/mol
25	-515.64	132.85	-512.55	240.85	-509.57
26.85	-515.59	134.85	-512.50	242.85	-509.51
28.85	-515.53	136.85	-512.44	244.85	-509.46
30.85	-515.47	138.85	-512.38	246.85	-509.40
32.85	-515.41	140.85	-512.33	248.85	-509.35
34.85	-515.35	142.85	-512.27	250.85	-509.29
36.85	-515.29	144.85	-512.22	252.85	-509.24
38.85	-515.24	146.85	-512.16	254.85	-509.18
40.85	-515.18	148.85	-512.10	256.85	-509.13
42.85	-515.12	150.85	-512.05	258.85	-509.07
44.85	-515.06	152.85	-511.99	260.85	-509.02
46.85	-515.00	154.85	-511.94	262.85	-508.96
48.85	-514.94	156.85	-511.88	264.85	-508.91
50.85	-514.88	158.85	-511.83	266.85	-508.85
52.85	-514.83	160.85	-511.77	268.85	-508.80
54.85	-514.77	162.85	-511.72	270.85	-508.74
56.85	-514.71	164.85	-511.66	272.85	-508.69
58.85	-514.65	166.85	-511.61	274.85	-508.63
60.85	-514.60	168.85	-511.55	276.85	-508.58
62.85	-514.54	170.85	-511.49	278.85	-508.52
64.85	-514.48	172.85	-511.44	280.85	-508.47
66.85	-514.42	174.85	-511.38	282.85	-508.41
68.85	-514.36	176.85	-511.33	284.85	-508.36
70.85	-514.31	178.85	-511.27	286.85	-508.30
72.85	-514.25	180.85	-511.22	288.85	-508.24
74.85	-514.19	182.85	-511.16	290.85	-508.19
76.85	-514.13	184.85	-511.11	292.85	-508.13
78.85	-514.08	186.85	-511.05	294.85	-508.08
80.85	-514.02	188.85	-511.00	296.85	-508.02
82.85	-513.96	190.85	-510.94	298.85	-507.97
84.85	-513.91	192.85	-510.89	300.85	-507.91
86.85	-513.85	194.85	-510.83	302.85	-507.86
88.85	-513.79	196.85	-510.78	304.85	-507.80
90.85	-513.74	198.85	-510.72	306.85	-507.75
92.85	-513.68	200.85	-510.67	308.85	-507.69
94.85	-513.62	202.85	-510.61	310.85	-507.63
96.85	-513.56	204.85	-510.56	312.85	-507.58
98.85	-513.51	206.85	-510.50	314.85	-507.52
100.85	-513.45	208.85	-510.45	316.85	-507.47
102.85	-513.39	210.85	-510.39	318.85	-507.41
104.85	-513.34	212.85	-510.34	320.85	-507.36

Temp, °C	ΔHr, kJ/mol	Temp, °C	ΔHr, kJ/mol	Temp, °C	ΔHr, kJ/mol
106.85	-513.28	214.85	-510.28	322.85	-507.30
108.85	-513.23	216.85	-510.23	324.85	-507.25
110.85	-513.17	218.85	-510.17	326.85	-507.19
112.85	-513.11	220.85	-510.12	328.85	-507.13
114.85	-513.06	222.85	-510.06	330.85	-507.08
116.85	-513.00	224.85	-510.01	332.85	-507.02
118.85	-512.94	226.85	-509.95	334.85	-506.97
120.85	-512.89	228.85	-509.90	336.85	-506.91
122.85	-512.83	230.85	-509.84	338.85	-506.85
124.85	-512.78	232.85	-509.79	340.85	-506.80
126.85	-512.72	234.85	-509.73	342.85	-506.74
128.85	-512.66	236.85	-509.68	344.85	-506.69
130.85	-512.61	238.85	-509.62	346.85	-506.63

Calibration of mass flow controller.

The mass flow controllers were calculated by measuring the flow rate with an electronic gas flow meter at several setpoints.

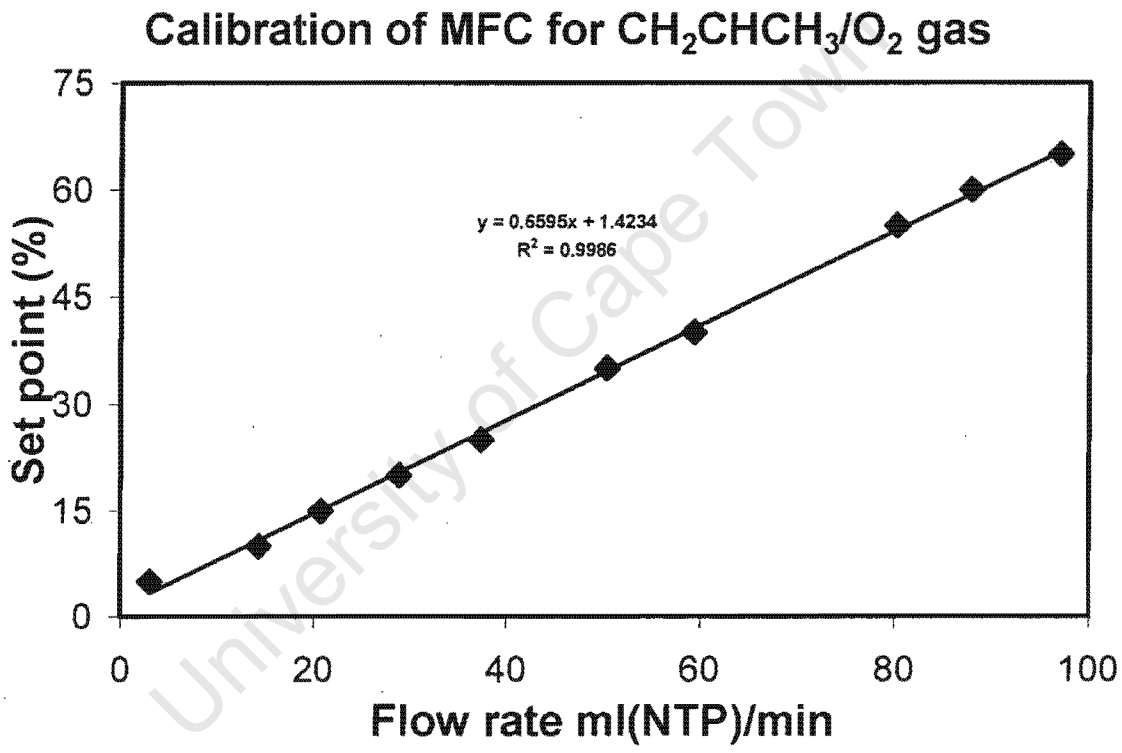

The GC operation conditions and the GC calibrations for the determination of response factor (f)

Detector

The GC has two FID detectors - with FID1 mainly COx is analysed, but ethane, ethylene, acetylene, etc. can also be seen. Attached to FID1 is a methanizer, which convert CO and CO_2 to methane in order to be detected by the FID. FID2 is essentially for oxygenates and the rest of the products like acrolein, acrylic acid, acrylonitrile, acetic acid, acetone and. The table below is a summary of the specifications and conditions of each detector.

Detector specifications

Detector	**FID1**	**FID2**
Column	Packed	Capillary
	0.6m Chromosorb WHP-SP OV-225 Pre-column (10wt%) & 6m Hayesepp D_B	30m CP Sil 24
Components	COx, methane, ethane	Propane, Propene oxygenates, acrylonitrile
Injector temperature	200°C	200°C
Detector temperature	370°C[1]	250°C

The calibration factor for an FID was determined as follows:

Diffrent moles of a gas are injected manually in a GC. The corresponding area in response to that particular concentration is obtained. The slope of the plot for an area versus mole represents a calibration factor: $f_{compound}$.

$$n_{compound} = f_{compound} \cdot Area_{compound}$$

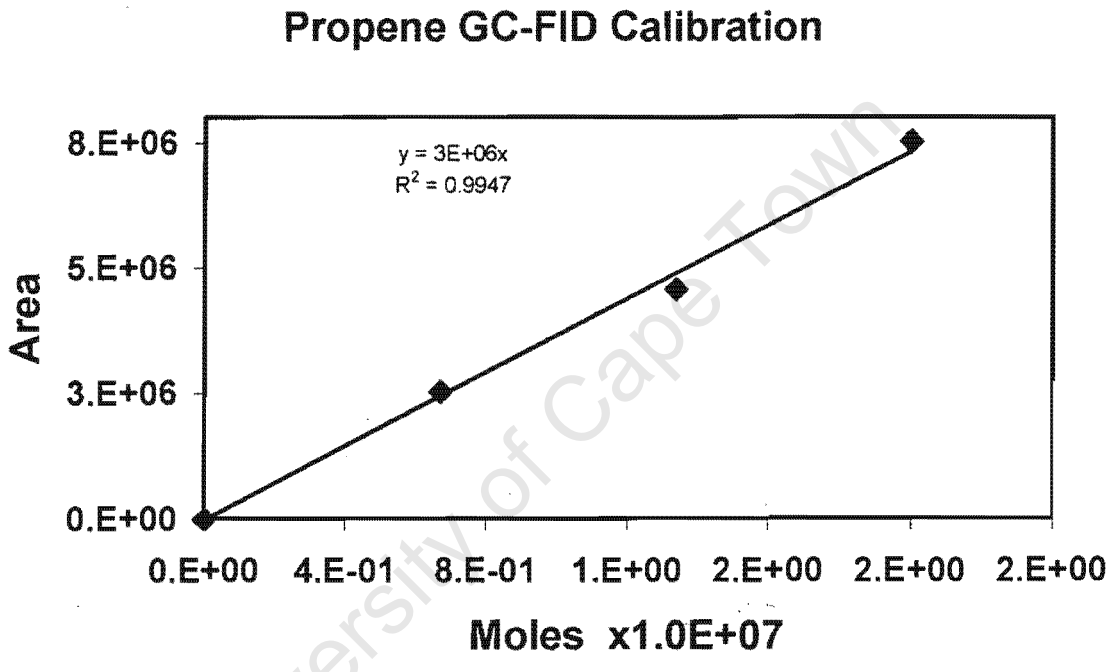

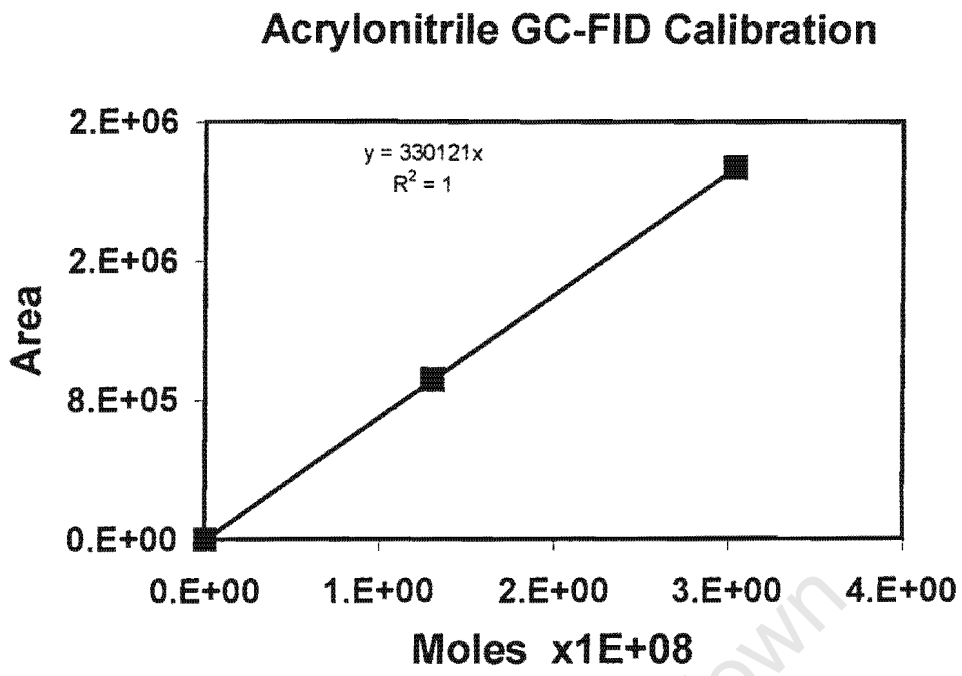

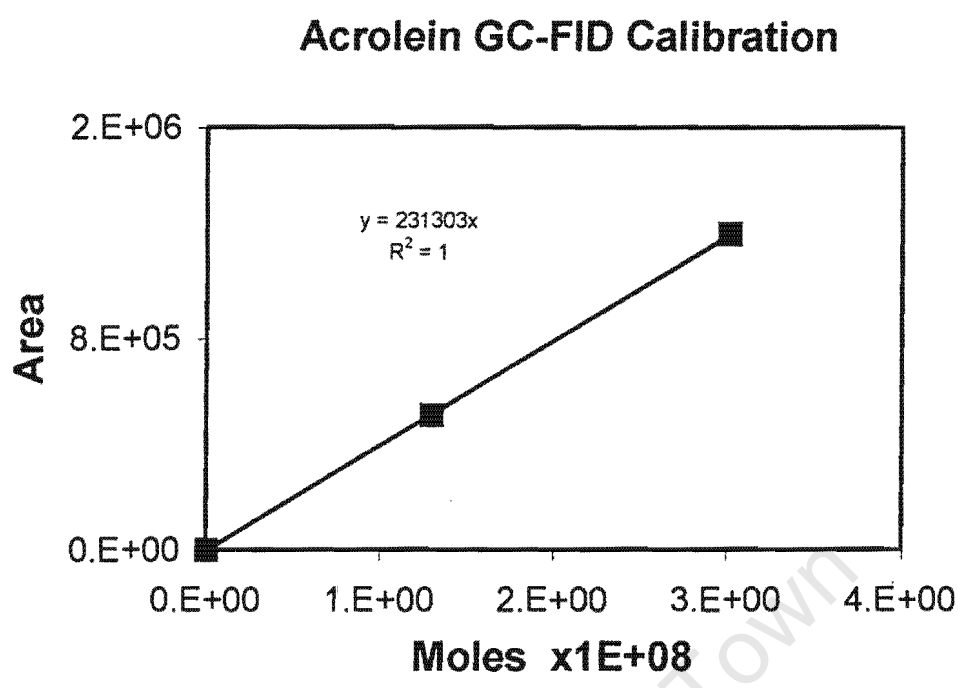

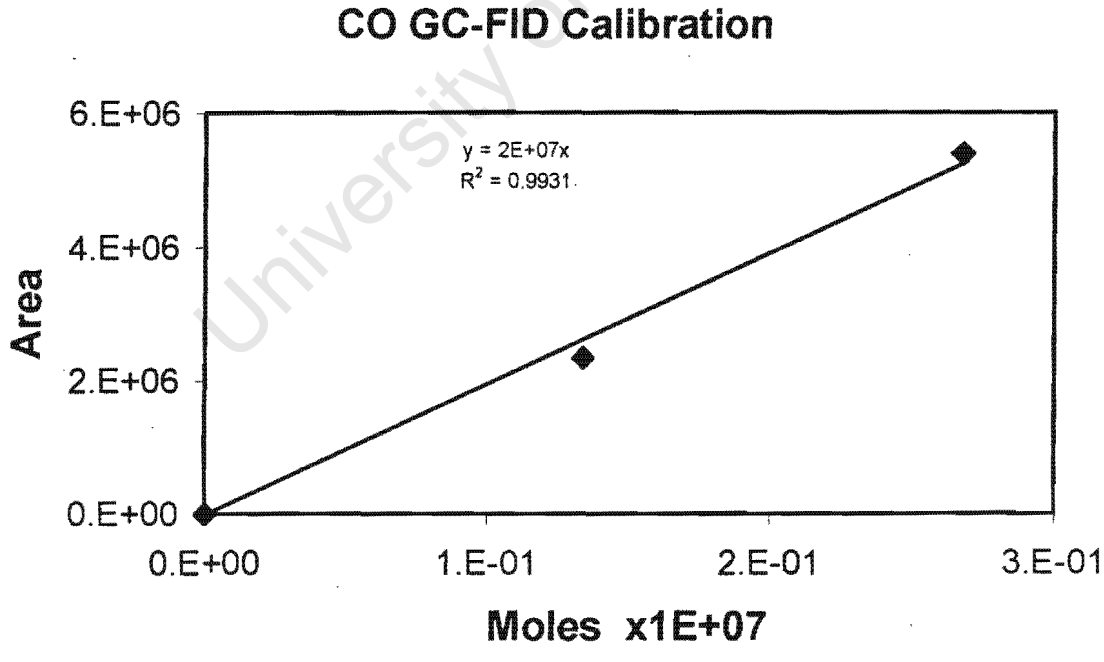

X: conversion; Y_{POX}: Yield to partial oxidation products; Y_{TOX}: Yield to total oxidation products; S_{TOX}: Selectivity to total oxidation products; S_{POX}: Selectivity to partial oxidation products;

$Bi_2Mo_3O_{12}$				
F_{NH3} (ml.min^{-1})	C-% XC3	mol-% XNH3	C-% Y_{TOX}	C-% Y_{POX}
3.295	10.79	1.54	0.31	0.53
5.475	6.28	2	0.39	0.78
13.4	4.76	2.4	0.44	1.94
16.528	3.19	1.1	0.31	3.36
20.068	1.58	0.63	0.21	1.14
22.918	1.25	0.43	0.85	1.26

$Bi_2Mo_3O_{12}/Fe_2Mo_3O_{12}$				
F_{NH3} (ml.min^{-1})	C-% XC3	mol-% XNH3	C-% Y_{TOX}	C-% Y_{POX}
3.295	10.16	6.92	2.31	5.4
5.475	9.5	5.5	1.78	6.13
13.4	9.2	5	1.47	7.5
16.528	9.13	2.62	0.72	5.18
20.068	8.32	1.13	0.6	5.02
22.918	7.97	0.76	0.65	4.86

$Bi_3FeMo_2O_{12}/Fe_2Mo_3O_{12}$				
F_{NH3} (ml.min^{-1})	C-% XC3	mol-% XNH3	C-% Y_{TOX}	C-% Y_{POX}
3.295	10.31	2.31	1.29	6.63
5.475	9.21	4	0.62	7.05
13.4	7.83	6	0.47	7.94
16.528	7.39	1.54	1.83	4.49

$Fe_2Mo_3O_{12}$

F_{NH3} (ml.min^{-1})	C-% XC3	mol-% XNH3	C-% Y_{TOX}	C-% Y_{POX}
3.295	5.44	7.69	22.25	8.13
5.475	0.87	7	36.28	8.05
13.4	31.14	10	19.98	5.04
16.528	-8.	2.77	3.03	8.05

$Bi_2Mo_3O_{12}$

Carbon balance	C-% S_{TOX}	C-% S_{POX}	CO cont	ACN cont
90.23	37.04	62.96	21.33	57.96
94.96	33.35	66.65	40.64	73.1
97.64	18.4	81.57	48.04	74.65
100.56	8.5	91.47	36.94	53.26
99.91	15.47	84.53	19.83	50.88
101.6	40.3	59.69	6.31	45.76

$Bi_2Mo_3O_{12}/Fe_2Mo_3O_{12}$

Carbon balance	C-% S_{TOX}	C-% S_{POX}	CO cont	ACN cont
98.39	29.94	70.06	31.79	77.39
98.58	22.53	77.47	44.63	78.48
99.51	16.43	83.57	59.14	80.23
96.33	12.2	87.8	80.49	78.49
96.74	10.64	89.37	96.43	78.43
96.96	11.85	88.15	95.27	78.46

$Bi_3FeMo_2O_{12}/Fe_2Mo_3O_{12}$

Carbon balance	C-% S_{TOX}	C-% S_{POX}	CO cont	ACN cont
98.46	16.35	83.65	17.73	73.52
98.63	8.06	91.94	36.5	68.9
100.36	5.58	94.41	73.12	85.37
100.34	28.99	71	11.35	86.92

$Fe_2Mo_3O_{12}$

Carbon balance	C-% S_{TOX}	C-% S_{POX}	CO cont	ACN cont
145.9	73.24	26.76	2.86	88.68
178.77	81.83	18.17	1.35	84.07
113	79.86	20.13	2.04	84.6
121.63	27.38	72.62	8.87	66.48

SEM pictures

Bismuth molybdate

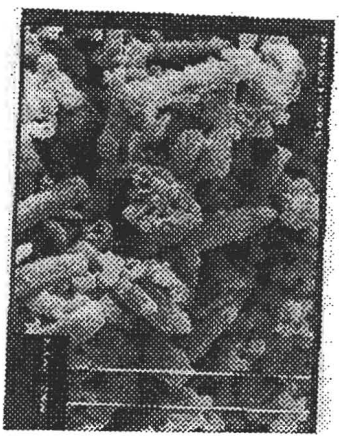

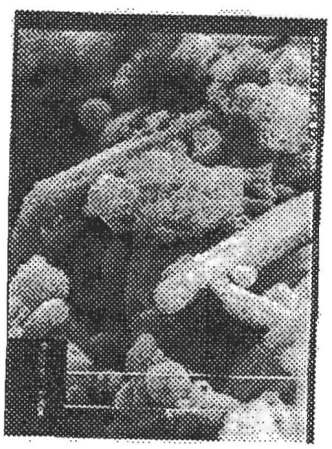

SEM pictures of iron bismuth molybdate (Bi:Fe=3)

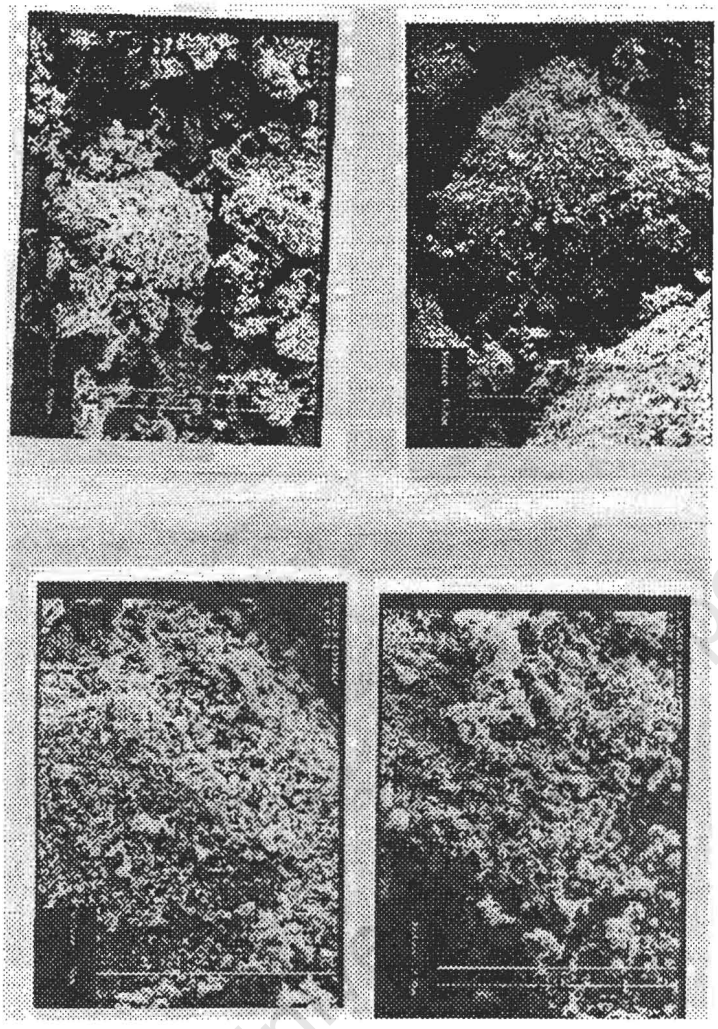

SEM pictures of iron molybdate

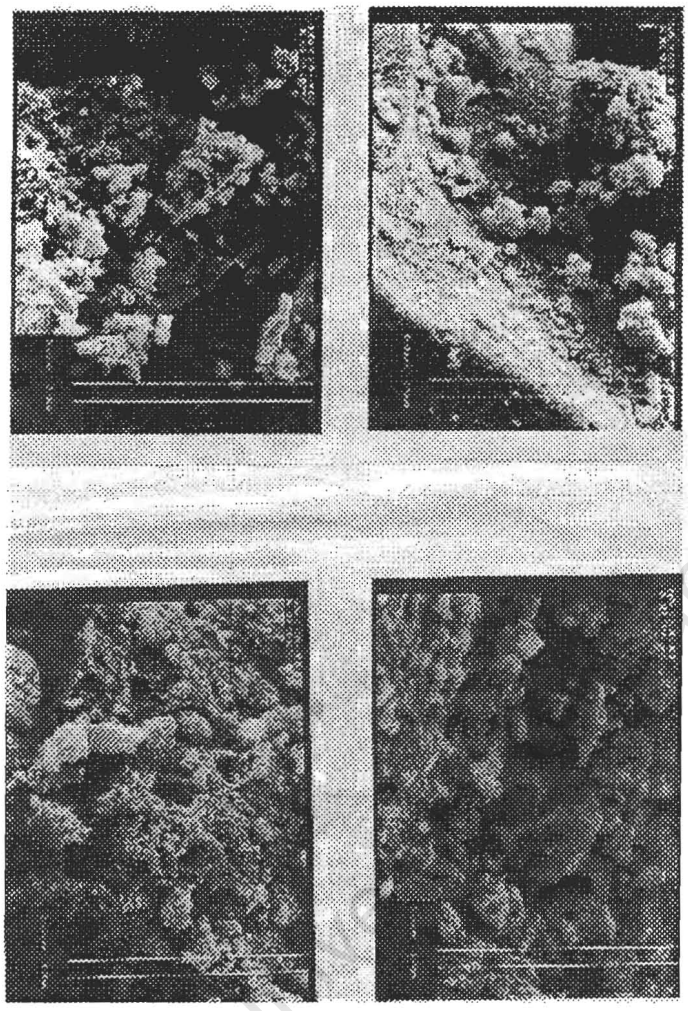

SEM pictures of iron bismuth molybdate (Bi:Fe=1)

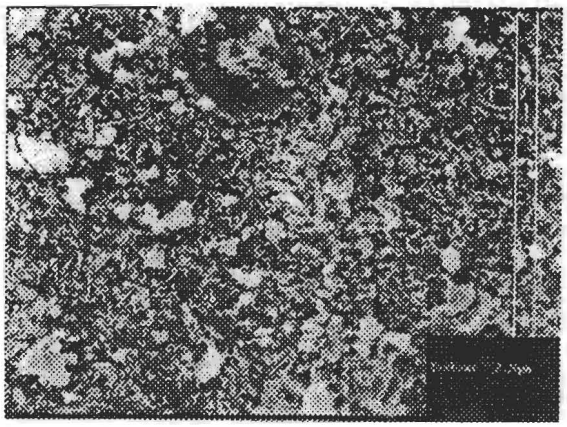

BET surface measurements
Bismuth molybdate

$$\frac{p}{V_{AD}(P_O - P)} = \frac{1}{CV_M} + \frac{C-1}{CV_M}\left(P/P_O\right)$$

$$A_{SP}\left(m^2/g\right) = \frac{V_M\left(ml/g, STP\right)}{22.4\times10^3\left(ml/mol\right)} N_A\left(molecules/mol\right) A_C\left(nm^2/molecules\right) 10^{-18}\left(m^2/nm^2\right)$$

Vad: Volume adsorbed
Vm: Volume of the monolayer
Ac: Cross sectional area of adsorbing molecule
P/Po: Relative pressure

The volume of the monolayer, Vm can be obtained by linearising the BET equation. The volume of the monolayer can be obtained from ratio of intercepts and slope, from the plot of Vads*1/(1-Po/P) versus P/Po below lead to

Bismuth molybdate

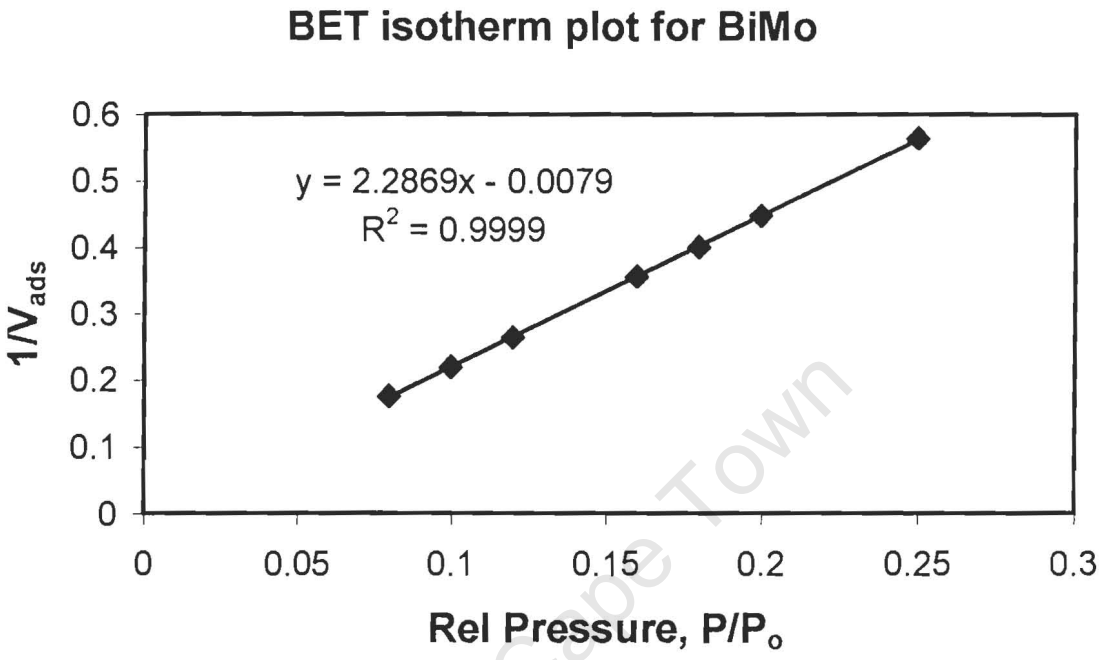

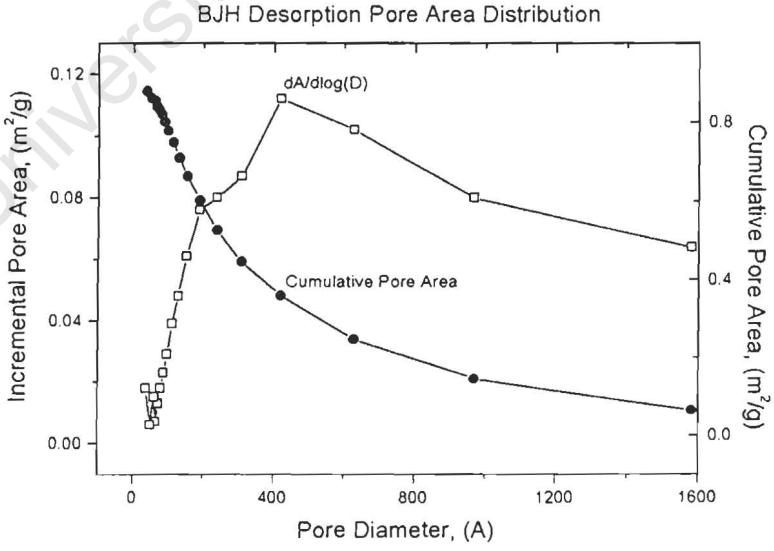

Bismuth molybdate

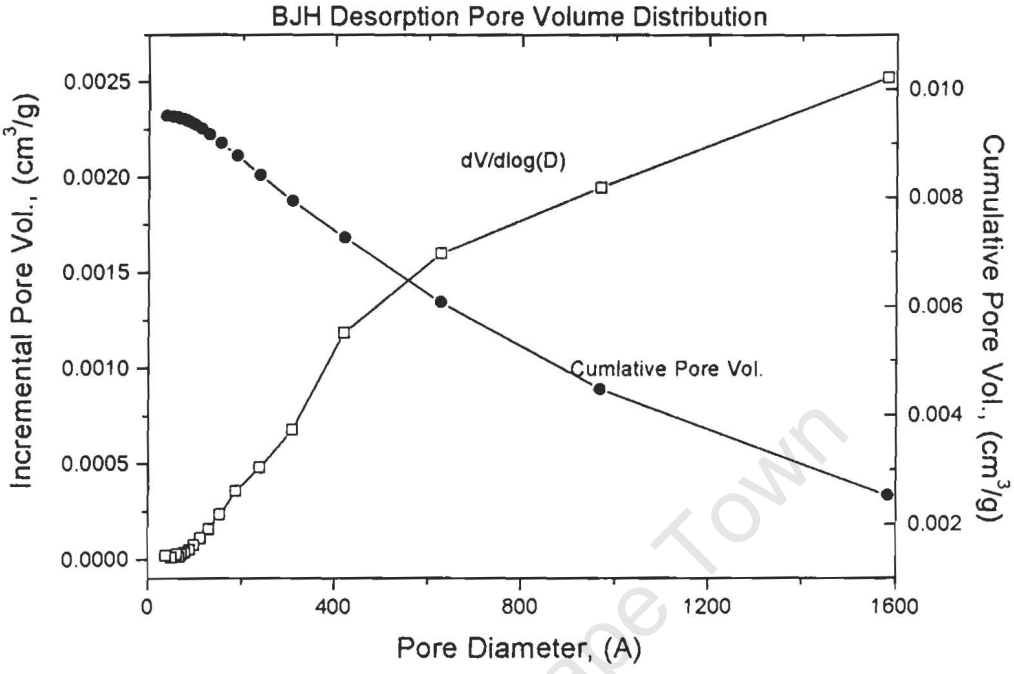

Iron bismuth molybdate (Bi:Fe=3)

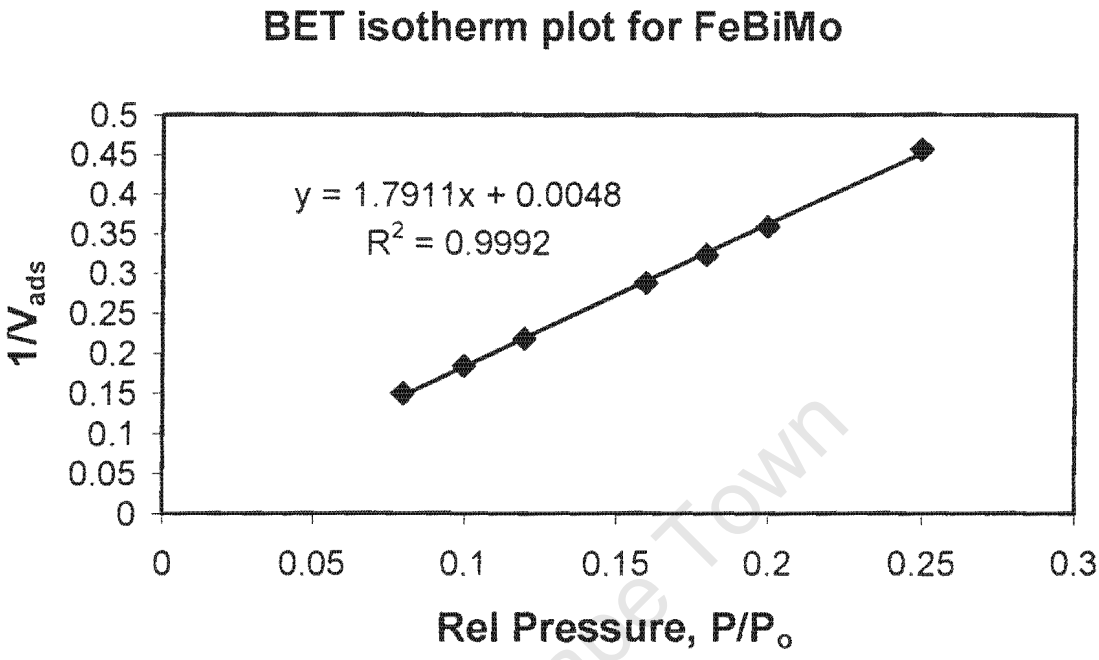

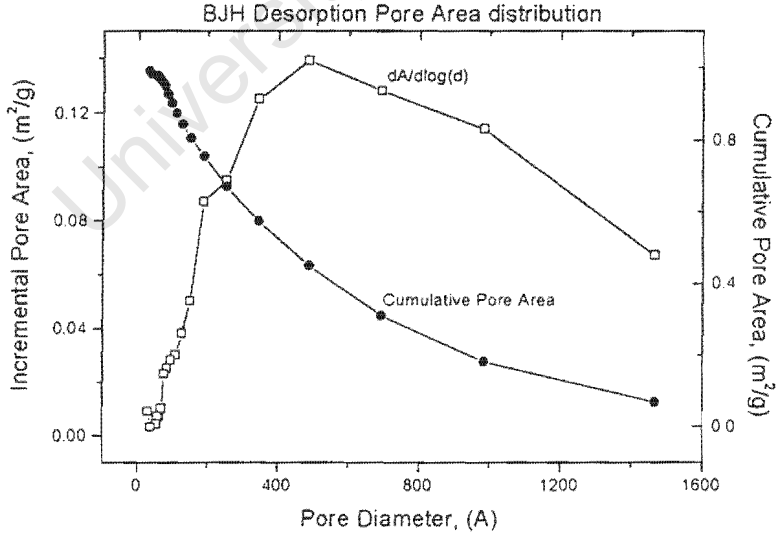

Iron bismuth molybdate (Bi:Fe=3)

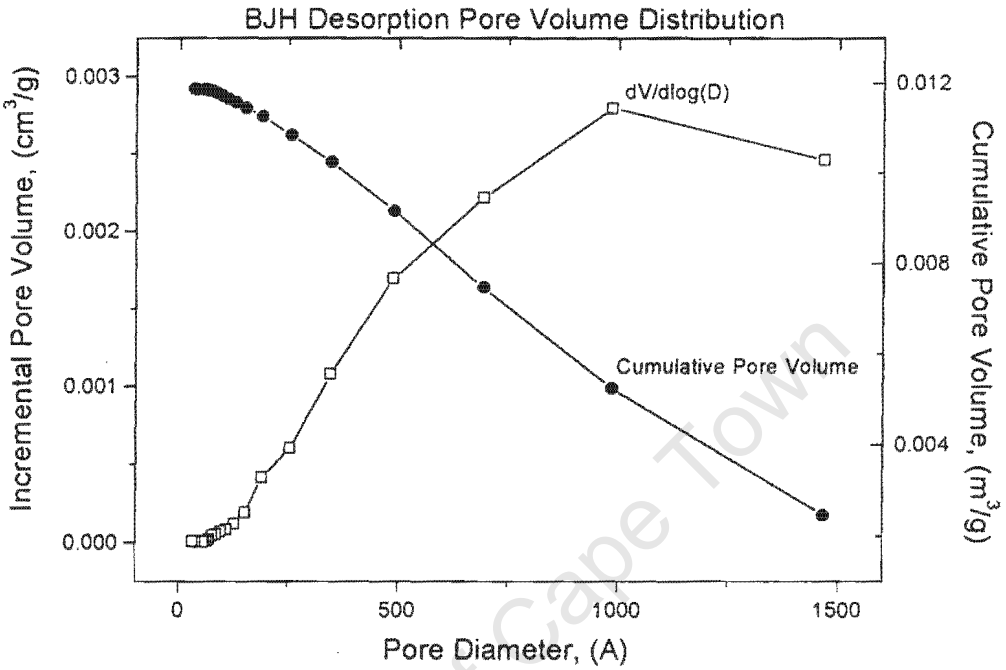

Iron bismuth molybdate (Bi:Fe=1)

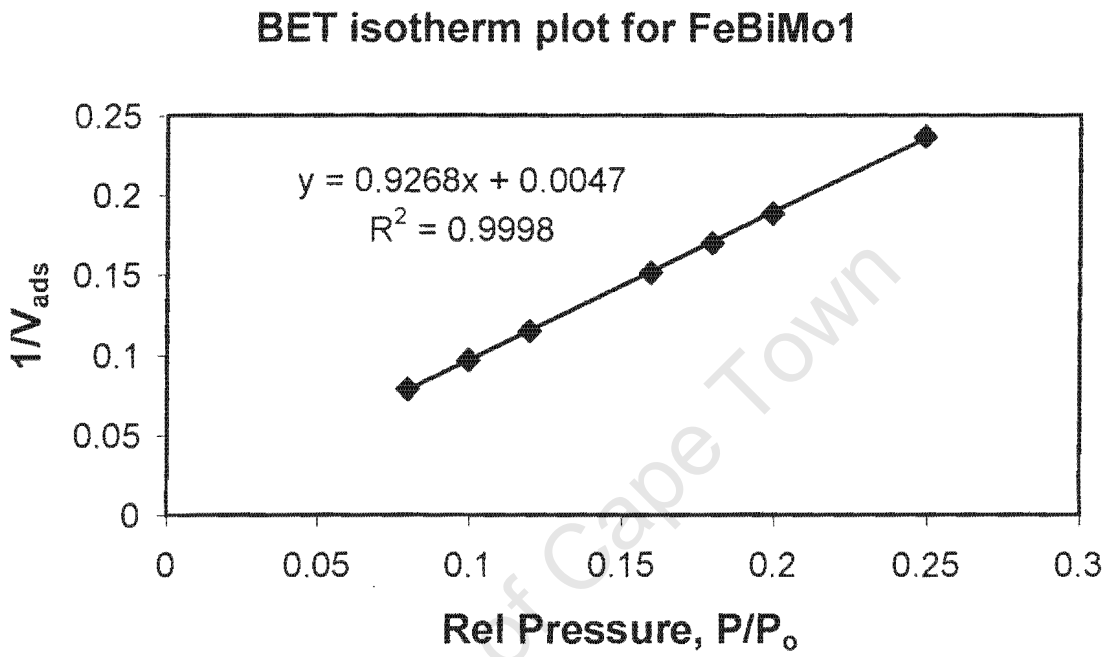

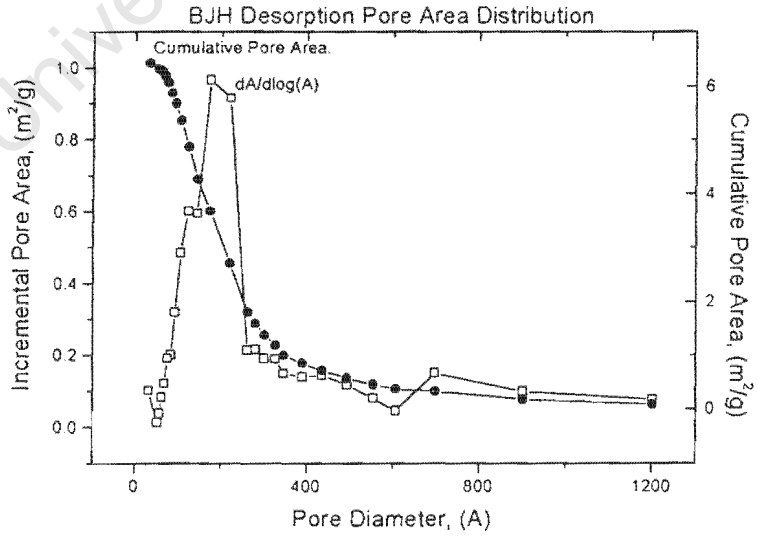

Iron bismuth molybdate (Bi:Fe=1)

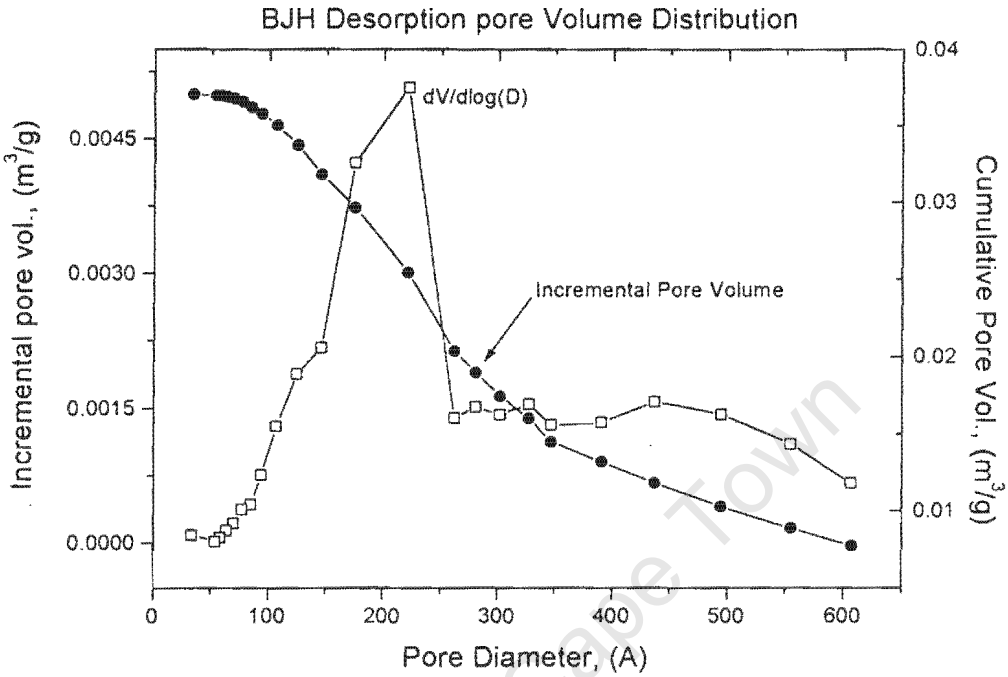

Iron molybdate catalyst

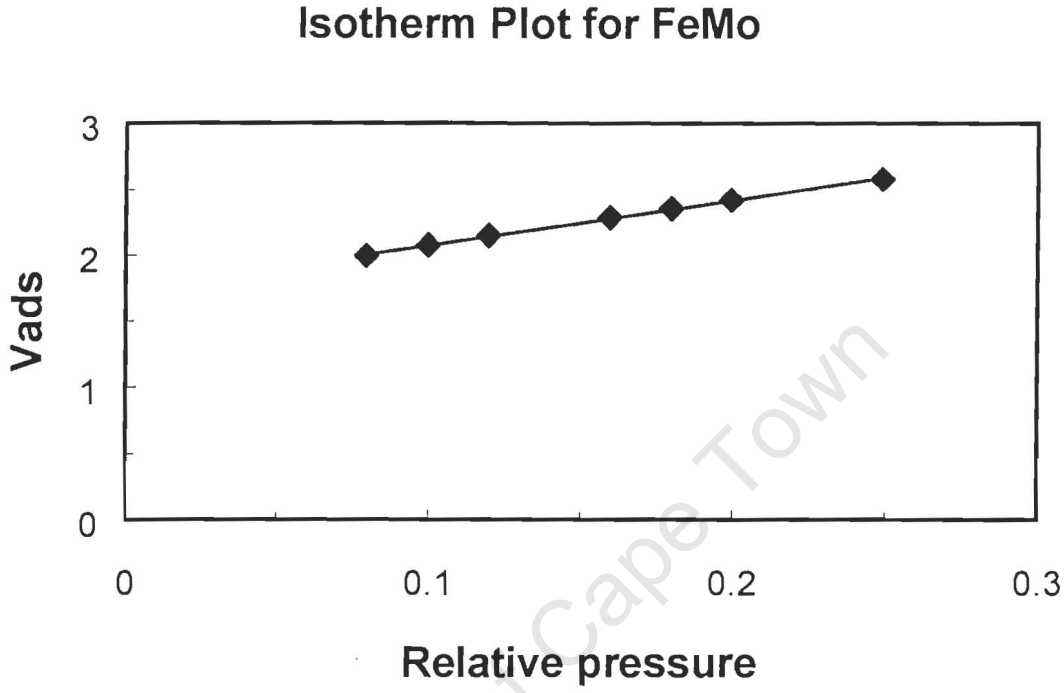

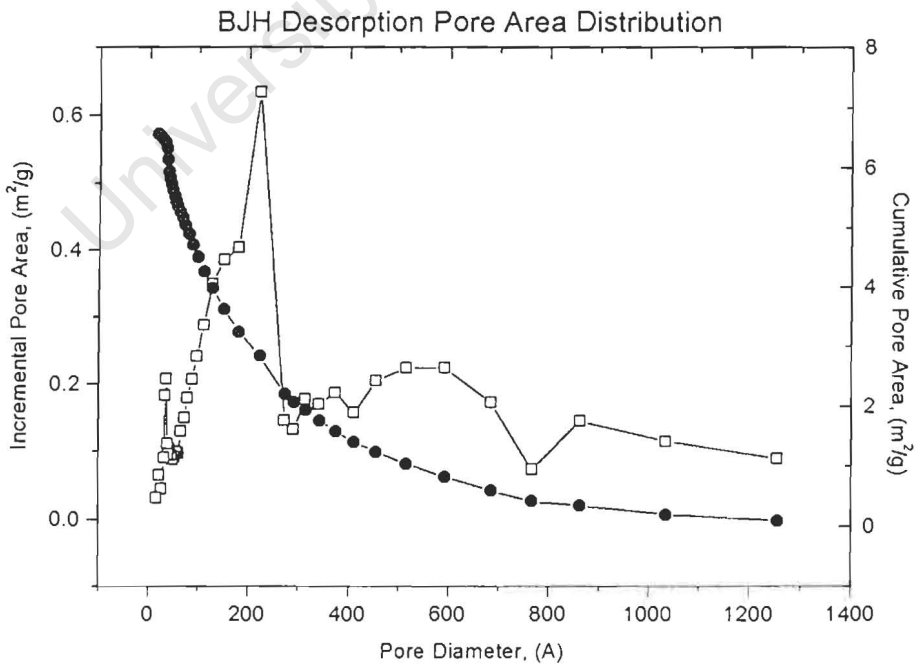

Iron molybdate

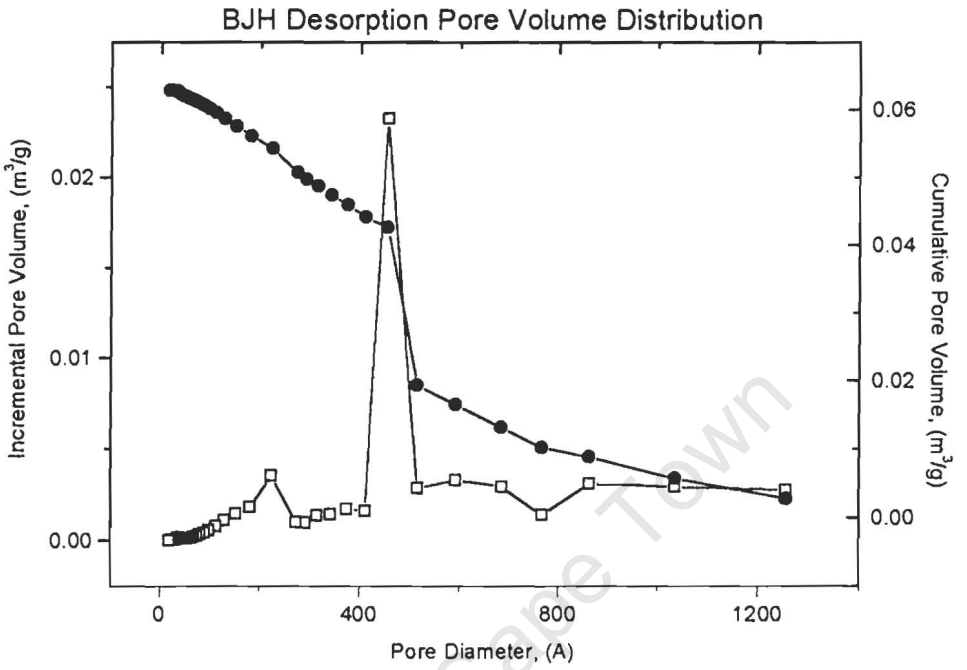

Mössbauer spectrum of iron molybdate

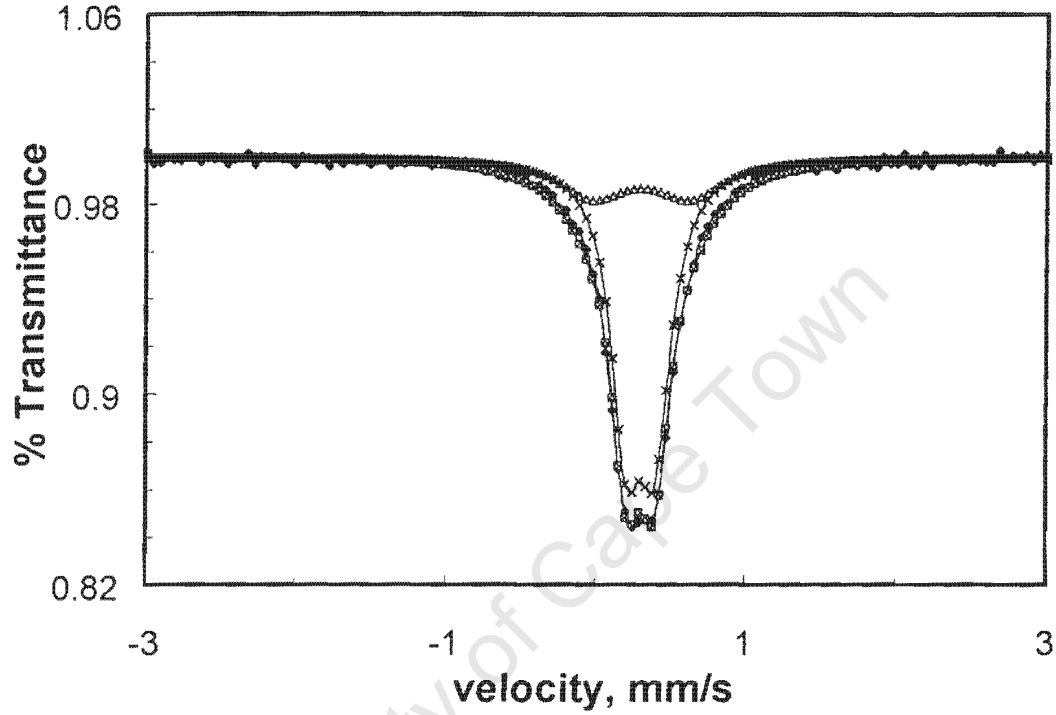

Mössbauer spectrum of iron bismuth molybdate (Bi:Fe=1)

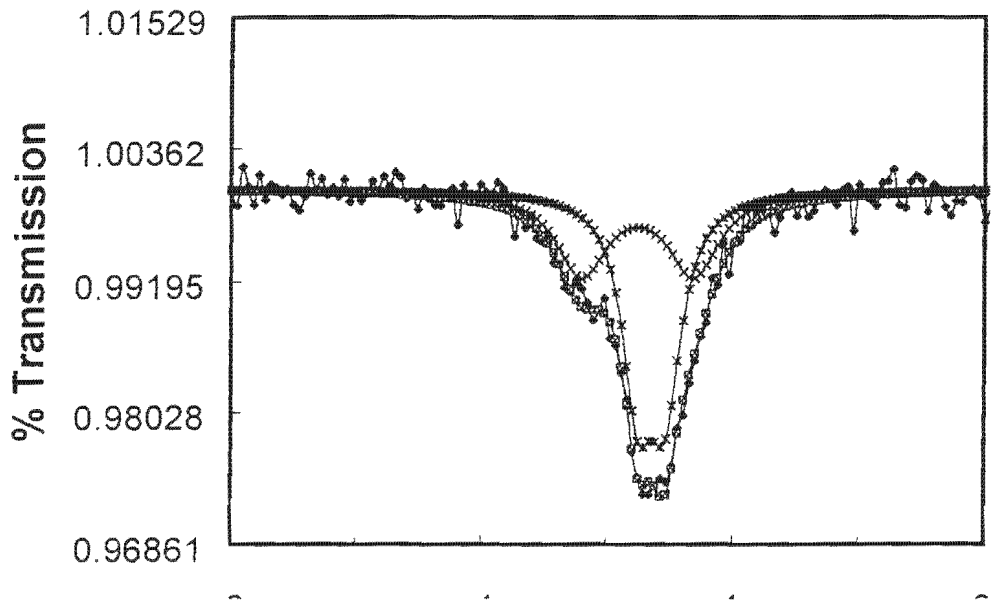

Mössbauer spectrum of iron bismuth molybdate (Bi:Fe=3)